

Generative AI for Cold Atom Interferometry

MLBD MRes Project Report

Project Code: MLBD_33

Name: Alex Evans

CID: 02525873

Supervisor: Mikael Mieskolainen & Charles Baynham

Assessor: Robert Bainbridge

Word Count: 9015

Date of Submission: 20/09/2024

Abstract

Developing an accurate model of an ultra-cold cooling sequence enables the potential optimisation of cold atom interferometry sequences, either through the training of a reinforcement learning agent or statistical inference. Pre-existing physics simulations are computationally intensive, however by training a generative AI model on data obtained from the physics simulation a speed-up factor of approximately 175x was achieved. The model itself is factorised into two parts, a deterministic model of the probability of an atom being transmitted to the next chamber, and a probabilistic model of the distributions of position and velocity vectors of the transmitted atoms. For the first part, a deep neural network was found to significantly out-perform a boosted decision tree, particularly in the tail-end of the distribution. For the probabilistic model, the introduction of diffusion Bayesian inference methods and diffusion inspired modifications was found to have significant improvements on conditional normalising flows in preventing manifold overfitting. This paper introduces the concept of "pre-diffusion" rounds in flows, in which the model is trained on a gradually denoising representation of the data, "smoothing" out training and drastically reducing manifold overfitting in as few as ten "pre-diffusion" rounds. Similarly, the application of a diffusion based Bayesian inference model with attention based conditioning led to even greater results in the prevention of manifold overfitting. The inclusion of second order information in the loss function of diffusion models has somewhat of a precedent, with these models approximating the trace of the Hessian using Hutchinson's estimator leading to more realistic results in image super-resolution. This paper introduces the first application of this second order term to diffusion-based Bayesian inference, and has been found to prevent overfitting in certain situations. On our dataset, the first order model was not particularly prone to overfitting, and therefore the impact was somewhat limited. In some areas of the parameter space it did however provide a significantly better fit, in particular distributions with long "tail-ends" - although a novel and experimental method such as this requires extensive scrutiny and testing before it can be applied with confidence. The application of diffusion on the whole had a significant impact on modelling the "global" distribution, rather than overfitting to local optima. In this context this is an essential characteristic, particularly for training a reliable reinforcement learning algorithm or obtaining meaningful statistical inference - of which a Bayesian optimisation example was demonstrated. The models applied are effective in achieving this global representation, and should set a precedent for modelling the entirety of the cooling sequence.

Contents

1	Introduction	1
2	2D Magneto-Optical Trap Simulation	2
2.1	Simulation Mechanics	2
2.1.1	Initialisation	3
2.1.2	Atom Generation	4
2.1.3	Dynamics	5
2.1.4	Transmission	7
2.2	Simulation Parameters	7
2.2.1	Constants	7
2.2.2	Input Variables (θ)	8
2.2.3	Target Variables (X)	8
2.3	Sampling	9
2.3.1	Cluster Optimisation	9
2.3.2	Sampling Technique	9
2.3.3	Sampling Execution	9
3	Normalising Flow Bayesian Inference	10
3.1	Conditional Normalising Flows	10
3.2	Data Mollification	11
3.2.1	CNF with Pre-Diffusion	12
4	Diffusion Bayesian Inference	12
4.1	1st Order Diffusion Bayesian Inference	14
4.2	2nd Order Diffusion Bayesian Inference	14
5	Results	15
5.1	Predicting Transmission Probability	15
5.1.1	Training	16
5.1.2	Evaluation	18
5.2	Modelling Vector Distributions	19
5.2.1	Initial Model	20
5.2.2	Adaptive Sampling	21
5.2.3	CNF with Pre-Diffusion	22
5.2.4	Diffusion Bayesian Inference	23
5.2.5	Evaluation	25
5.3	Unified Model Optimisation Example	28
5.3.1	Sensitivity Analysis	29
6	Conclusion	30
A	Deterministic Prediction Methods	36
A.1	Boosted Decision Trees	36
A.2	Deep Neural Networks	36

B Diffusion Bayesian Inference	38
B.1 Derivation of the Score Matching Objective	38
B.2 SLCP Dataset Loss Curve	39
C Parameter Quartile χ^2 Values	40
C.1 CNF	40
C.1.1 Natural Distribution	40
C.1.2 Adaptive Sampling	42
C.2 CNF-PD	45
C.2.1 Natural Distribution	45
C.2.2 Adaptive Sampling	47
C.3 1ODBI	50
C.3.1 Natural Distribution	50
C.3.2 Adaptive Sampling	52
C.4 2ODBI	55
C.4.1 Natural Distribution	55
C.4.2 Adaptive Sampling	57

1 Introduction

The Atom Interferometer Observatory and Network (AION) [1] project applies single-photon strontium atom interferometry to detect ultra-light dark matter (ULDM) and gravitational waves (GWs) in the deci-Hz frequency band; from sources including first-order phase transitions from the early Universe, cosmic strings and the merger of black-holes with masses existing detectors LIGO [2] and Virgo [3] are not sensitive to. Initial 10 m and 100 m instruments will serve as a test for kilometre-scale terrestrial instruments, before ultimately a satellite based instrument akin to AEDGE [4]. Strontium atom interferometry was chosen due to the long lifetime of the narrow line-width of the $^1S_0 - ^3P_0$ 698 nm wavelength clock transition to reduce coherence loss during the interferometer sequences [5, 6] and ideal optical transitions for trapping in magneto-optical traps (MOTs) [7–9].

In an AION detector (Figure 1), ultra-cold strontium atoms are launched in an “atomic fountain” configuration; a cloud of atoms is cooled to near absolute zero (a) and launched vertically in a vacuum tube shielded from residual magnetic fields [10]. Once in free-fall and effectively isolated from external forces excluding gravity, the atoms are placed into a quantum superposition of states via laser pulses (b) before recombined via a subsequent set of pulses, the influence of ULDM and GWs on the atom’s transition frequency causing an interference pattern [11]. Multiple interferometers (c) are placed at varying heights within the vacuum tube, the difference in laser phase measured at each cancels out laser noise and isolates the influence of GWs; detected via the light propagation time caused by the strain GWs create in the space between the free-falling atoms. ULDM is detected via its differential effects on the atom’s transition frequency [1].

To provide ultra-cold atoms for interferometry, a set of ultra-high vacuum (UHV) chambers attached to the vertical detector act as the atom source (a) shown in Figure 1. To reach the

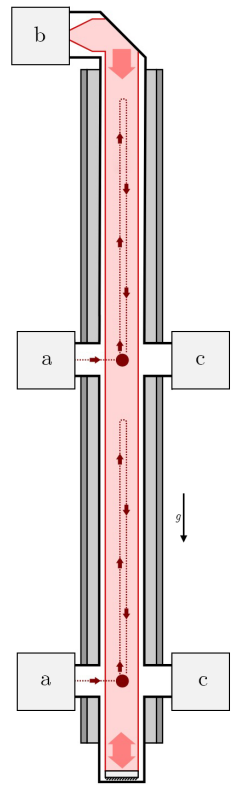


Figure 1:
Conceptual AION detector. Adapted from [1].

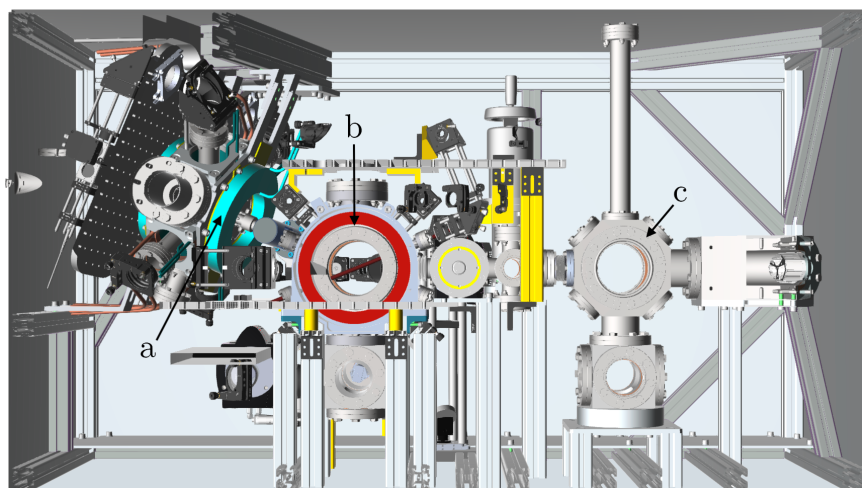


Figure 2: 3D cross-sectional view of a model AION sequence, showing: (a) UHV chamber 1 (2D+ MOT); (b) UHV chamber 2 (blue/red 3D MOT and dipole trap); (c) test conceptual atom interferometer as shown in Figure 1.

nano-kelvin temperatures necessary, a series of ultra-cold cooling techniques are used [9] (Figure 2). The atoms are initially fired from an atomic oven into a 2D+ "blue" MOT, where they are cooled and trapped by a two dimensional laser and magnetic field gradient before transmitted by a push beam into the 3D MOT. The 3D MOT, with an initial "blue" and further "red" phase, traps the atoms using a three dimensional configuration, bringing them down to micro-kelvin temperatures. Finally an optical dipole trap cools atoms to nano-kelvin levels through evaporative cooling, whilst confining the atoms in a small, dense region [12]. Each stage of the sequence involves various adjustable parameters that are currently manually tuned - however, recent research [13–15] indicates that more sophisticated techniques could be applied to optimise the cooling process.

AtomECS [16] is a simulation package designed to model the interactions of atoms with near-resonant laser light, as used in MOTs. AtomECS was developed in Rust utilising the Entity Component System (ECS) architecture for optimal CPU parallelisation and computational efficiency. The application of a reinforcement learning (RL) agent on a physical ultra-cold setup has been shown to be successful (Ref. [13]), with the study mitigating the "cold start problem" [17] by pre-training on sampled data. Through the use of AtomECS, simulated data could be obtained upon which the model is trained, therefore mitigating the need to directly sample the physical sequence. Not only would this minimise cost outlay, but new samples could be generated with relative ease, leading to a "deeper" pre-trained RL agent. Statistical inference on this model could also be performed, leading to a deeper understanding of AION's cooling process.

The wider goal is to develop a full AI (rather than physical) simulation of the cooling process for both inference and optimisation using an RL agent. Within AtomECS, each section of the sequence (2D MOT, blue/red 3D MOT and dipole trapping) is factorised into distinct simulations. To accurately model the atoms transmitted to the 3D MOT, simulated atom vectors dependent on the 2D MOT parameters are necessary. The AI model will replicate the relationship between these vectors and the parameters, rather than the underlying physical processes. This enables efficient sampling of the 2D MOT without the heavy computational outlay of operating a physical simulator.

Initially, the simulation itself is introduced in Section 2 including experimental parameters and techniques to sample mass data for training the AI model. The model is factorised into a deterministic prediction for probability of transmission (theory available in Appendix A) and a probabilistic model to generate atoms at a specified threshold. The theory behind the probabilistic models developed is given in Section 3 for normalising flows, and Section 4 for diffusion based techniques. The application of these techniques in the development of the model including results and optimisation example is detailed in Section 5.

2 2D Magneto-Optical Trap Simulation

The following looks to introduce the workings and fundamental mechanics of the AtomECS 2D MOT simulation (Section 2.1), including context into the parameters within the simulation and resultant model (values tabulated in Section 2.2), and how the simulation may be run to obtain large-scale datasets (Section 2.3).

2.1 Simulation Mechanics

Presented is an overview of the 2D MOT AtomECS simulation mechanics as demonstrated in Ref. [16]. The emphasis here is placed on introducing the simulation constants (Section 2.2.1) and

input variables θ (Section 2.2.2) and their effect on the target variables X (Section 2.2.3) within the physics simulation. This section does *not* intend to serve as an accurate quantum description of MOTs, but rather a description of the simulation mechanics to add context to the wider study. The rate equations for example (Equations (4) and (5)) are classical approximations used within the simulation. It's worth noting that the simulation does not account for the broadening effect due to saturation intensity or interactions between atoms.

2.1.1 Initialisation

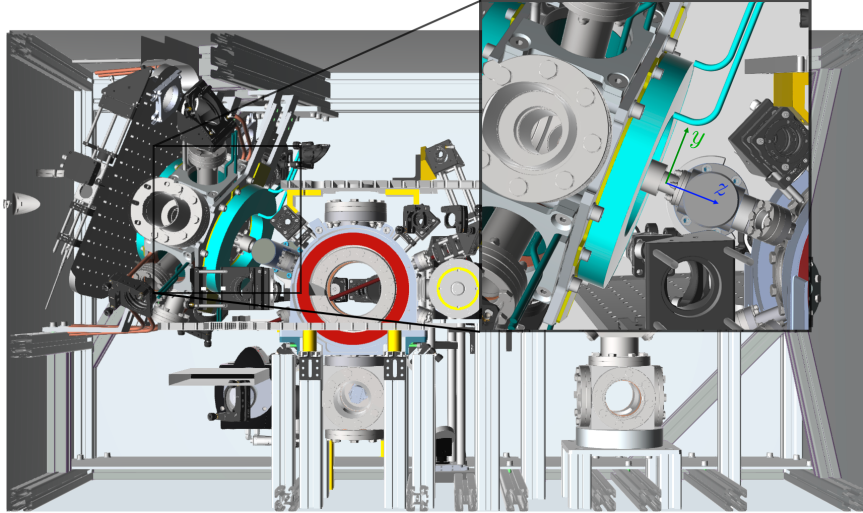


Figure 3: 3D cross-sectional view of a model AION sequence showing the alignment of the co-ordinate system. The x -axis is aligned perpendicular to the cross-sectional view.

Each atom's trajectory is presented in this paper using a spherical co-ordinate system, with θ representing the polar angle and ϕ the azimuth, as illustrated in plot (a) of Figure 4. Figure 3 shows the relation of this co-ordinate to the AION cooling sequence. At a given time-step such that elapsed time $t = n_t \Delta t$, where n_t represents the total number of elapsed time-steps and Δt a fixed increment of time simulated by an individual time-step, the simulation updates the position and velocity vectors (Cartesian) of each atom stored in the ECS based on the effects of the dynamics of the system described in this section.

To reduce computational outlay various limits are placed within the simulation to remove atoms with an improbable chance of being captured. A defined velocity cap v_{cap} is implemented, such that if an atom's magnitudinal velocity v exceeds this cap they are deleted from the simulation. Physical boundaries (b) are also defined to similar effect, this includes the main simulation bounds \mathbf{D}_{sim} defining the dimensions of a cuboid centred on the origin, and pipe length L_{pipe} , pipe radius r_{pipe} and pipe offset d_{pipe} defining the dimensions of a cylinder along the z -axis. This cylinder is designed to model the differential pumping apparatus through which the atoms are transmitted to the 3D MOT [16].

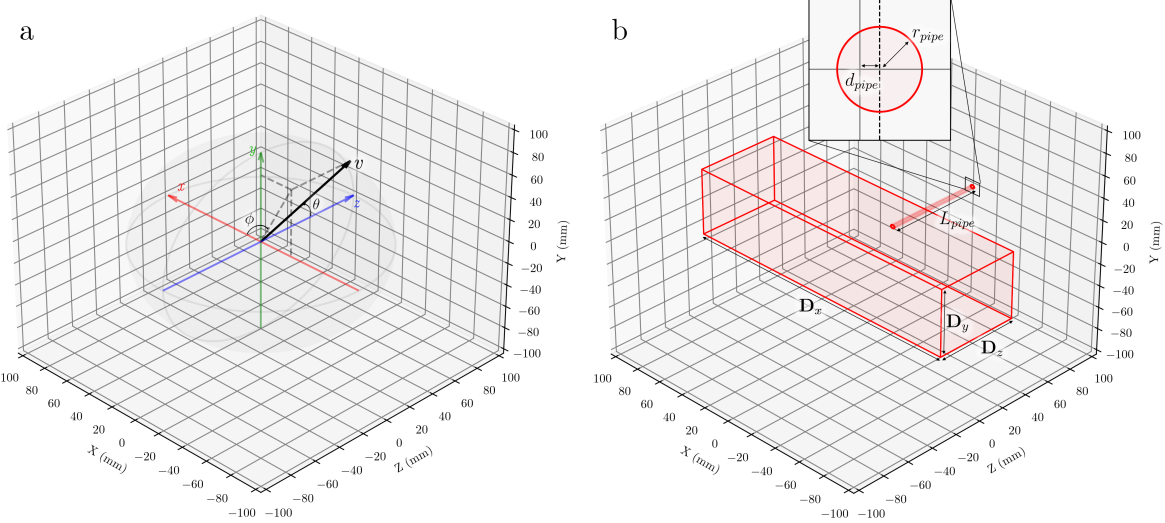


Figure 4: 3D diagram illustrating: (a) the spherical co-ordinate system used to define the trajectory of an atom, showing the magnitudinal velocity v , polar angle θ and azimuthal ϕ ; (b) the simulation bounds \mathbf{D}_{sim} dimensions \mathbf{D}_x , \mathbf{D}_y , \mathbf{D}_z , pipe length L_{pipe} , pipe radius r_{pipe} and pipe offset d_{pipe} fixed parameters - representing the physical bounds beyond which atoms are removed from the simulation.

2.1.2 Atom Generation

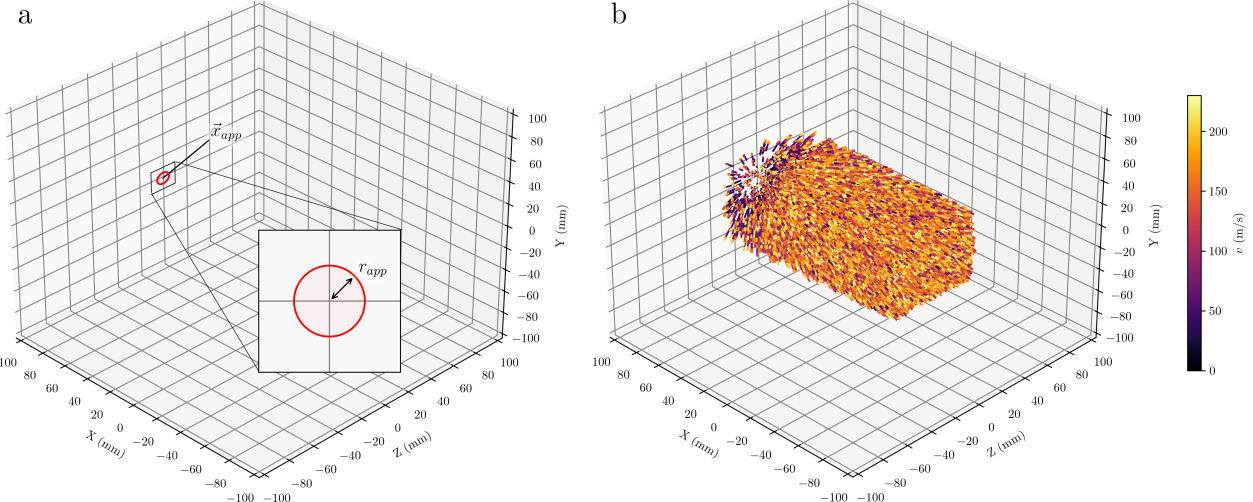


Figure 5: 3D diagrams illustrating: (a) aperture position \vec{x}_{app} and aperture radius r_{app} , from which the atoms are generated; (b) simulation $N_{atoms} = 5 \times 10^5$, $n_t = 320$: hot atoms fired from the oven along the negative x -axis, each arrow represents an individual atom colour coded according to the magnitude of its velocity vector.

Within the ultra-cold atom cooling sequence, the atomic oven acts as the source of atoms. The oven typically contains a source material, strontium in the case of AION, which is heated to a high temperature such that it emits a vapour of atoms. These vaporised atoms are emitted from an aperture following an array of micro-channels which collimate the atoms into a 'beam'. Within the simulation, the aperture position \vec{x}_{app} vector defines the point at which a number of atoms N_{atoms}

are generated from an aperture of radius r_{app} and fired along the negative x-axis. Their velocity and angular directions are sampled from a v^3 -Boltzmann and $j(\theta)$ distribution respectively; the former dependent on the oven temperature T_{oven} and the latter on the micro-channel radius r_{mc} and micro-channel length L_{mc} [16].

2.1.3 Dynamics

The magnetic field is modelled as a 2D quadrupole gradient ∇B , with a null point at the centre that increases linearly with distance from this central point; although the null point may be shifted through the presence of a vertical bias field B_v [18]. Additionally there are four cooling lasers which intersect at the centre, the intensity $I_i(\vec{x})$ of an individual beam i at position \vec{x} is given by:

$$I_i(\vec{x}) = I_{0,i} \exp\left(-\frac{2r^2}{w_c^2}\right) \quad (1)$$

where r is the radial distance from the beam's axis, w_c the waist of the cooling beam and $I_{0,i}$ the peak intensity [19] - dependent on the cooling beam power P_c by the relation:

$$I_{0,i} = \frac{2P_i}{\pi w_i^2} \quad (2)$$

In AtomECS, the rate R_i at which an atom absorbs photons from a laser beam i is given by:

$$R_i = \frac{I_i(\vec{x})}{I_{sat}} \frac{\Gamma}{2} \frac{\Gamma^2/4}{\delta(\vec{x}, \vec{v}, \delta_c)^2 + \Gamma^2} \quad (3)$$

where I_{sat} is the saturation intensity, Γ is the linewidth of the atomic transition, and $\delta(\vec{x}, \vec{v}, \delta_c)$ is the effective angular detuning [16]. The static baseline detuning of the cooling beam δ_c is defined as the difference between the angular frequency of the laser light, ω_L , and the natural angular frequency of the atomic transition ω_0 - however due to the Zeeman [20] and Doppler [21] effects $\delta(\vec{x}, \vec{v}, \delta_c)$ is dependent on both the position \vec{x} and velocity \vec{v} of the atom respectively. In the presence of a magnetic field, the energy levels of the atom are shifted, changing the natural frequency ω_0 - this is the Zeeman effect; and so due to the gradient ∇B , the atom's position determines the level of shift in energy levels [22]. Through the Doppler effect, the motion of an atom relative to the laser beams shifts the perceived angular frequency of the light, altering the effective detuning based on the atom's velocity [23].

The shift in angular velocity due to both the Zeeman and Doppler effects can put the atom into resonance with the detuned beams based on the position and velocity of the atom, therefore determining the rate of absorption, R_i [24]. When an atom absorbs a photon from the laser beam, it receives a momentum kick in the direction of the photon's propagation, pushing them towards the centre of the MOT. Similarly if an already excited atom encounters another photon of the same energy, it can be stimulated to emit a photon in the same direction as the incoming photon - this process redistributes the atom's momentum away from the MOT [18]. Atoms in the excited state will spontaneously emit photons in a random direction, returning to the ground state and providing a momentum kick; however due to random nature the net effect over many emissions is isotropic, therefore making the resultant impact of emission of the atom's trajectory insignificant [25].

The rate equation is used to describe the population dynamics of atomic states under the influence of laser light - in the context of a MOT, it can be used to describe population densities

of whether an atom is in the ground state, ρ_{gg} , or the excited state, ρ_{ee} . The rate equation for each state can be expressed as follows:

$$\dot{\rho}_{gg} = -\rho_{gg}A_{eg} - \left(\sum_i R_i \right) (\rho_{gg} - \rho_{ee}) \quad (4)$$

$$\dot{\rho}_{ee} = +\rho_{gg}A_{eg} + \left(\sum_i R_i \right) (\rho_{gg} - \rho_{ee}) \quad (5)$$

where A_{eg} is the Einstein A coefficient (rate of spontaneous emission), such that $-\rho_{gg}A_{eg}$ and $+\rho_{gg}A_{eg}$ represent the decay of atoms from the excited to the ground state and the ground to excited state respectively [16]. The rate equations are solved in the limit $t \rightarrow \infty$ to give steady-state solutions of the population densities:

$$\rho_{gg} = \frac{\sum_i R_i}{A_{eg} + 2 \sum_i R_i} \quad (6)$$

$$\rho_{ee} = 1 - \rho_{gg} \quad (7)$$

The average total number of photons absorbed and spontaneously emitted by an atom in a given time-step Δt is equal to:

$$N_\gamma = \Delta t \cdot \rho_{gg} \cdot \Gamma \quad (8)$$

and the expected number of photons scattered by an individual laser beam N_i distributed according to R_i :

$$N_i = \frac{R_i}{\sum_i R_i} N_\gamma \quad (9)$$

with the actual number of photons \tilde{N}_i drawn from a Poisson distribution with a mean of N_i , taking into account the stochastic nature of the scattering process [16]. When an atom absorbs a photon from a laser beam, it receives a momentum kick in the direction of the photon's wave-vector. The force due to the absorption of photons from laser beam i during the time-step Δt is given by:

$$\tilde{F}_{A,i} = \frac{\hbar \mathbf{k}_i \tilde{N}_i}{\Delta t} \quad (10)$$

where \hbar represents the reduced Planck constant and \mathbf{k}_i the wave-vector of the beam; $\hbar \mathbf{k}_i$ therefore representing the momentum of a single photon from laser beam. Similarly, the force from emission is given by:

$$\tilde{F}_{E,i} = \sum_{j=1}^{\tilde{N}_i} \frac{\hbar |\mathbf{k}_i|}{\Delta t} \hat{e}_j \quad (11)$$

where \hat{e}_j is a unit vector that points in a random direction [16]. The net force enacted on an atom in a time-step Δt as a result of a collective number of absorptions and emissions can be approximated by a single force sampled from a Gaussian distribution with standard deviation:

$$\sigma_F = \sqrt{\frac{\tilde{N}_i}{3} \cdot \frac{\hbar |\mathbf{k}_i|}{\Delta t}} \quad (12)$$

the simulation updates the atom's velocity and position vectors with the sampled force using the velocity-Verlet algorithm (Ref. [26]), before repeating the process for the next time-step [16].

2.1.4 Transmission

To simulate the transmission of atoms to the 3D MOT, a push beam along the z-axis transfers momentum onto cooled atoms trapped in the MOT to "push" them through the pipe. In a similar manner to the momentum transfer in the cooling beams, when the atoms absorb a photon from the beam they gain a shift in momentum in the direction of the photon's propagation before emitting it in a random direction - the net result is a shift in momentum in the direction of the beam dependent on the push beam power P_p and waist w_p . To align with a shifted null point in the magnetic field under the presence of vertical bias B_v , the push beam may be offset distance d_p . The push beam detuning δ_p is typically red-detuned to preferentially interact with atoms moving towards the beam due to the Doppler effect, this selective interaction allows the push beam to target and slow down faster-moving atoms [24]. At thresholds τ_z of 5 mm intervals along the z -axis, the atom x and y -axis positions \vec{r}_x , \vec{r}_y , velocity magnitude v , polar angle θ and azimuthal angle ϕ of the velocity trajectory are recorded. The transmission probability \mathcal{P} represents the percentage of N_{atoms} that reach a given τ_z .

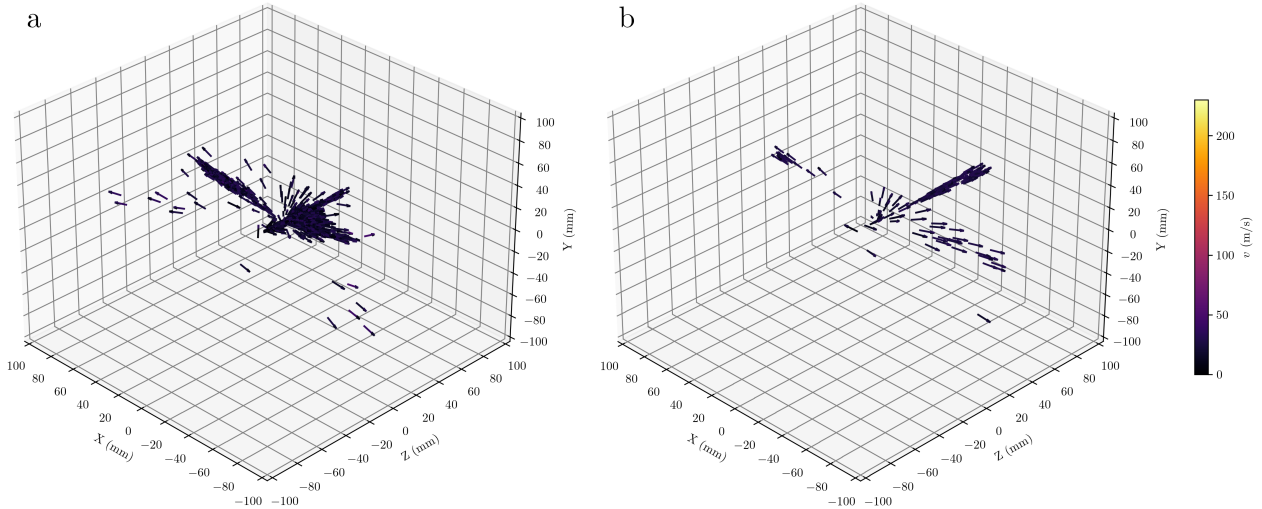


Figure 6: 3D diagrams of simulations $N_{atoms} = 5 \times 10^5$ at: (a) $n_t = 2560$: here some atoms have become trapped by the laser and magnetic field configuration and have begun to be pushed by the push beam; (b) $n_t = 3840$: the atoms are traversing through the pipe to the 3D MOT.

2.2 Simulation Parameters

2.2.1 Constants

When generating samples from AtomECS, parameters associated with the fundamental design of the chamber such as the oven position remain fixed. Similarly by minimising the number of parameter relationships within the model down to those feasibly optimisable, its dimensionality reduces significantly, therefore also reducing the number of samples necessary to adequately cover the parameter space.

Table 1: Fixed simulation parameters with corresponding symbols, values, and units.

Symbol	Parameter	Value	Units
N_{atoms}	Atoms Generated	5×10^6	atoms
\vec{x}_{app}	Aperture Position	83, 0, 0	mm
r_{app}	Aperture Radius	5	mm
L_{mc}	Micro-Channel Length	4.0	mm
r_{mc}	Micro-Channel Radius	0.2	mm
T_{oven}	Oven Temperature	776	K
L_{pipe}	Pipe Length	70	mm
r_{pipe}	Pipe Radius	1.5	mm
d_{pipe}	Pipe Offset	0	mm
\mathbf{D}_{sim}	Simulation Bounds	200, 60, 60	mm
τ_z	Slice Threshold	30	mm
Δt	Time-Step	2.0	μ s
v_{cap}	Velocity Cap	230	m/s

2.2.2 Input Variables (θ)

In total, nine parameters were varied throughout the data sampling process. The ranges were chosen based on prior knowledge from manual tuning of the 2D+ MOT and initial test sampling of the simulation.

Table 2: Free simulation parameters with corresponding symbols, units, and range of values sampled and modelled in a MOT setup.

Symbol	Parameter	Minimum Value	Maximum Value	Units
δ_c	Cooling Beam Detuning	-250	0	MHz
P_c	Cooling Beam Power	50	350	mW
w_c	Cooling Beam Waist	7	15	mm
δ_p	Push Beam Detuning	-350	0	MHz
P_p	Push Beam Power	0	20	mW
w_p	Push Beam Waist	0	3	mm
d_p	Push Beam Offset	0	5	mm
∇B	Quadrupole Gradient	0	100	G/cm
B_v	Vertical Bias Field	-20	20	G

2.2.3 Target Variables (X)

Although the positions and velocity vectors of each atom are saved at thresholds τ_z of 5 mm intervals along the pipe, this paper models exclusively the threshold at $\tau_z = 30$ mm along the z-axis from the origin, effectively the inlet to the pipe. This value was chosen due to uncertainty in the modelling of dynamics in the pipe, although the model could easily be retrained on a different value of τ_z . The target parameters represent the parameters dependent on the varying free parameters, with the relationship between the two sets to be modelled.

Table 3: Target parameters and their corresponding units, recorded at threshold $\tau_z = 30$ mm.

Symbol	Parameter	Units
\mathcal{P}	Transmission Probability	
v	Velocity Magnitude	m/s
θ	Polar Angle	radians
ϕ	Azimuthal Angle	radians
\vec{r}_x	x-Axis Position	mm
\vec{r}_y	y-Axis Position	mm

2.3 Sampling

2.3.1 Cluster Optimisation

Operating AtomECS on the scale required to gain a sufficient number of samples to adequately cover the parameter space requires the use of high-performance computing (HPC) clusters with many instances running in parallel. To operate AtomECS in this manner, the program must be adapted to enforce a thread limit, otherwise it will attempt to exceed the quota defined in the batch request. Within the raw Rust files, Rayon library is added into the cargo.toml file and the number of threads in the pool is limited to 8. For additional libraries, OpenBlas, MKL and OMP, the number of threads is similarly constricted to 8.

2.3.2 Sampling Technique

Using a lower-discrepancy sequence such as Sobol would enable the parameter space to be covered more uniformly than a purely random sequence; Sobol sampling outperforms random sampling by reducing variance, this is particularly valuable when sampling the simulation’s high-dimensional parameter space. Sobol is based on the Van der Corput sequence, a method of generating points by reversing the digits of the sequence index in its binary representation (see Ref. [27]), which is then amplified to multiple dimensions. This is achieved by combining the binary digits of the index with direction vectors that are generated using primitive polynomials over a finite Galois field of order 2 [28].

2.3.3 Sampling Execution

The sampling was executed on the Imperial College London HPC clusters with an array of 500 8 core 4GB memory instances each sampling the simulation in a Sobol Sequence, taking ≈ 22 minutes to complete an individual sample. Each run of the simulation outputs the position and velocity vectors of each atom at each Δt . The sampler processes this data, extracting the vectors of each atom as they pass the thresholds τ_z at increments of 5 mm along the pipe. An additional script compiles and clears any finished instances. In total 2^{19} Sobol distributed variations of θ samples were taken with in total 2.62×10^{12} atoms generated from the atomic oven, 3.88×10^8 vectors recorded for 4.35×10^7 unique atoms. Total computation time $\approx 1 \times 10^7$ minutes or ≈ 20 years spread across up to 500 concurrent samplers. Sampling scripts are open-sourced on [GitHub](#).

3 Normalising Flow Bayesian Inference

To model the atom vectors at the point of transmission (denoted by X , although without including \mathcal{P}) probabilistic machine learning methods are used. This provides a model that captures the uncertainty and variance within the data, providing a probabilistic output rather than a deterministic value - essential for sampling a set of atoms for a given $\boldsymbol{\theta}$. Theory on the deterministic methods used to model \mathcal{P} is available in Appendix A.

3.1 Conditional Normalising Flows

The Kullback-Leibler (KL) divergence [29], provides a measure of how one probability distribution diverges from another. Minimising the KL divergence is equivalent to maximising the likelihood of the observed data under our model, with conditional normalising flows (CNFs) trained to minimise the KL divergence through a series of transformations. For a CNF at iteration t the KL divergence D_{KL} is given by:

$$D_{KL}[p(X|\boldsymbol{\theta}) \parallel p(\hat{X}_t|\boldsymbol{\theta})] = \int_{-\infty}^{\infty} p(X|\boldsymbol{\theta}) \log \frac{p(X|\boldsymbol{\theta})}{p(\hat{X}_t|\boldsymbol{\theta})} dx \quad (13)$$

effectively measuring the expected amount of information lost when approximating $p(X|\boldsymbol{\theta})$ as the model's density $p(\hat{X}_t|\boldsymbol{\theta})$ at iteration t .

Through a series of K bijective transformations $f_{\varphi_1}, \dots, f_{\varphi_K}$ applied to a base distribution $p_0(\mathbf{u})$ (e.g. Figure 7), CNFs [30] model the density of a set of target parameters X dependent on input parameters $\boldsymbol{\theta}$ as an invertible transformation f_φ of a sampled vector \mathbf{u} from $p_0(\mathbf{u})$; i.e. $p_K(\hat{X}|\boldsymbol{\theta}) = f_\varphi(\mathbf{u}, \boldsymbol{\theta})$ where $\mathbf{u} \sim p_0(\mathbf{u})$. The invertible nature of f_φ , and also the differentiability of both f_φ and its inverse f_φ^{-1} , ensures the structure of the probability density is maintained during the transformation from one density $p_{k-1}(\mathbf{z}_{k-1}|\boldsymbol{\theta})$ to another $p_k(\mathbf{z}_k|\boldsymbol{\theta})$ (such that $\mathbf{z}_0 = \mathbf{u}$ and $\mathbf{z}_K = \hat{X}$); the equation for which can be given by the change of variables formula (Ref [31, 32]):

$$p_k(\mathbf{z}_k|\boldsymbol{\theta}) = p_{k-1}(\mathbf{z}_{k-1}|\boldsymbol{\theta}) \left| \det J_{f_{\varphi_k}}(\mathbf{z}_{k-1}, \boldsymbol{\theta}) \right|^{-1} \quad (14)$$

where $J_{f_{\varphi_k}}(\mathbf{z}_{k-1}, \boldsymbol{\theta})$ is the Jacobian - a $D \times D$ matrix of all partial derivatives of $f_{\varphi_k}(\mathbf{z}_{k-1}, \boldsymbol{\theta})$; or alternatively in terms of the Jacobian of $f_{\varphi_k}^{-1}(\mathbf{z}_k, \boldsymbol{\theta})$:

$$p_k(\mathbf{z}_k|\boldsymbol{\theta}) = p_{k-1}(f_{\varphi_k}^{-1}(\mathbf{z}_k|\boldsymbol{\theta})) \left| \det J_{f_{\varphi_k}^{-1}}(\mathbf{z}_k, \boldsymbol{\theta}) \right| \quad (15)$$

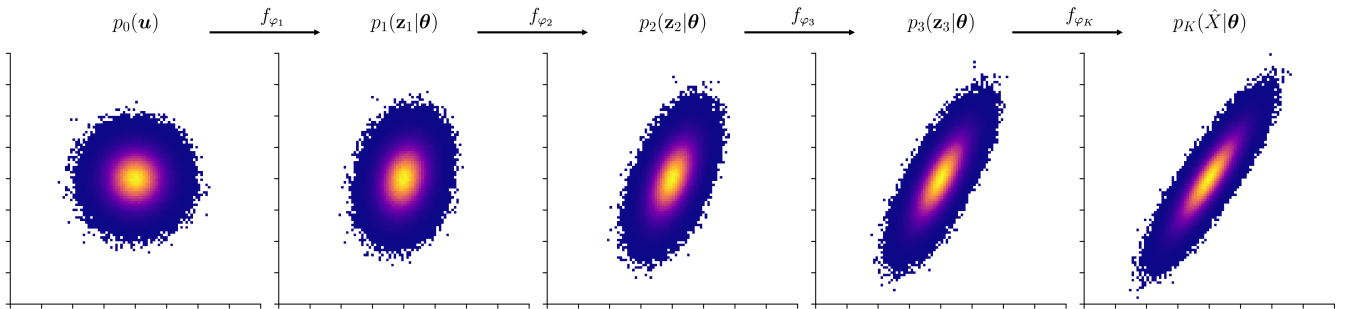


Figure 7: Diagram illustrating a series of hypothetical transformations f_{φ_k} being applied to a base Gaussian distribution $p_0(\mathbf{u})$ to result in a model $p_K(\hat{X}|\boldsymbol{\theta})$.

such that the inverse flow $f_{\varphi_K}^{-1}, \dots, f_{\varphi_1}^{-1}$ enables any point in the target space to be mapped back through to the original sample from the base distribution \mathbf{u} . This traceability allows the model to correctly adjust $p_K(\hat{X}|\boldsymbol{\theta})$ so that the total probability mass remains constant and normalised [33].

Within this framework many styles of transformations for normalising flows have been developed [34–39], typically involving "coupling" [35]. A coupling layer partitions \mathbf{z} into two parts, the "identity" part is unchanged $\mathbf{z}_{\mathbb{I}}$, while the other \mathbf{z}_{f_φ} undergoes a transformation. Splines are a common example of transformation, in which \mathbf{z}_{f_φ} is divided into several intervals, and within each interval a polynomial (often a cubic or quadratic) function is applied - rational splines can also be used in this context, where the transformation is defined as a ratio of two polynomial functions. This transformation is "coupled" based on $\mathbf{z}_{\mathbb{I}}$, i.e. the specific parameters of the spline φ such as the locations and shapes of the segments are parameterised by $\mathbf{z}_{\mathbb{I}}$ [37].

3.2 Data Mollification

By "mollifying" the data, i.e. iteratively reducing Gaussian noise $\epsilon \sim \mathcal{N}(0, I)$ perturbing X , a CNF begins by learning a "smoother" representation of the data, before moving onto a more refined representation where it can capture the intricate details - therefore capturing a more global and realistic representation of the data. The mollified data \tilde{X}_t at iteration t is given by:

$$\tilde{X}_t = \alpha_t X + \sigma_t \epsilon \quad (16)$$

where α_t and σ_t determine the signal-to-noise ratio at t controlled by the noise schedule function $\gamma(t/T)$, given by:

$$\gamma(t/T) = \text{sigmoid}\left(\frac{-t}{\tau \cdot T}\right) \quad (17)$$

where T is the total number of iterations and τ is a constant controlling the steepness of the sigmoid curve. α_t and σ_t are derived from $\gamma(t/T)$ as follows:

$$\sigma_t^2 = \gamma(t/T) \quad (18)$$

$$\alpha_t = \sqrt{1 - \sigma_t^2} \quad (19)$$

As $\gamma(t/T)$ decreases, σ_t decreases, and α_t increases, effectively starting with a high noise level and gradually reducing to zero as the training progresses [40].

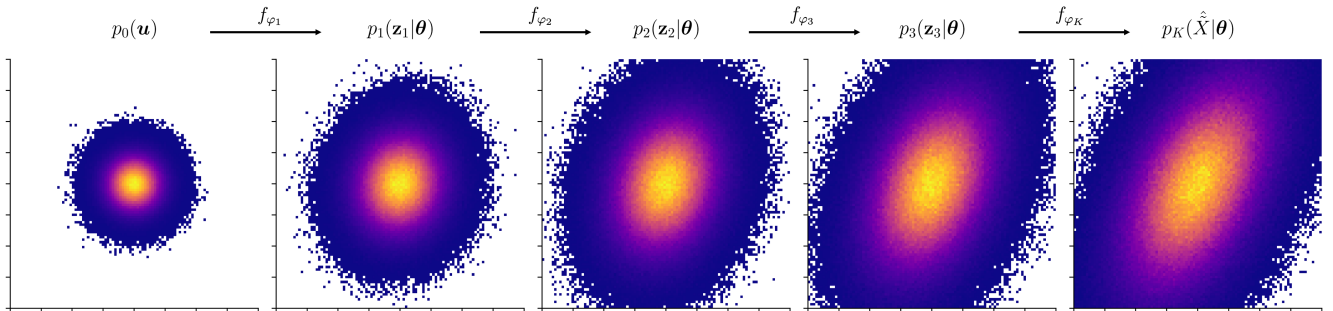


Figure 8: Diagram illustrating a single iteration t such that target distribution $p_K(\hat{X}|\boldsymbol{\theta})$ is perturbed by noise. A series of hypothetical transformations f_{φ_k} are applied to a base Gaussian distribution $p_0(\mathbf{u})$ to result in a model of the perturbed data $p_K(\hat{X}|\boldsymbol{\theta})$.

3.2.1 CNF with Pre-Diffusion

Data mollification in normalising flows, as introduced in (Ref. [40]), deploys a continuous noise reduction process. The application of a learning rate scheduler in this setup would require extensive tuning with the denoising schedule. Early stopping rounds would also be redundant since the denoising schedule is derived from a pre-defined number of epochs T . This paper, however, introduces CNF with Pre-Diffusion (CNF-PD) in which for an initial set of rounds T_ϵ the data is mollified according to schedule $\gamma(t \cdot T_\epsilon^{-1})$, before then a typical CNF training phase with learning rate decay and early stopping rounds. A "pre-diffusion" stage can be introduced to any existing CNF without requiring extensive tuning or adjustment, in contrast to continuous mollification.

4 Diffusion Bayesian Inference

Score matching, as introduced by Hyvärinen (Ref. [41]), is a method to infer the parameters $\boldsymbol{\theta}$ of an unnormalised probability density $q(X|\boldsymbol{\theta})$. In many statistical or machine learning models, the density $p(X|\boldsymbol{\theta})$ is often given in terms of a multiplicative normalisation constant $Z(\boldsymbol{\theta})$ such that:

$$p(X|\boldsymbol{\theta}) = \frac{q(X|\boldsymbol{\theta})}{Z(\boldsymbol{\theta})} \quad (20)$$

where $Z(\boldsymbol{\theta})$ is given by an often analytically intractable integral:

$$Z(\boldsymbol{\theta}) = \int_{X \in \mathbb{R}^n} q(X|\boldsymbol{\theta}) dX \quad (21)$$

making direct computation of the probability density challenging and practically impossible for higher dimensions.

Score matching minimises the expected square distance between the gradient of the log probability density $\nabla_X \log p(X)$ of the data X and the model's prediction of the log density gradient with respect to $\boldsymbol{\theta}$, i.e. the model's prediction of $\nabla_X \log p(X|\boldsymbol{\theta})$. Since $Z(\boldsymbol{\theta})$ is constant with respect to X , it drops out when differentiating, the objective function $J(\boldsymbol{\theta})$ is therefore not dependent on $Z(\boldsymbol{\theta})$:

$$J(\boldsymbol{\theta}) = \frac{1}{2} \int_{X \in \mathbb{R}^n} p_X(X) \|\psi(X; \boldsymbol{\theta}) - \nabla_X \log p(X)\|^2 dX \quad (22)$$

such that the estimator of $\boldsymbol{\theta}$ is given by $\hat{\boldsymbol{\theta}} = \arg \min_{\boldsymbol{\theta}} J(\boldsymbol{\theta})$. Assuming differentiability, through partial integration $J(\boldsymbol{\theta})$ can be expressed without the non-normalised model (full derivation given in Appendix B.1):

$$J(\boldsymbol{\theta}) = \int_{X \in \mathbb{R}^n} p_X(X) \sum_{i=1}^n \left[\frac{\partial \psi_i(X; \boldsymbol{\theta})}{\partial X_i} + \frac{1}{2} \psi_i(X; \boldsymbol{\theta})^2 \right] dX + \text{const.} \quad (23)$$

In practice, the integral over the data distribution $p_X(X)$ is often approximated by an empirical expectation over the observed data. This gives the empirical version of the objective function:

$$\tilde{J}(\boldsymbol{\theta}) = \mathbb{E}_{X \sim p_X} \left[\sum_{i=1}^n \left(\frac{\partial \psi_i(X; \boldsymbol{\theta})}{\partial X_i} + \frac{1}{2} \psi_i(X; \boldsymbol{\theta})^2 \right) \right] + \text{const.} \quad (24)$$

Upon reformulating the objective function, $J(\boldsymbol{\theta})$ now includes the derivative of $\psi_i(X; \boldsymbol{\theta})$, effectively the model's approximation of the i -th diagonal component of the Hessian matrix $\nabla_X^2 \log p(X)$. The summation of each of these points gives the model's approximation $\text{Trace}(\nabla_X \psi(X; \boldsymbol{\theta}))$ of the trace of the Hessian $\text{Trace}(\nabla_X^2 \log p(X))$, a measure of the total curvature of the log-density with respect to X across all dimensions. $\tilde{J}(\boldsymbol{\theta})$ can therefore be represented as:

$$\tilde{J}(\boldsymbol{\theta}) = \mathbb{E}_{X \sim p_X} \left[\text{Trace}(\nabla_X \psi(X; \boldsymbol{\theta})) + \sum_{i=1}^n \left(\frac{1}{2} \psi_i(X; \boldsymbol{\theta})^2 \right) \right] + \text{const.} \quad (25)$$

Although a product of the reformulation, this 2nd order term penalises large score functions values and stabilises the model. When averaged over the data distribution, this term ensures that the model's parameters $\boldsymbol{\theta}$ are adjusted to match the empirical distribution as closely as possible [41].

While Hyvärinen score matching aims to minimise an objective function to infer model parameters $\boldsymbol{\theta}$, diffusion uses the concept of score matching to infer the parameters φ of a neural network (i.e., weights and biases); therefore modelling the underlying distribution $p(X|\boldsymbol{\theta})$. Diffusion involves both a forward and reverse process (Figure 9). In the forward process, Gaussian noise is iteratively added to X until the distribution is indistinguishable from complete Gaussian noise, transforming a complex distribution into a more simple one. The forward process may be modelled by an Itô stochastic differential equation as follows:

$$dX_t = \mu(X_t, t)dt + \sigma(t)dW_t \quad (26)$$

where $\mu(X_t, t)$ represents the drift coefficient that models the deterministic part of the process, $\sigma(t)$ is the diffusion coefficient that scales the noise, and dW_t denotes the differential of a Wiener process (or Brownian motion), which introduces the stochastic component.

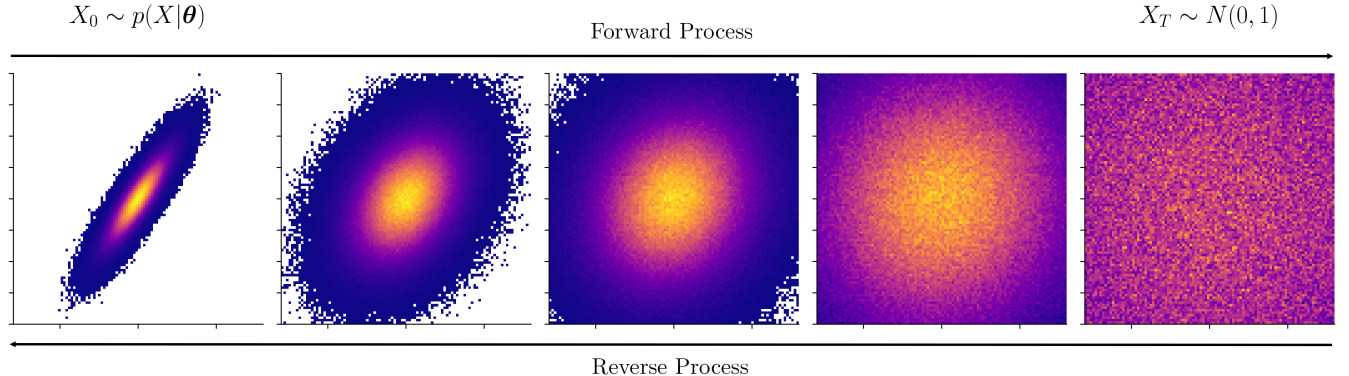


Figure 9: Diagram illustrating a hypothetical diffusion process involving: the forward process - noise is iteratively added to the target distribution $X_0 \sim p(X|\boldsymbol{\theta})$ resulting in Gaussian noise $X_T \sim N(0, 1)$; and the reverse score-matching process where the distribution is iteratively denoised.

Conversely, the reverse process involves gradually removing the noise, aiming to recover the original data distribution from the noisy observations. The score function $\psi_\varphi(\hat{X}_t, t)$ approximates the gradient of the log probability density $\nabla_{\hat{X}_t} \log p_t(\hat{X}_t | \hat{X}_0)$ of the noisy data \hat{X}_t given the clean data \hat{X}_0 at each time-step t . A neural network is trained (see Appendix A.2 for theory) to minimise the discrepancy between the model's approximation and the true gradient, with the loss function given as:

$$L(\varphi) = \mathbb{E}_{t, \hat{X}_0, \hat{X}_t} \left[\lambda(t) \left\| \psi_\varphi(\hat{X}_t, t) - \nabla_{\hat{X}_t} \log p_t(\hat{X}_t | \hat{X}_0) \right\|_2^2 \right] \quad (27)$$

where $\lambda(t)$ is a weighting function that adjusts the contribution of each time-step to the loss.

With a model trained on the reverse process, samples can then be generated by recreating that reverse process. Starting with $X_T \sim N(0, 1)$ (a sample drawn from pure Gaussian noise), the model iteratively denoises this sample by stepping backwards through time. At each step t , the trained neural network estimates the $\psi_\varphi(\hat{X}_t, t)$, guiding sample generation towards regions of high probability. After iterating to $t = 0$, the resulting X_0 represents a sample from the learned data distribution [41].

4.1 1st Order Diffusion Bayesian Inference

By integrating a transformer attention mechanism into a diffusion model, MackeLab's Simformer (see Ref. [42]) model encodes dependencies on parameters θ within the diffusion process. The condition state $M_C \in \{0, 1\}^d$ is a binary variable that determines whether each $(X, \theta) \in \mathbb{R}^d$ pair at each iteration is conditioned. The attention mask M_A is learnt throughout training and influences the attention score \mathcal{A} by modulating the importance assigned to each variable. The attention mechanism, given by:

$$\mathcal{A}(Q, K, V) = \sum \text{softmax} \left(\frac{QK^\top}{\sqrt{d_k}} + M_A \right) V \quad (28)$$

computes weighted sums of input values V based on the similarity between query Q and key K vector pairs derived from the input data, quantified by the dot product over the dimensionality d_k . This is then adjusted by M_A , representing the learnt importance of the relationship between Q and K [43]. Accounting for conditioning, the loss function can be represented as:

$$L_1(\varphi) = \mathbb{E}_{M_A, M_C, t, \hat{X}_0, \hat{X}_t} \left[\lambda(t) \left\| (1 - M_C) \cdot \left[\psi_\varphi^{\mathcal{A}}(\hat{X}_t^{M_C}, t) - \nabla_{\hat{X}_t} \log p_t(\hat{X}_t | \hat{X}_0) \right] \right\|_2^2 \right] \quad (29)$$

[42] however, for simplicity the role of conditioning may be simply denoted by super-script \mathcal{A} :

$$L_1(\varphi) = \mathbb{E}_{t, \hat{X}_0, \hat{X}_t} \left[\lambda(t) \left\| \psi_\varphi^{\mathcal{A}}(\hat{X}_t, t) - \nabla_{\hat{X}_t} \log p_t(\hat{X}_t | \hat{X}_0) \right\|_2^2 \right] \quad (30)$$

4.2 2nd Order Diffusion Bayesian Inference

Although Hyvärinen score matching reformulates the objective function $J(\theta)$, it does introduce the trace of the Hessian, as shown in Equation (25). In reality this is highly computationally expensive to compute, however the application of Hutchinson's estimator has been found to be an efficient substitute [44].

Hutchinson's estimator [45] estimates the trace of the hessian matrix H , given by:

$$\text{Trace}(H) = \mathbb{E}_\epsilon [\epsilon^T H \epsilon] \quad (31)$$

through the use of a stochastic approximation:

$$\text{Trace}(H) \approx \mathbb{E}_\epsilon [\epsilon^T (f(X + \epsilon) - f(X))] \quad (32)$$

effectively perturbing the data with random noise ϵ sampled from a distribution (often Gaussian) to provide an estimate of the curvature of the loss landscape, without the need to calculate the full Hessian.

So called 1st order diffusion models include only approximations of the first order gradient, however within other domains such as image super-resolution [46] 2nd order information has been incorporated into the loss function resulting in more realistic sample generation. By incorporating 2nd order information into diffusion models, information on the curvature of the log-probability density function is introduced. In theory this should lead to a more global representation of the underlying distribution, rather than overfitting to local optima.

This paper introduces 2nd order diffusion Bayesian inference (2ODBI), a Bayesian inference model which incorporates 2nd order information into the loss function by approximating the trace of the Hessian through Hutchinson's estimator. In this instance a Rademacher distribution [47, 48] was chosen due to reduced computational complexity, with the sampled noise added to the representation at t and the expectation found naturally through stochastic averaging in the batch processing; in the same manner as the expectation in the standard loss function (Equation 30).

The trace of the hessian for the model's prediction of the gradient of log probability density at iteration t can be estimated by:

$$\text{Trace}(\nabla\psi_{\varphi}^{\mathcal{A}}(\hat{X}_t, t)) \approx \mathbb{E}_{\epsilon} \left[\epsilon^T (\psi_{\varphi}^{\mathcal{A}}(\hat{X}_t + \epsilon, t) - \psi_{\varphi}^{\mathcal{A}}(\hat{X}_t, t)) \right] \quad (33)$$

by including this approximation the loss function becomes:

$$L_2(\varphi) = \mathbb{E}_{t, \hat{X}_0, \hat{X}_t} \left[\lambda(t) \left\| \psi_{\varphi}^{\mathcal{A}}(\hat{X}_t, t) - \nabla_{\hat{X}_t} \log p_t(\hat{X}_t | \hat{X}_0) \right\|_2^2 \right] + \gamma \mathbb{E}_{\epsilon} \left[\epsilon^T (\psi_{\varphi}^{\mathcal{A}}(\hat{X}_t + \epsilon, t) - \psi_{\varphi}^{\mathcal{A}}(\hat{X}_t, t)) \right] \quad (34)$$

where γ is the 2nd order coefficient, controlling the contribution of the 2nd order information to the loss function.

5 Results

The unified model AION 2D MOT model is factorised into two subsections, an initial model that predicts \mathcal{P} for a given θ , and a further probabilistic model that generates a number of remaining target parameters X equal to a defined N_{atoms} multiplied by \mathcal{P} as predicted by the first model. The models in this subsection were trained on data taken at a $\tau_z = 30$ mm, with the pipe radius extended to 7.85 mm. By significantly increasing the proportion of atoms recorded, there is a significant increase in the data available for the model to be trained on. By clipping samples generated by the unified model, values of r_{pipe} and d_{pipe} may be chosen retrospectively, whilst also not limiting the training of the model. For each model, the features were normalised and data split into train, test and validation (70%, 15% and 15% of the dataset respectively). Each model is open sourced and available on [GitHub](#).

5.1 Predicting Transmission Probability

To model \mathcal{P} , a boosted decision tree (BDT) [49] and a deep neural network (DNN) [50] were chosen due to their capability to capture complex relationships in large datasets. Theory on these models is available in Appendix A.

5.1.1 Training

The BDT regression model was trained using the XGBoost Python library (Ref. [51]) with the objective to minimise the root mean squared error (RMSE). The model was tuned into a deep but regularised model that captures deep relationships between the parameters whilst also being conservative when it comes to splitting into a new leaf [49]. The full hyperparameters are denoted in Table 8:

Table 4: *BDT model hyperparameters.*

Hyperparameter
Learning Rate: 0.01
Max Depth: 12
L1 Regularisation: 3
Early Stopping: 20 rounds

Model optimisation was benchmarked against a "vanilla" model of 6 max-depth and no regularisation, the comparison of their loss curves is shown in Figure 10:

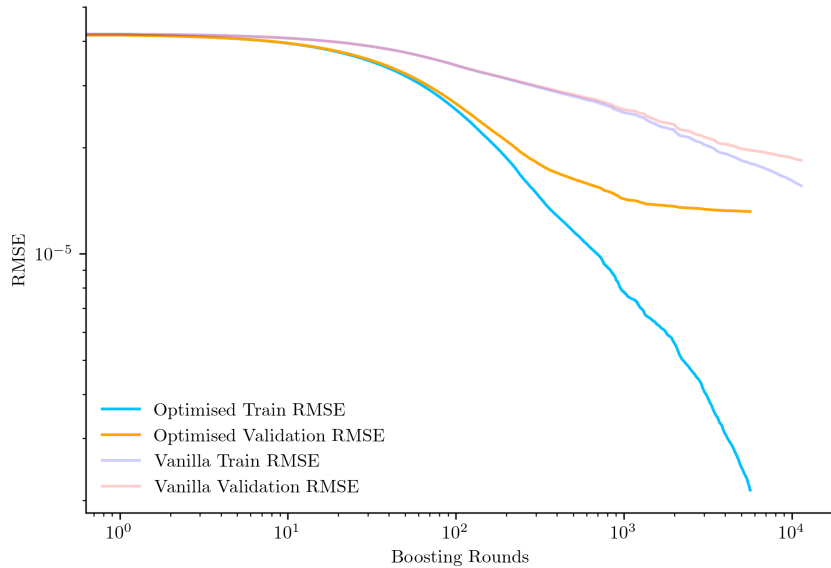


Figure 10: *BDT RMSE loss curve; demonstrating the "optimised" loss (max depth = 12 and L1 = 3), to a "vanilla" model (max depth = 6 and L1 = 0).*

The DNN model was built using PyTorch (Ref. [52]) in Python, with the objective to minimise the mean squared error (MSE) (within results and figures the RMSE is shown for parity). The model architecture and hyperparameters are tabulated in Table 5:

Table 5: DNN architecture and hyperparameters.

Component	Parameters
Model Architecture	Input Layer: 9 neurons Hidden Layers: 3 (ReLU activation) - Layer 1: 128 neurons - Layer 2: 64 neurons - Layer 3: 32 neurons Output Layer: 1 neuron
Training	Optimiser: L-BFGS Learning Rate: 0.1 Max Iterations: 20 History Size: 20 Early Stopping: 10 epochs

An L-BFGS (Ref. [53]) optimiser was found to be marginally superior to an Adam optimiser model with a learning rate of 10^{-3} and exponential decay scheduler with gamma = 0.95. The loss curves of each are shown in Figure 11.

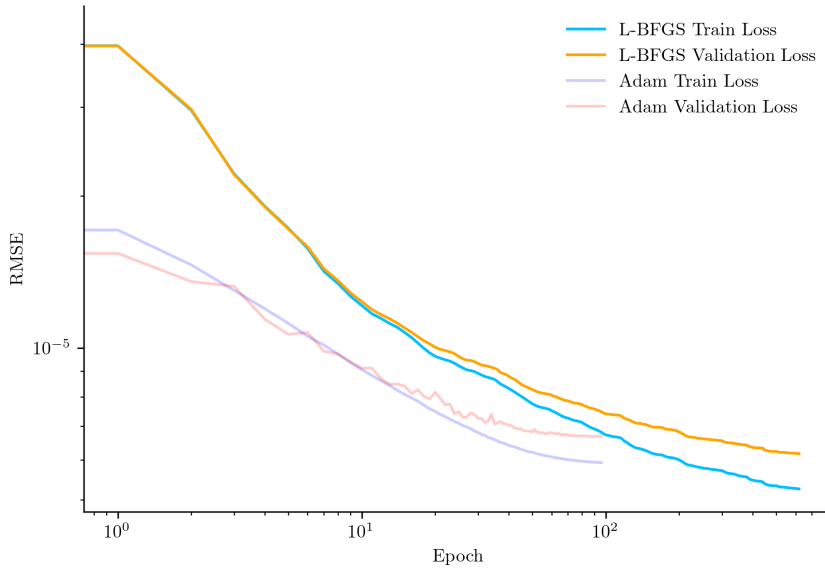


Figure 11: DNN RMSE loss curve; demonstrating the loss comparison of a model trained with L-BFGS and Adam optimisers respectively.

5.1.2 Evaluation

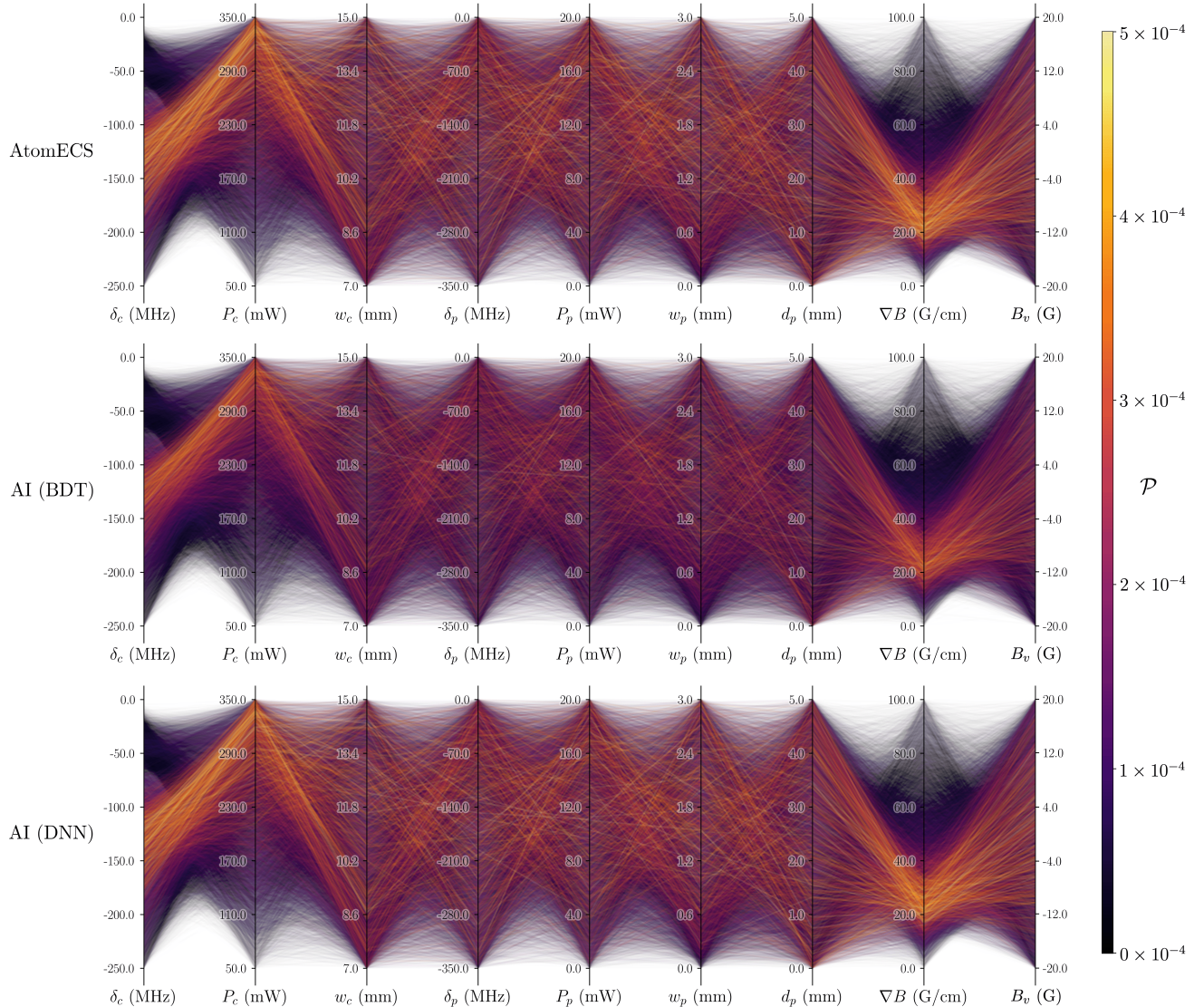


Figure 12: Parallel co-ordinate plots of the ground-truth (GT) unseen test data and predicted boosted decision tree (BDT) and deep neural network (DNN) values of \mathcal{P} (for 3.5×10^4 random samples). Colour coded based on \mathcal{P} , colour scaling capped at 5×10^{-4} .

From qualitative comparison (Figure 12), the DNN appears to very accurately capture the complex relationships between the θ and \mathcal{P} , including making accurate predictions of high values. The BDT on the other hand, appears to be much more conservative in its predictions and therefore fails to accurately capture the complex relationships that lead to high values of \mathcal{P} . This is further supported by the histogram of \mathcal{P} values predicted versus the ground-truth (GT) (Figure 13), which shows that the BDT fails to replicate the tail-end of the distribution. From the bin ratio segment of the figure, it's apparent that the BDT is also over-confident in predictions with significant residuals, whereas the DNN is capable of providing appropriate uncertainty in these bins.

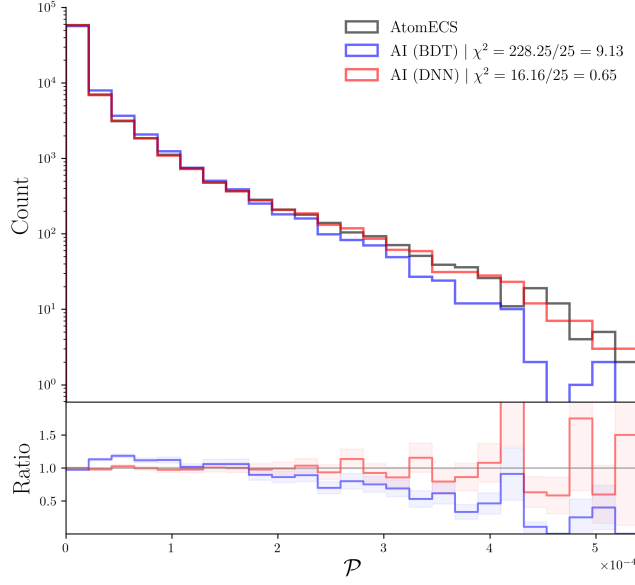


Figure 13: Histogram and bin ratio plot of the ground-truth (GT) unseen test data and predicted boosted decision tree (BDT) and deep neural network (DNN) values of \mathcal{P} . Shaded areas on the ratio plot represent prediction uncertainty.

The DNN quantitatively outperforms the BDT in terms of both the overall error and the proportion of variance explained by the model (RMSE and R^2 score; Table 6). Despite the BDT being tuned to capture deeper relationships without over-fitting, BDTs are typically more conservative in their predictions due to prioritising minimising the error in the majority of data points in their iterative correction process - therefore neglecting the rare extreme values. DNNs on the other-hand learn a global approximation from the entire dataset, therefore more accurately representing the full distribution.

Table 6: Comparison of RMSE, R^2 , and χ^2 values (as in Figure 13) for BDT and DNN models.

Model	RMSE ↓	$R^2 \uparrow$	$\chi^2 \downarrow$
BDT (Optimised)	1.33×10^{-5}	0.901	9.13
DNN (L-BFGS)	6.14×10^{-6}	0.979	0.65
BDT (Vanilla)	1.84×10^{-5}	0.809	35.45
DNN (Adam)	6.40×10^{-6}	0.977	0.76

Inaccurate tail-end predictions would likely lead to poor exploration strategies by a RL agent, with the agent unlikely to explore high-probability transmission scenarios due to the distorted reward landscape - therefore less likely to adapt well following domain transfer. The DNN however is mostly successful in mitigating these potential issues by accurately capturing the breadth of the distribution. The DNN also captures uncertainty more effectively than the BDT, which could potentially be weighted into an RL agent's learning process.

5.2 Modelling Vector Distributions

The remaining target parameters (denoted by X , however now excluding \mathcal{P}) will be modelled through the use of Bayesian inference methods. This provides a model that captures the uncertainty

and variance within the data, providing a probabilistic output rather than a deterministic value.

5.2.1 Initial Model

An initial CNF model using the NormFlows (Ref [54]) Python library was developed with architecture and hyperparameters defined in Table 7:

Table 7: *CNF architecture and hyperparameters.*

Component	Parameters
Flow Architecture	Transformations: 4 Type: Coupled Rational Quadratic Spline Base Distribution: Diagonal Gaussian
Neural Architecture	Hidden Layers: 4 Units per Layer: 128
Training	Batch Size: 128 Loss Function: Kullback-Leibler Divergence (KLD) Early Stopping: 5 epochs
Optimiser	Type: AdamW Initial Learning Rate: 10^{-3} Weight Decay: 10^{-5}
Learning Rate Schedule	Type: Exponential Decay Decay Factor: 0.96 per epoch

A dataset of 10^6 randomly chosen sets of vectors across all simulations was used to reduce computational load to feasible levels. The model was trained on transform $\ln(1 + v)$ rather than v . This transforms the target distribution closer to a Gaussian, making the CNF transformations much more simple to learn and drastically improving the training. This transformation is reversed during sampling. The loss curve for the CNF is shown in Figure 14:

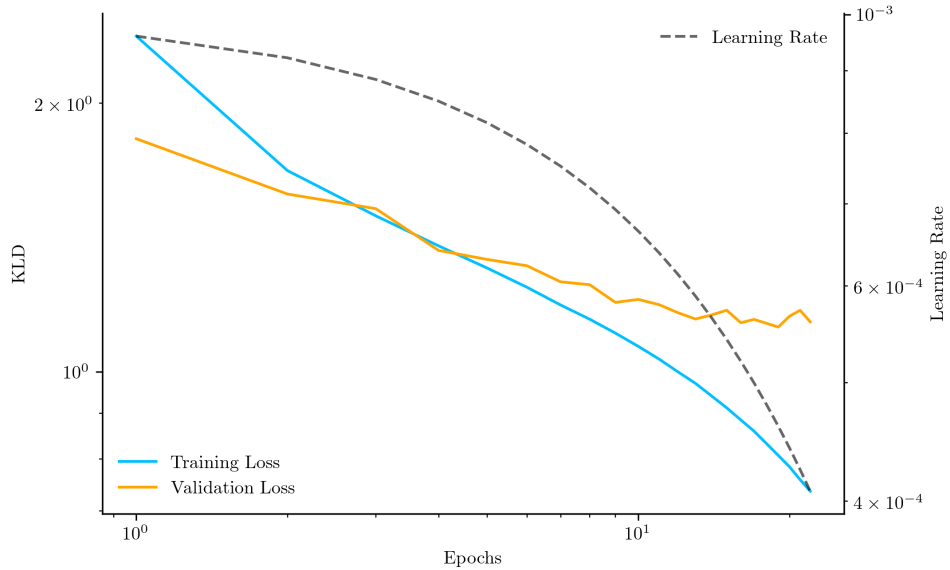


Figure 14: *Initial CNF model KLD loss curve with learning rate.*

Although θ for each simulation was sampled from a Sobol sequence (as described in Section 2.3.2), Figure 12 shows that varying areas of the parameter space result in drastically varying quantities of atoms transmitted, and therefore vectors to train a Bayesian inference model on. The variance in density of the parameter space can often lead to significant problems in training, notably manifold overfitting. Machine learning models typically represent high-dimensional data distributions as low-dimensional manifolds embedded in a high-dimensional space; however, the true underlying distribution may not be confined to this manifold. Manifold overfitting occurs when the model’s posterior distribution over parameters concentrates too strongly around values that fit the observed data manifold, rather than capturing the full underlying distribution. In regions where the data is sparse, the model may extrapolate the manifold structure from denser regions, leading to poor fit and unreliable predictions. This leads to an unrealistic representation of the underlying distribution, hampering statistical inference or optimisation methods including the pre-training of an RL agent.

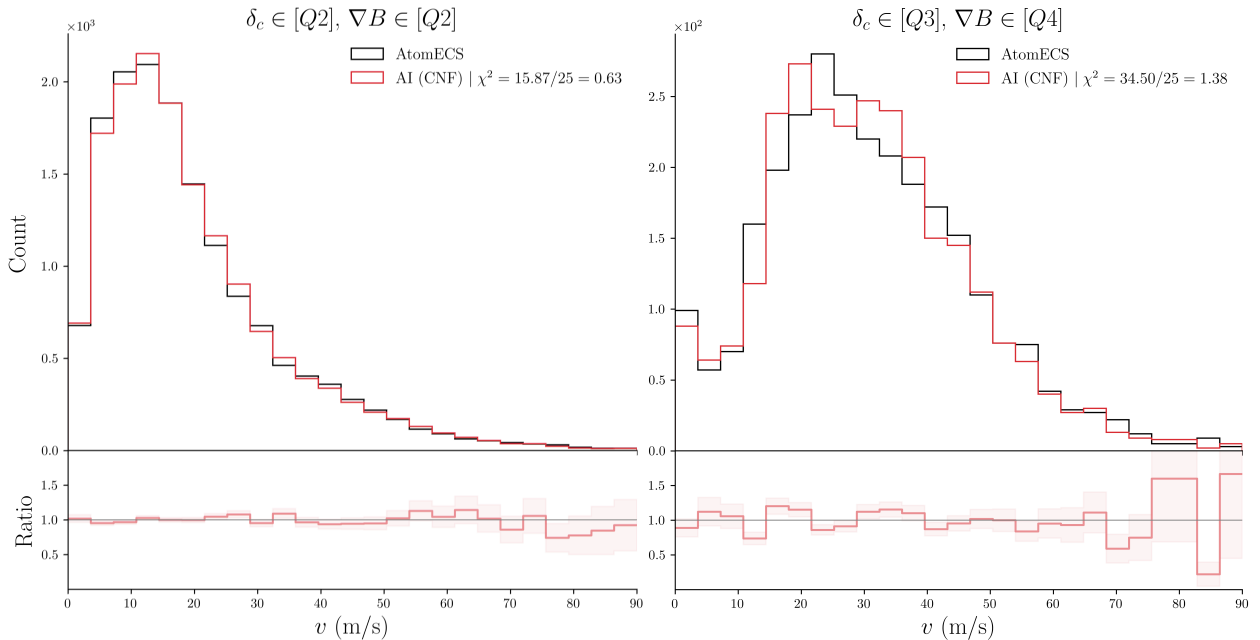


Figure 15: An area of high density $\delta_c \in [Q2], \nabla B \in [Q2]$ (left), compared with manifold overfitting in an area of low density $\delta_c \in [Q3], \nabla B \in [Q4]$ (right); $[Qn]$ denotes the n th quartile of the parameter’s range of values as defined in Section 2.2.2.

5.2.2 Adaptive Sampling

To mitigate the skew in the parameter space as a result of varying values of \mathcal{P} , an adaptive sampling (AS) algorithm is introduced to bolster sparse areas of the data distribution whilst still respecting the natural distribution of the parameter space. This prevents manifold overfitting to the sparse areas whilst still ensuring the model focuses learning resources on the high-density areas, since these are likely to produce the best results for AION. The AS algorithm takes an initial “slice” of the dataset, before counting the number of vectors for each unique simulation and the proportion of vectors each simulation represents in the total slice. For the target data size (10^6 vectors), it calculates a proportional sample size based on its representation in the full dataset. Rows from each simulation are sampled based on the calculated proportion with a minimum of 20

and maximum of 500 per simulation. The result (shown in Figure 16) is a more balanced dataset that does not entirely distort the natural underlying distribution.

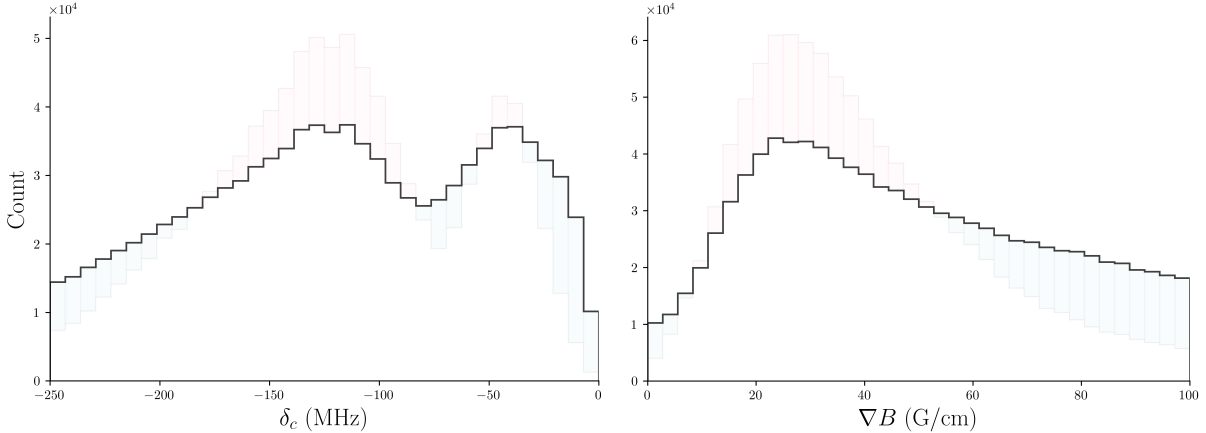


Figure 16: Histograms demonstrating the rebalancing of the distributions of δ_c (left) and ∇B (right) through AS. Blue/red shading represents an increase/decrease in sample density from the natural distribution.

5.2.3 CNF with Pre-Diffusion

By adding Gaussian noise to the data, mollification effectively "blurs" or smooths the manifold structure, preventing the model from fitting too tightly to the specific details. Throughout training the noise level is gradually reduced, forcing the model to initially learn broader, more general features first. As noise decreases, the model gradually refines its understanding. The changing noise levels ensures the model explores a wider range of possible parameter configurations, rather than getting stuck in poor local optima that might result from overfitting to the manifold.

Data mollification in CNFs as introduced in Ref. [40] deploys a continuous denoising process and found $\tau = 0.7$ to be optimal. The application of a learning rate scheduler in this setup would require extensive tuning with the denoising schedule. Early stopping rounds would also be redundant since the denoising schedule is derived from a pre-defined number of epochs T . Through tuning and experimentation with the values of τ and T , an extensive number of epochs would be required to capture the distribution of the AtomECS simulated data to the same degree as the initial CNF model. CNF-PD mitigates these issues through an initial "diffusion" stage where the data is denoised with a static learning rate for a number of epochs T_ϵ , followed by a typical CNF training process with a learning rate scheduler and early stopping rounds.

A CNF-PD model with a pre-diffusion stage $T_\epsilon = 10$ epochs and $\tau = 0.7$ was trained on both the natural distribution and AS data. After the pre-diffusion stage, exponential decay of the learning rate begins by a factor of 0.98 per epoch. The specifications otherwise were the same as for the initial model in Section 5.2.1. In Figure 17, the training for the CNF-PD is compared to a mollified CNF with $T = 100$ epochs and $\tau = 0.7$ with otherwise the same architecture. The continuous mollification model fails to capture the distribution within the set number of epochs. Compared to an almost equivalent standard CNF loss curve (Figure 14), training with CNF-PD is significantly smoother, suggesting it may be effective at mitigating manifold overfitting.

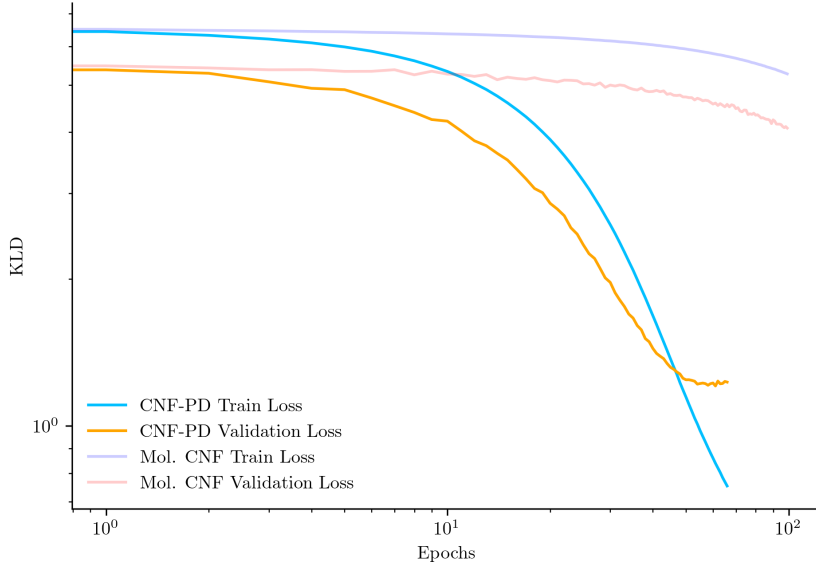


Figure 17: *CNF-PD loss curve T_ϵ compared with standard mollification $T = 100$, each trained with adaptive sampling.*

5.2.4 Diffusion Bayesian Inference

Whereas CNFs involve a series of discrete invertible transformations applied to a base distribution, diffusion models learn to denoise data gradually. This allows for "hierarchical" learning, where the model initially learns high-level features before the finer details - therefore preventing overfitting to the training data manifold. Similarly, transformers excel at capturing "long-range" dependencies in the data, which could help in learning global structure rather than overfitting to local optima in the data manifold. The application of a diffusion model could therefore address the issues with the initial model and provide a deeper representation of the relationships in the parameter space. The chosen model architecture and hyperparameters (Table 8) aim to capture deep relationships within the data, whilst also not being unnecessarily computationally intensive.

By incorporating 2nd order information into the loss function, 2ODBI aims to "ground" the training of the model to realistic approximations of the score function. In theory, the result would be the prevention of manifold overfitting and a more "global" and realistic representation of the underlying distribution, however even with a reasonably complex structure 1ODBI isn't prone to overfitting to this dataset (as shown in Figure 18). 2ODBI is a novel and experimental method of Bayesian inference, the full possibilities are therefore yet to be explored. On toy data, e.g. the SLCP example shown in Appendix B.2, 2ODBI has demonstrated a significant regularisation effect on an otherwise overfit model. 2ODBI is a method that requires deeper testing and analysis to understand fully, perhaps there are strategies involving a low learning rate and the 2nd order term that lead to optimal results - however, it's impossible to judge any kind of impact, at least solely from the loss curve for this study.

Table 8: Diffusion Bayesian inference model architecture and hyperparameters.

Component	Parameters
Model Structure	Dimension Value: 64 Dimension ID 64: Dimension Condition: 32
Transformer Architecture	Number of Heads: 4 Number of Layers: 4 Attention Size: 32 Widening Factor: 4
Diffusion Process (VESDE)	T: 1.0 T min: 10^{-2} Sigma min: 10^{-3} Sigma max: 32.0
Training	Epochs: 100 Steps per Epoch: 5000 Batch Size: 2048
Optimiser	Adam Optimiser Gradient Clipping Norm: 1.0
Learning Rate (LR) Schedule	Linear Warm-Up \rightarrow Cosine Decay Initial LR: 10^{-4} Peak LR: 10^{-3} Warm-Up Steps: 10000

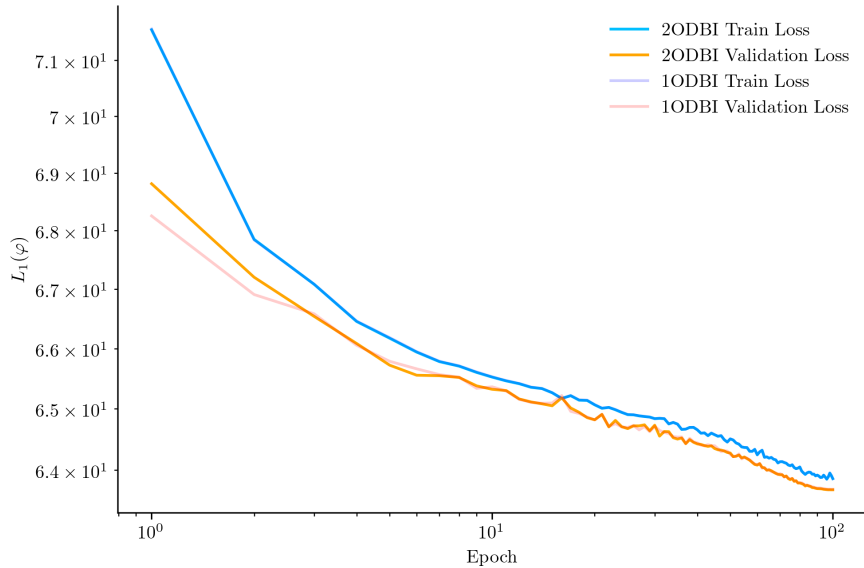


Figure 18: Diffusion Bayesian inference (Simformer) loss curve, showing the original model (1ODBI) and the inclusion of 2nd order information in the loss function (2ODBI) with $\gamma = 10^{-4}$. Although trained using $L_2(\varphi)$, the loss shown for 2ODBI excludes the 2nd order term for parity with 1ODBI.

5.2.5 Evaluation

The following metrics were chosen to give a holistic and balanced overview of the performance of each model: the negative log-likelihood (NLL) a general measure of how well the model fits the AtomECS data [55], perplexity a multiplicative transformation of the NLL - therefore sensitive to extreme residuals [56], Wasserstein-2 the geometric distance between distributions - or "work" required to transform one to another [57], and C2ST the distinguishability of the predicted data from the ground-truth [58, 59]. For C2ST, the AtomECS and model data was merged and a random forest binary classifier with 100 estimators was applied trained with the aim of distinguishing between the two sets of data. The C2ST score shown in Table 9 represents the accuracy score of the classification model. KLD was neglected due to potential bias introduced by being used as the loss function for the CNF models.

Table 9: Comparison of the NLL, perplexity, Wasserstein-2 and C2ST values for each model trained on both the natural distribution and an AS sampled dataset.

Data	Model	NLL ↓	Perplexity ↓	Wasserstein-2 ↓	C2ST ↓
Natural	CNF	11.4363	1.0793	0.5743	0.5082
Natural	CNF-PD	11.4354	1.0785	0.5748	0.5077
Natural	1ODBI	11.4336	1.0903	0.5747	0.5229
Natural	2ODBI	11.4336	1.0893	0.5744	0.5266
Adaptive	CNF	11.5695	1.0841	0.5791	0.5137
Adaptive	CNF-PD	11.5695	1.0841	0.5723	0.5082
Adaptive	1ODBI	11.5685	1.0956	0.5711	0.5000
Adaptive	2ODBI	11.5684	1.0956	0.5714	0.5004

Seemingly, the AS on the whole had either a neutral or negative impact on each model. However, due to the significant imbalance of the natural distribution these models may instead be heavily biased towards high density regions, therefore minimising loss without giving a global representation of the parameter space. From the metrics shown, there is no significant distinction between 1ODBI and 2ODBI, although both models trained on the adaptive dataset were near indistinguishable from AtomECS by the classifier. The lower NLL but higher perplexity score suggests however that although the diffusion models were on average a better representation of AtomECS, there were more significant outliers within the predictions - perplexity being a multiplicative metric compared to additive NLL. In order to deeply analyse the impact of these models on manifold overfitting, each input parameter was divided into quartiles [Q_n] based on their range as defined in Section 2.2.2. Figure 19 shows histograms/box-plots of the χ^2 values calculated for each permutation of quartiles, with the full set of values available in Appendix C.

The effect of the "pre-diffusion" stage on the CNF is immediately apparent from Figure 19, causing a highly significant shift in the distribution of χ^2 values across the parameter space - suggesting the introduction of the "pre-diffusion" stage to be highly effective in mitigating manifold overfitting. The use of adaptive sampling also had a significant impact on the CNF, reducing manifold overfitting fairly although not as effectively as the introduction of the "pre-diffusion" stage. Curiously, CNF-PD seemed to be less prone to manifold overfitting on the natural distribution as opposed to the adaptive sampling dataset, with less outliers also. Table 10 shows that 2ODBI has a marginally lower mean χ^2 and each quartile than 1ODBI, however not to the point of major significance. 2ODBI was however able to achieve a significantly lower χ^2 value in certain select areas of the parameter space, including a significantly lower minimum. The maximum χ^2

for 2ODBI is also higher than 1ODBI, suggesting a higher range in modelling efficacy based on area of the parameter space.

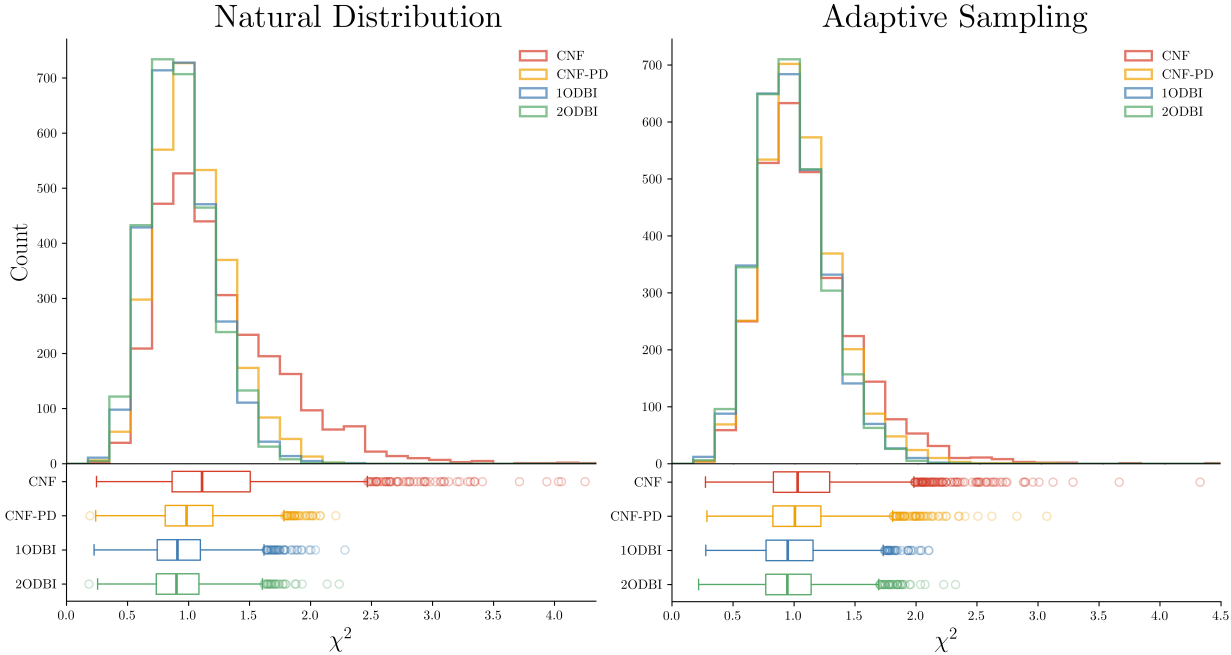


Figure 19: χ^2 histograms and box plots for each model trained on the natural distribution (left) and AS sampled data (right).

Table 10: χ^2 distribution statistics. Q_{25} , Q_{50} and Q_{75} represent the box plot boundaries (25th percentile, median and 75th percentile respectively).

Data	Model	μ_{χ^2}	σ_{χ^2}	Min	Q_{25}	Q_{50}	Q_{75}	Max
Natural	CNF	1.2295	0.5028	0.2461	0.8652	1.1105	1.5066	4.2493
Natural	CNF-PD	1.0177	0.2950	0.1922	0.8097	0.9841	1.1997	2.2068
Natural	1ODBI	0.9334	0.2684	0.2257	0.7437	0.9090	1.0978	2.2820
Natural	2ODBI	0.9255	0.2658	0.1832	0.7362	0.9013	1.0863	2.3343
Adaptive	CNF	1.1014	0.3987	0.2741	0.8320	1.0292	1.2925	4.3282
Adaptive	CNF-PD	1.0433	0.3169	0.2864	0.8281	1.0075	1.2206	3.0718
Adaptive	1ODBI	0.9778	0.2886	0.2778	0.7714	0.9476	1.1564	2.1058
Adaptive	2ODBI	0.9727	0.2840	0.2188	0.7683	0.9452	1.1409	2.3238

By bolstering samples taken from simulations that transmit fewer atoms, the distribution of certain areas of the parameter space can be reshaped significantly, an extreme example shown in *row 1* of Figure 20. This can prevent manifold overfitting in areas of low density, however could potentially introduce bias itself due to the distortion of the underlying distribution. Figure 20 illustrates examples of the CNF performing better on the adaptive data compared to the natural distribution, and also the significant impact of CNF-PD in preventing manifold overfitting in areas of low density. However when these areas are rebalanced through adaptive sampling, CNF-PD performs significantly worse than on the natural distribution. 1ODBI in each of these examples provide generally a better fit to the data than the CNF models, the performance of 2ODBI compared to other models seems to fluctuate quite heavily.

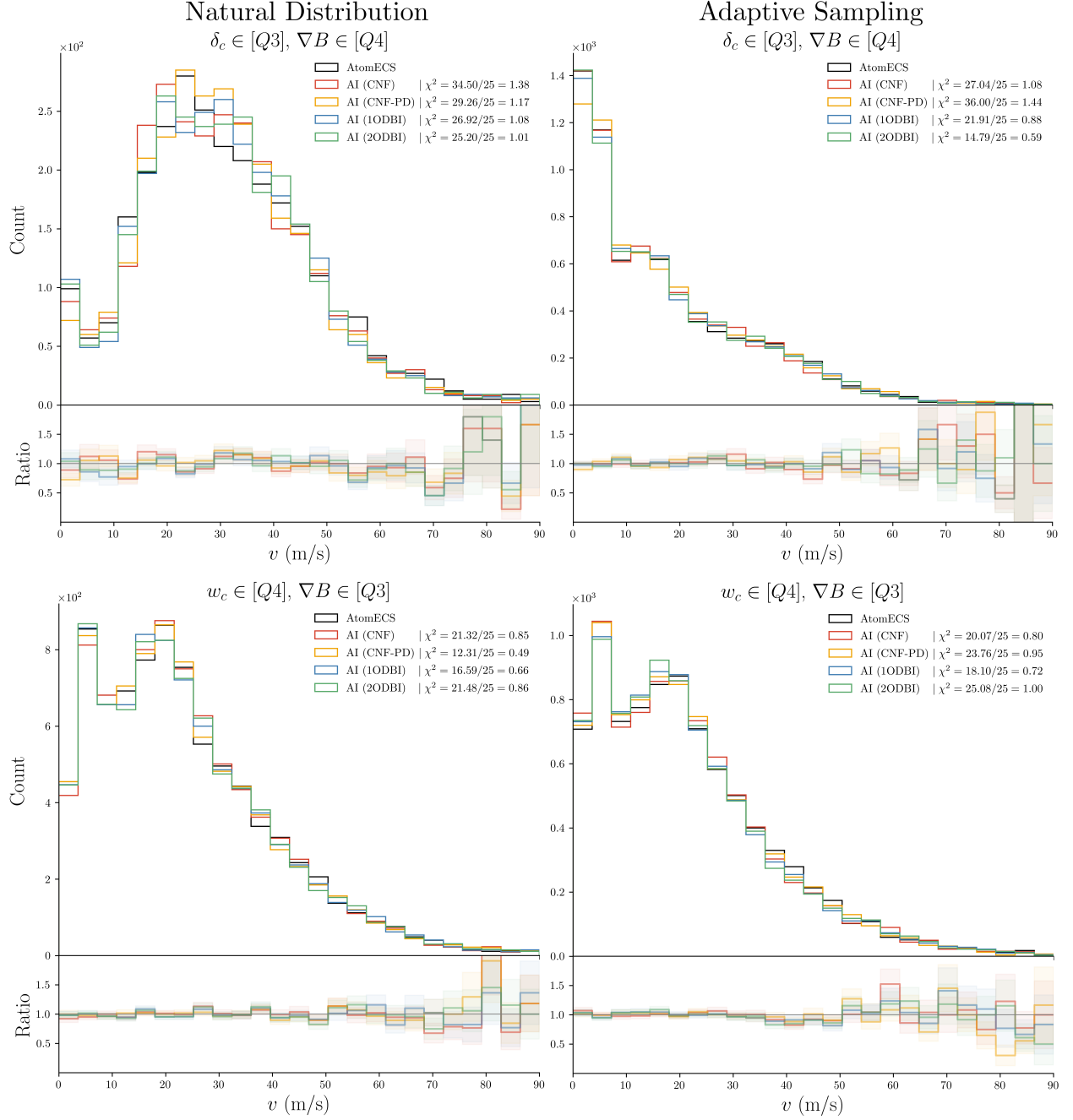


Figure 20: Histogram and bin ratio plots of two slices of the distribution: top $\delta_c \in [Q3], \nabla B \in [Q4]$; bottom $w_c \in [Q4], \nabla B \in [Q3]$. Trained and evaluated on the natural distribution (left) and AS sampled data (right).

Exploring areas of extreme low χ^2 values for 2ODBI, particularly compared to 1ODBI, (examples shown in Figure 21), 2ODBI does appear to be effective at accurately capturing the rare observations at the extreme tail-end of the distribution with often reduced uncertainty. It is vital however to be considerate of confirmation bias with such an experimental technique, its usage should therefore warrant additional scrutiny. The results obtained for 2ODBI aren't significant enough for AION, and the use of a model not thoroughly reviewed could pose the risk of introducing uncertainty and bias into the final model. 2ODBI does however show some promise, particularly on toy data (Appendix B.2), and is a technique that should be explored in greater detail.

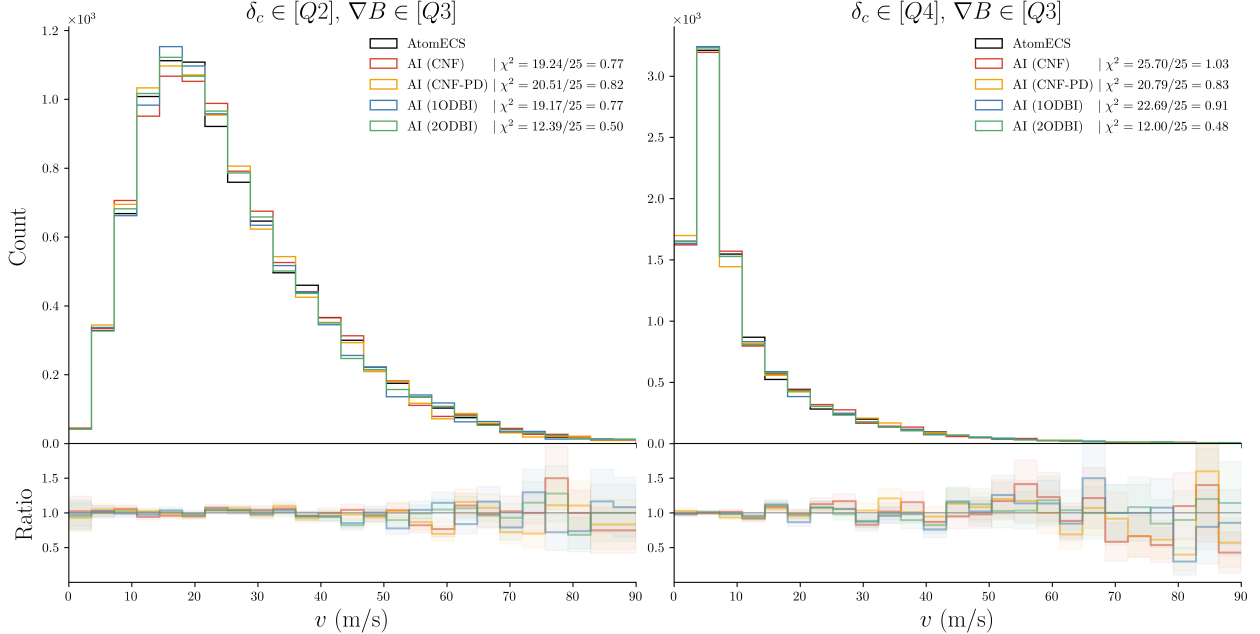


Figure 21: Histogram and bin ratio plots showing two slices, $\delta_c \in [Q3], \nabla B \in [Q4]$ (left), and $\delta_c \in [Q4], \nabla B \in [Q3]$ (right), where 2ODBI performs significantly better than 1ODBI.

Although models have demonstrated capability to accurately capture the global distribution of the AtomECS, particularly those involving or influenced by diffusion, the true accuracy of the model is limited by the accuracy of AtomECS in relation to the real cooling sequence. As discussed in the introduction to Section 2.1, particle interactions and the broadening effect are not currently modelled. With real experimental data the model built here could be calibrated to real cooling sequence, therefore replicating the real relationships between parameters rather than those in AtomECS.

5.3 Unified Model Optimisation Example

An example here is given of the inference that can be obtained from the complete simulation. Here the DNN trained in Section 5.1 predicts \mathcal{P} , a set of vectors is then sampled from the probabilistic model, for this example the CNF-PD trained on the natural distribution is used. The percentage of vectors within the pipe dimensions as defined by r_{pipe} and d_{pipe} is multiplied by the original \mathcal{P} to give the probability of an atom reaching the true transmission threshold $\mathcal{P}_{\text{pipe}}$.

This model takes ≈ 3 ms to create sample a vector on a Nvidia RTX 3080 GPU, with the total simulation time therefore highly dependent on $\boldsymbol{\theta}$. From Figure 12 we can infer that a highly

successful $\boldsymbol{\theta}$ would give $\mathcal{P} \approx 5 \times 10^{-4}$. For $N_{atoms} = 5 \times 10^6$, as used in the AtomECS sampling, this would result in 2.5×10^3 vectors sampled, giving us a conservative estimate of ≈ 7.5 s per simulation run. The equivalent AtomECS sample time is ≈ 22 minutes (Section 2.3.3), resulting in an AI model speed-up factor of $\approx 175x$ without any optimisation. This efficiency enables the application of optimisation techniques that wouldn't be as easily applicable to AtomECS.

Here we apply Bayesian optimisation (Ref. [60]) to the unified model, in which the objective function minimised is dependent on \mathcal{P}_{pipe} , the average sample atom velocity \tilde{v} and the standard deviation of displacement from the z-axis $\sigma_{\vec{r}}$, the aim being to find $\boldsymbol{\theta}$ that results in a large number of slow moving collimated atoms transmitted from the 2D MOT; these characteristics making atoms more likely to be trapped by the following stages of the cooling process. The objective function J_τ is given by:

$$J_\tau = \frac{N_{atoms} \mathcal{P}_{pipe}}{k_1 \tilde{v} + k_2 \sigma_{\vec{r}}} \quad (35)$$

where k_1 and k_2 are coefficients controlling the contribution of \tilde{v} and $\sigma_{\vec{r}}$ respectively. A multiplicative rather than additive objective function was chosen such that the properties of the transmitted atoms act as a scaling factor to the transmission count. An additive objective function would also be well motivated.

In this instance N_{atoms} was set to 5×10^6 as used in AtomECS sampling resulting in $N_{atoms} \mathcal{P}_{pipe}$ vectors sampled from the CNF-PD model. k_1 and k_2 were set to 0.25 and 1.1 respectively and Bayesian optimisation was ran using the HyperOpt (Ref. [61]) library for 1000 iterations. The top results are given in Table 11:

Rank	δ_c (MHz)	P_c (mW)	w_c (mm)	δ_p (MHz)	P_p (mW)	w_p (mm)	d_p (mm)	∇B (G/cm)	B_v (G)	\mathcal{P}_{pipe} ($\times 10^{-3}$)	\tilde{v} (m/s)	$\sigma_{\vec{r}}$ (mm)	J_τ ($\times 10^3$)
1	-146.44	304.79	11.33	-260.07	2.30	8.01	1.98	27.11	0.16	0.26	9.08	0.36	0.49
2	-139.22	316.48	11.34	-294.06	2.51	8.64	2.04	25.84	-2.44	0.25	10.29	0.35	0.41
3	-180.66	340.39	12.50	-287.02	1.55	7.27	2.51	32.26	0.07	0.19	9.32	0.37	0.34
4	-116.44	210.93	8.95	-176.23	3.81	6.71	2.61	26.35	-0.14	0.15	7.55	0.34	0.32
5	-112.10	334.36	8.47	-181.94	2.92	12.66	2.38	28.24	-1.30	0.25	13.84	0.35	0.32
6	-109.83	325.69	11.12	-176.36	3.01	12.69	2.06	18.65	-1.80	0.31	17.67	0.34	0.32
7	-180.39	337.92	11.92	-346.66	1.76	7.20	2.53	31.39	0.09	0.14	7.27	0.36	0.30
8	-110.94	301.42	9.53	-189.55	3.00	10.95	2.40	26.47	-1.19	0.22	13.01	0.35	0.30
9	-119.46	251.06	9.25	-145.26	3.17	13.33	2.74	28.34	-2.54	0.24	14.83	0.35	0.29
10	-90.73	326.33	10.59	-189.92	2.96	11.18	1.94	15.23	0.73	0.18	11.22	0.35	0.28

Table 11: Rank of the top 10 sets of input parameters $\boldsymbol{\theta}$ found through Bayesian optimisation, with their optimised characteristics (\mathcal{P}_{pipe} , \tilde{v} , $\sigma_{\vec{r}}$) and value of the objective function J_τ .

The results shown in Table 11 suggest that the objective function used is effective at balancing both \mathcal{P}_{pipe} and \tilde{v} , although $\sigma_{\vec{r}}$ doesn't tend to vary much between runs. Most significantly, however, it demonstrates the insights that can be gained from an accurate AI model of AION's cooling process.

5.3.1 Sensitivity Analysis

As a demonstration of sensitivity analysis, the top ranked set of parameters from Table 11 was used as a benchmark and the average \mathcal{P}_{pipe} , \tilde{v} , $\sigma_{\vec{r}}$, J_τ over 10 executions found. Each parameter $\boldsymbol{\theta}$ was then iterated $\pm 5\%$ of its range as defined in Section 2.2.3, with the objective metrics then

averaged at this "perturbed" point. Figure 22 shows the range of percentage shifts in each of these objective metrics as a result of the shifts in each parameter value.

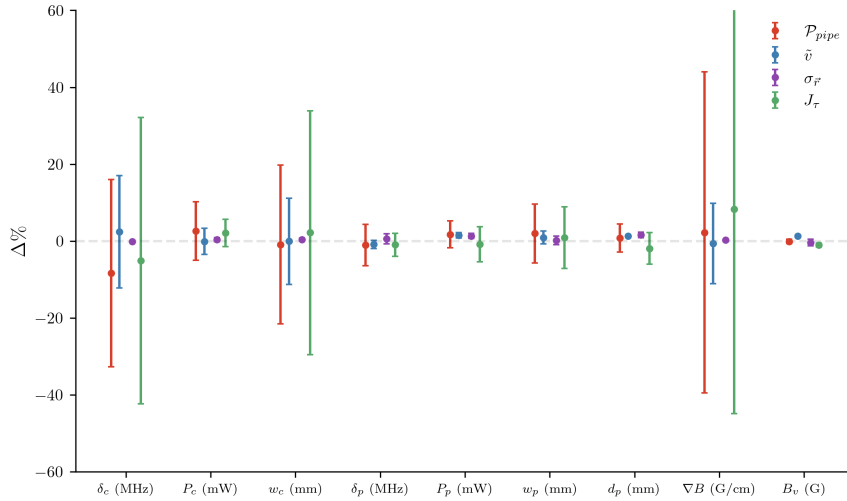


Figure 22: Error bar plot showing the percentage shift ($\Delta\%$) in $\mathcal{P}_{\text{pipe}}$, \tilde{v} , σ_r and J_τ as a result of minor shifts in the input parameters.

Even with a simple example inference into the reaction caused by small shifts in the input parameters on this locality is immediately apparent. For example $\mathcal{P}_{\text{pipe}}$ in this local region is most sensitive to small changes in ∇B , however ∇B does not influence \tilde{v} as much as δ_c . More advanced global methods would be the rational next-step; the Sobol' indices method (Ref. [62]) for example quantifies how much each variable and its combinations contribute to the overall variance of the model.

6 Conclusion

The dynamics and relationships between parameters within AtomECS have been accurately modelled by the AI methods in this paper with a significant degree of confidence. The DNN in Section 5.1 is capable of accurately predicting the probability of transmission, and therefore vectors to be generated by the probabilistic model. A range of probabilistic methods were studied, a well-tuned CNF gave an impressive NLL, however resulted in significant manifold overfitting in areas of the parameter space that transmit fewer atoms. Rebalancing the distribution through adaptive sampling led to an improvement, however this was eclipsed by the use of diffusion based Bayesian inference and diffusion inspired adjustments to the CNF.

In as few as 10 "diffusion" rounds, CNF-PD drastically reduced manifold overfitting in the CNF, significantly narrowing the range of χ^2 values across slices of the distribution. The use of diffusion-based Bayesian inference with an attention-based conditioning mechanism had a similar but slightly greater effect. By initially learning a "smooth" representation of the data, diffusion models (and CNF-PD) begin by learning the high-level details, with finer details gradually introduced into training. This encourages the model to avoid overfitting to manifolds in the early rounds and instead learn a global representation of the data.

The introduction of a 2nd order approximation to diffusion Bayesian inference, as applied to diffusion models in other domains, was found to significantly prevent overfitting on toy data,

however when applied to the dataset had a somewhat insignificant impact; likely due to the 1st order model not being prone to overfitting. In a few areas of the parameter space, particularly in the tail-ends, 2ODBI seemed to perform best suggesting it to be effective in accurately generating rare outcomes. A novel experimental method such as this requires much more extensive scrutiny before it can be recommended with any form of confidence, particularly due to confirmation bias.

By developing a globally accurate model of the parameter space, rather than one biased towards areas with high transmission probability, a model was developed that was shown to provide effective and reliable inference through optimisation techniques and analyses - with a simple Bayesian optimisation and sensitivity analysis example provided. Similarly when combined with the other simulated chambers the model will enable a RL agent to explore an environment and reward landscape accurate to AtomECS. As it stands, the model is limited by the accuracy of the AtomECS simulation to the real sequence; the lack of broadening factor for example is a source of uncertainty in the accuracy of the simulation. This could however be mitigated through calibration with experimental data.

This paper provides a comprehensive review of the methodology in modelling a 2D MOT, with the same methods also applicable to the later stages of the sequence - or even an improved or modified 2D MOT. Two novel methods have been introduced, with CNF-PD significantly mitigating the manifold overfitting apparent when training on the natural distribution of transmitted atoms. 2ODBI has shown some promise, however requires a deeper more extensive review and is therefore at this stage not recommended. On the whole, the application of diffusion and diffusion inspired processes shows significant promise in Bayesian inference and has taken AION a step closer to an optimised cooling process for atom interferometry.

Acknowledgements

Thank you to my supervisors, Mikael Mieskolainen and Charles Baynham for their continued support throughout this project. This report was only possible through their patience and attention to detail.

Thank you to Elliot Bentine for building the physical simulation of the AION 2D MOT and his support in working with the simulation.

Thank you to Elizabeth Pasatembou for her support in interpreting the quantum physics behind the simulation.

Thank you to Xavier Loizeau at NPL for first introducing me to various prominent areas of research which eventually led me to 2ODBI.

Thank you to Dr. Tobias, my supervisor at Birmingham University, for initially sparking my interest for research.

Thank you to Yubo from Tokyo Institute of Technology for his passion for the project, I hope this paper continues to inspire him.

Thank you to MackeLab for developing the Simformer, which proved an effective framework for implementing the 2nd order approximation.

References

- [1] L. Badurina et al. “AION: an atom interferometer observatory and network”. In: *Journal of Cosmology and Astroparticle Physics* 2020.05 (May 2020), pp. 011–011. ISSN: 1475-7516. DOI: [10.1088/1475-7516/2020/05/011](https://doi.org/10.1088/1475-7516/2020/05/011). URL: <http://dx.doi.org/10.1088/1475-7516/2020/05/011>.
- [2] B P Abbott et al. “LIGO: the Laser Interferometer Gravitational-Wave Observatory”. In: *Reports on Progress in Physics* 72.7 (June 2009), p. 076901. ISSN: 1361-6633. DOI: [10.1088/0034-4885/72/7/076901](https://doi.org/10.1088/0034-4885/72/7/076901). URL: <http://dx.doi.org/10.1088/0034-4885/72/7/076901>.
- [3] F Acernese et al. “Virgo detector characterization and data quality: results from the O3 run”. In: *Classical and Quantum Gravity* 40.18 (Aug. 2023), p. 185006. ISSN: 1361-6382. DOI: [10.1088/1361-6382/acd92d](https://doi.org/10.1088/1361-6382/acd92d). URL: <http://dx.doi.org/10.1088/1361-6382/acd92d>.
- [4] Y. A. El-Neaj, C. Alpigiani, S. Amairi-Pyka, et al. “AEDGE: Atomic Experiment for Dark Matter and Gravity Exploration in Space”. In: *EPJ Quantum Technology* 7.1 (2020), p. 6. DOI: [10.1140/epjqt/s40507-020-0080-0](https://doi.org/10.1140/epjqt/s40507-020-0080-0). URL: <https://doi.org/10.1140/epjqt/s40507-020-0080-0>.
- [5] J. Rudolph et al. “Large momentum transfer clock atom interferometry on the 689 nm intercombination line of strontium”. In: *Physical Review Letters* 124 (2019), p. 083604. DOI: [10.1103/PhysRevLett.124.083604](https://doi.org/10.1103/PhysRevLett.124.083604).
- [6] L. Hu et al. “Atom interferometry with the Sr optical clock transition”. In: *Physical Review Letters* 119 (2017), p. 263601. DOI: [10.1103/PhysRevLett.119.263601](https://doi.org/10.1103/PhysRevLett.119.263601).
- [7] H. Katori et al. “Magneto-optical trapping and cooling of strontium atoms down to the photon recoil temperature”. In: *Physical Review Letters* 82 (1999), pp. 1116–1119.
- [8] F. Sorrentino et al. “Laser cooling and trapping of atomic strontium for ultracold atoms physics, high-precision spectroscopy and quantum sensors”. In: *Modern Physics Letters B* 20 (2006), pp. 1287–1320.
- [9] E. Pasatembou et al. *Progress towards ultracold Sr for the AION project – sub-microkelvin atoms and an optical-heterodyne diagnostic tool for injection-locked laser diodes*. 2023. arXiv: [2310.08500 \[physics.atom-ph\]](https://arxiv.org/abs/2310.08500). URL: <https://arxiv.org/abs/2310.08500>.
- [10] T. Kovachy. “Progress toward large-area strontium atom interferometry for precision gravitational measurements”. In: 11700 (2021). DOI: [10.1111/12.2595546](https://doi.org/10.1111/12.2595546).
- [11] Ya-jie Wang et al. “Modeling gravitational wave detection with atom interferometry”. In: *Classical and Quantum Gravity* 38 (2021). DOI: [10.1088/1361-6382/ac0236](https://doi.org/10.1088/1361-6382/ac0236).
- [12] B. Stray et al. *Centralised Design and Production of the Ultra-High Vacuum and Laser-Stabilisation Systems for the AION Ultra-Cold Strontium Laboratories*. 2023. arXiv: [2305.20060 \[physics.atom-ph\]](https://arxiv.org/abs/2305.20060). URL: <https://arxiv.org/abs/2305.20060>.
- [13] N Milson et al. “High-dimensional reinforcement learning for optimization and control of ultracold quantum gases”. In: *Machine Learning: Science and Technology* 4.4 (Dec. 2023), p. 045057. DOI: [10.1088/2632-2153/ad1437](https://doi.org/10.1088/2632-2153/ad1437). URL: <https://dx.doi.org/10.1088/2632-2153/ad1437>.
- [14] Sangwon Seo et al. “Maximized atom number for a grating magneto-optical trap via machine-learning assisted parameter optimization.” In: *Optics express* 29 22 (2021), pp. 35623–35639. DOI: [10.1364/oe.437991](https://doi.org/10.1364/oe.437991).

- [15] T. Lausch et al. “Optimizing quantum gas production by an evolutionary algorithm”. In: *Applied Physics B* 122 (2016), pp. 1–7. DOI: [10.1007/s00340-016-6391-2](https://doi.org/10.1007/s00340-016-6391-2).
- [16] X. Chen et al. “AtomECS: Simulate laser cooling and magneto-optical traps”. In: *Journal of Physics* 50.2 (2024). *Corresponding author: elliot.bentine@physics.ox.ac.uk, pp. 123–130.
- [17] Saurav Kadavath, Samuel Paradis, and Brian Yao. “Pretraining and Reinforcement Learning: Sharpening the Axe Before Cutting the Tree”. In: *ArXiv* abs/2110.02497 (2021).
- [18] Martin Weidemüller and Claus Zimmermann. *Cold Atoms and Molecules*. Wiley-VCH, 2009.
- [19] Anthony E. Siegman. *Lasers*. Mill Valley, CA: University Science Books, 1986. ISBN: 978-0935702118.
- [20] Geoffrey Brooker. “The Zeeman effect”. In: *Essays in Physics* (2021). DOI: [10.1888/0333750888/4955](https://doi.org/10.1888/0333750888/4955).
- [21] H. Günther. “The Doppler Effect”. In: *Elementary Approach to Special Relativity* (2020). DOI: [10.1007/978-981-15-3168-2_18](https://doi.org/10.1007/978-981-15-3168-2_18).
- [22] N. Sagna, G. Dudle, and P. Thomann. “The capture process in spherical magneto-optical traps: experiment and 1D magnetic field models”. In: *Journal of Physics B* 28 (1995), pp. 3213–3224. DOI: [10.1088/0953-4075/28/15/013](https://doi.org/10.1088/0953-4075/28/15/013).
- [23] Michael Drewsen et al. “Investigation of sub-Doppler cooling effects in a cesium magneto-optical trap”. In: *Applied Physics B* 59 (1994), pp. 283–298. DOI: [10.1007/BF01081396](https://doi.org/10.1007/BF01081396).
- [24] Harold J. Metcalf and Peter van der Straten. *Laser Cooling and Trapping*. Springer, 1999.
- [25] L. Allen and J.H. Eberly. *Optical Resonance and Two-Level Atoms*. Dover Publications, 1975.
- [26] J.M. Haile. *Molecular Dynamics Simulation: Elementary Methods*. John Wiley & Sons, 1992.
- [27] Henri Faure, Peter Kritzer, and Friedrich Pillichshammer. *From van der Corput to modern constructions of sequences for quasi-Monte Carlo rules*. 2015. arXiv: [1506.03764 \[math.NT\]](https://arxiv.org/abs/1506.03764). URL: <https://arxiv.org/abs/1506.03764>.
- [28] Jingrun Chen et al. *Quasi-Monte Carlo sampling for machine-learning partial differential equations*. 2019. arXiv: [1911.01612 \[math.NA\]](https://arxiv.org/abs/1911.01612). URL: <https://arxiv.org/abs/1911.01612>.
- [29] Solomon Kullback and Richard A. Leibler. “On information and sufficiency”. In: *Annals of Mathematical Statistics* 22.1 (1951), pp. 79–86.
- [30] Christina Winkler et al. “Learning Likelihoods with Conditional Normalizing Flows”. In: *Preprint* (2023). Institute of Informatics, University of Amsterdam, Netherlands. URL: <https://arxiv.org/abs/1912.00042>.
- [31] Roger Ernest Cooke. “Real and Complex Analysis”. In: 2011. URL: <https://api.semanticscholar.org/CorpusID:118286458>.
- [32] Oliver Fest. “Measure theory”. In: *A Tool Kit for Groupoid *-Algebras* (2019). URL: <https://api.semanticscholar.org/CorpusID:2320788>.
- [33] G. Papamakarios et al. “Normalizing Flows for Probabilistic Modeling and Inference”. In: *J. Mach. Learn. Res.* 22 (2019), 57:1–57:64.

- [34] Laurent Dinh, David Krueger, and Yoshua Bengio. *NICE: Non-linear Independent Components Estimation*. 2015. arXiv: [1410.8516 \[cs.LG\]](https://arxiv.org/abs/1410.8516). URL: <https://arxiv.org/abs/1410.8516>.
- [35] Laurent Dinh, Jascha Sohl-Dickstein, and Samy Bengio. *Density estimation using Real NVP*. 2017. arXiv: [1605.08803 \[cs.LG\]](https://arxiv.org/abs/1605.08803). URL: <https://arxiv.org/abs/1605.08803>.
- [36] George Papamakarios, Theo Pavlakou, and Iain Murray. *Masked Autoregressive Flow for Density Estimation*. 2018. arXiv: [1705.07057 \[stat.ML\]](https://arxiv.org/abs/1705.07057). URL: <https://arxiv.org/abs/1705.07057>.
- [37] Conor Durkan et al. *Neural Spline Flows*. 2019. arXiv: [1906.04032 \[stat.ML\]](https://arxiv.org/abs/1906.04032). URL: <https://arxiv.org/abs/1906.04032>.
- [38] Diederik P. Kingma and Prafulla Dhariwal. *Glow: Generative Flow with Invertible 1x1 Convolutions*. 2018. arXiv: [1807.03039 \[stat.ML\]](https://arxiv.org/abs/1807.03039). URL: <https://arxiv.org/abs/1807.03039>.
- [39] Diederik P. Kingma et al. *Improving Variational Inference with Inverse Autoregressive Flow*. 2017. arXiv: [1606.04934 \[cs.LG\]](https://arxiv.org/abs/1606.04934). URL: <https://arxiv.org/abs/1606.04934>.
- [40] Ba-Hien Tran et al. “One-Line-of-Code Data Mollification Improves Optimization of Likelihood-based Generative Models”. In: *Advances in Neural Information Processing Systems*. Ed. by A. Oh et al. Vol. 36. Curran Associates, Inc., 2023, pp. 6545–6567. URL: https://proceedings.neurips.cc/paper_files/paper/2023/file/1516a7f7507d5550db5c7f29e995ec8c-Paper-Conference.pdf.
- [41] Aapo Hyvärinen. “Estimation of Non-Normalized Statistical Models by Score Matching”. In: *J. Mach. Learn. Res.* 6 (Dec. 2005), pp. 695–709. ISSN: 1532-4435.
- [42] Manuel Gloeckler et al. *All-in-one simulation-based inference*. 2024. arXiv: [2404.09636 \[cs.LG\]](https://arxiv.org/abs/2404.09636). URL: <https://arxiv.org/abs/2404.09636>.
- [43] Ashish Vaswani et al. *Attention Is All You Need*. 2023. arXiv: [1706.03762 \[cs.CL\]](https://arxiv.org/abs/1706.03762). URL: <https://arxiv.org/abs/1706.03762>.
- [44] Yang Song et al. “Sliced Score Matching: A Scalable Approach to Density and Score Estimation”. In: *CoRR* abs/1905.07088 (2019). arXiv: [1905.07088](https://arxiv.org/abs/1905.07088). URL: [http://arxiv.org/abs/1905.07088](https://arxiv.org/abs/1905.07088).
- [45] Michael F Hutchinson. “A stochastic estimator of the trace of the influence matrix for Laplacian smoothing splines”. In: *Communications in Statistics-Simulation and Computation* 18.3 (1989), pp. 1059–1076.
- [46] Litu Rout et al. *Beyond First-Order Tweedie: Solving Inverse Problems using Latent Diffusion*. 2023. arXiv: [2312.00852 \[cs.LG\]](https://arxiv.org/abs/2312.00852). URL: <https://arxiv.org/abs/2312.00852>.
- [47] Morris H. DeGroot and Mark J. Schervish. *Probability and Statistics*. 4th. Pearson Education, 2012. ISBN: 978-0321500465.
- [48] Hans Rademacher. “Einige Sätze über Reihen von allgemeinen Orthogonalfunktionen”. In: *Mathematische Annalen* 87.1 (1922), pp. 112–138.
- [49] Tianqi Chen and Carlos Guestrin. “XGBoost: A Scalable Tree Boosting System”. In: *Proceedings of the 22nd ACM SIGKDD International Conference on Knowledge Discovery and Data Mining* (2016). DOI: [10.1145/2939672.2939785](https://doi.org/10.1145/2939672.2939785).
- [50] Chitta Baral, O. Fuentes, and V. Kreinovich. “Why Deep Neural Networks: A Possible Theoretical Explanation”. In: (2018), pp. 1–5. DOI: [10.1007/978-3-319-61753-4_1](https://doi.org/10.1007/978-3-319-61753-4_1).

- [51] Tianqi Chen and Carlos Guestrin. *XGBoost: A Scalable Tree Boosting System*. <https://xgboost.readthedocs.io/en/stable/>. Accessed: 2024-09-20. 2016.
- [52] Adam Paszke et al. “PyTorch: An Imperative Style, High-Performance Deep Learning Library”. In: *Advances in Neural Information Processing Systems 32*. Curran Associates, Inc., 2019, pp. 8024–8035. URL: <http://papers.neurips.com/paper/9015-pytorch-an-imperative-style-high-performance-deep-learning-library.pdf>.
- [53] Jorge Nocedal. “Updating quasi-Newton matrices with limited storage”. In: *Mathematics of computation* 35.151 (1980), pp. 773–782.
- [54] Michael Dittadi et al. *NormFlows: Normalizing Flows for Probabilistic Modeling*. 2021. arXiv: [2006.05545 \[stat.ML\]](https://arxiv.org/abs/2006.05545). URL: <https://arxiv.org/abs/2006.05545>.
- [55] Trevor Hastie, Robert Tibshirani, and Jerome Friedman. “Overview of Supervised Learning”. In: *The Elements of Statistical Learning: Data Mining, Inference, and Prediction*. Springer, 2009. Chap. 2, pp. 9–42.
- [56] Lalit R Bahl, Frederick Jelinek, and Robert L Mercer. “A maximum likelihood approach to continuous speech recognition”. In: *IEEE Transactions on Pattern Analysis and Machine Intelligence* 2 (1983), pp. 179–190.
- [57] Cédric Villani. *Optimal transport: old and new*. Vol. 338. Springer Science & Business Media, 2009.
- [58] Jerome H Friedman. “On multivariate goodness-of-fit and two-sample testing”. In: *Statistical Problems in Particle Physics, Astrophysics and Cosmology* (2004), pp. 311–313.
- [59] David Lopez-Paz and Maxime Oquab. “Revisiting classifier two-sample tests”. In: *International Conference on Learning Representations*. 2017.
- [60] Donald R Jones, Matthias Schonlau, and William J Welch. “Efficient global optimization of expensive black-box functions”. In: *Journal of Global optimization* 13.4 (1998), pp. 455–492.
- [61] James Bergstra, Dan Yamins, and David D. Cox. *Hyperopt: Distributed Asynchronous Hyperparameter Optimization*. <https://github.com/hyperopt/hyperopt>. Documentation available at <http://hyperopt.github.io/hyperopt/>. 2013.
- [62] I. M. Sobol’. “Sensitivity estimates for nonlinear mathematical models”. In: *Mathematical Modeling and Computational Experiment* 1.4 (1993), pp. 407–414.
- [63] Leo Breiman et al. *Classification and Regression Trees*. Monterey, CA: Wadsworth & Brooks/Cole Advanced Books & Software, 1984. ISBN: 9780412048418.
- [64] Jerome H Friedman. “Greedy function approximation: A gradient boosting machine”. In: *Annals of Statistics* 29.5 (2001), pp. 1189–1232.
- [65] Jan M. Lueckmann et al. “Benchmarking simulation-based inference”. In: *Proceedings of the National Academy of Sciences* 118.24 (2021), e2103564118.

A Deterministic Prediction Methods

The overall model will be split into two distinct sections, a model that predicts \mathcal{P} for a given $\boldsymbol{\theta}$, and a further probabilistic model that generates a number of remaining target parameters X equal to a defined number of atoms N_{atoms} multiplied by \mathcal{P} as predicted by the first model. To model \mathcal{P} , a boosted decision tree (BDT) [49] and a deep neural network (DNN) [50] were chosen due to their capability to capture complex relationships in large datasets.

A.1 Boosted Decision Trees

Decision trees are a class of supervised learning algorithm consisting of nodes representing decision points, edges representing the outcomes of decisions, and leaf nodes representing the final predictions. During training, the tree is constructed by splitting the data at each node based on the value of an input variable $\boldsymbol{\theta}$, the goal being to choose splits that best separate the data according to X ; in classification the criteria is typically the Gini impurity and variance reduction for regression. Once the data is split until a condition is met e.g. maximum depth or samples per leaf, the nodes at the end of each branch become leaf nodes which hold the predicted output [63].

To make a prediction, an individual data point is passed through the tree from the root to a leaf node, following the decision rules at each node. By "boosting" a decision tree, i.e. training multiple models sequentially, the performance can be improved significantly. In gradient boosting, an additional tree is fitted to train the residuals from the previous, learning the direction in which the predictions should be adjusted to minimise the loss function. The predictions are updated by adding the predictions from the new tree, scaled by a learning rate [64]. Extreme gradient boosting (XGBoost) [49] provides a number of further enhancements, including regularisation, enhanced tree pruning, and parallel processing, making XGBoost more effective on large datasets than typical BDTs.

A.2 Deep Neural Networks

DNNs consist of multiple layers of interconnected nodes known as neurons, typically an input layer, multiple hidden layers and an output layer, transforming the input data into increasingly abstract representations. For a given layer l , the output \mathbf{a}^l of the neurons is computed as follows:

$$\mathbf{a}^l = \sigma(\mathbf{W}^l \mathbf{a}^{l-1} + \mathbf{b}^l) \quad (36)$$

where \mathbf{W}^l is the weight matrix connecting layer $l-1$ to layer l , \mathbf{a}^{l-1} is the output from the previous layer, \mathbf{b}^l is the bias vector for the current layer, and σ is the non-linear activation function. Rectified linear unit (ReLU) activation $\sigma(x) = \max(0, x)$ being a common example. By applying a non-linear activation in a "deep" multi-layer architecture, the model can hierarchically learn complex non-linear relationships within the data.

DNNs learn through gradient descent, the gradient of the loss function with respect to the network's weights and biases are found and updated in the opposite direction of the gradient to reduce loss. The weight update rule for a given weight w at layer l is:

$$w_{ij}^l \leftarrow w_{ij}^l - \eta \frac{\partial \mathcal{L}}{\partial w_{ij}^l} \quad (37)$$

where η is the learning rate, determining the step size, which is multiplied by the gradient of the loss function with respect to the weight w_{ij}^l . The gradient is computed using backpropagation, this

involves a forward pass where the predicted output \hat{X} and resultant loss $\mathcal{L}(X, \hat{X})$ are found by propagating the input through the network, and a backward pass where the error from the output layer is propagated back through the network to compute the gradient of the loss with respect to each weight [50].

B Diffusion Bayesian Inference

B.1 Derivation of the Score Matching Objective

We start with the original score matching objective function:

$$J(\boldsymbol{\theta}) = \frac{1}{2} \int_{X \in \mathbb{R}^n} p_X(X) |\psi(X; \boldsymbol{\theta}) - \nabla_X \log p(X)|^2 dX \quad (38)$$

Expanding the squared norm:

$$J(\boldsymbol{\theta}) = \frac{1}{2} \int_{X \in \mathbb{R}^n} p_X(X) [|\psi(X; \boldsymbol{\theta})|^2 - 2\psi(X; \boldsymbol{\theta})^\top \nabla_X \log p(X) + |\nabla_X \log p(X)|^2] dX \quad (39)$$

The third term involving $\|\nabla_X \log p(X)\|^2$ is independent of $\boldsymbol{\theta}$, so it can be ignored for the purpose of optimisation. The second term, $-2 \int p_X(X) \psi(X; \boldsymbol{\theta})^\top \nabla_X \log p(X) dX$, is simplified using integration by parts:

$$-\int_X p_X(X) \nabla_X^\top \psi(X; \boldsymbol{\theta}) dX = \int_X p_X(X) \sum_{i=1}^n \frac{\partial \psi_i(X; \boldsymbol{\theta})}{\partial X_i} dX \quad (40)$$

Substituting back, the reformulated score matching objective becomes:

$$J(\boldsymbol{\theta}) = \int_{X \in \mathbb{R}^n} p_X(X) \sum_{i=1}^n \left[\frac{\partial \psi_i(X; \boldsymbol{\theta})}{\partial X_i} + \frac{1}{2} \psi_i(X; \boldsymbol{\theta})^2 \right] dX + \text{const.} \quad (41)$$

This final expression eliminates the need for the empirical score function.

B.2 SLCP Dataset Loss Curve

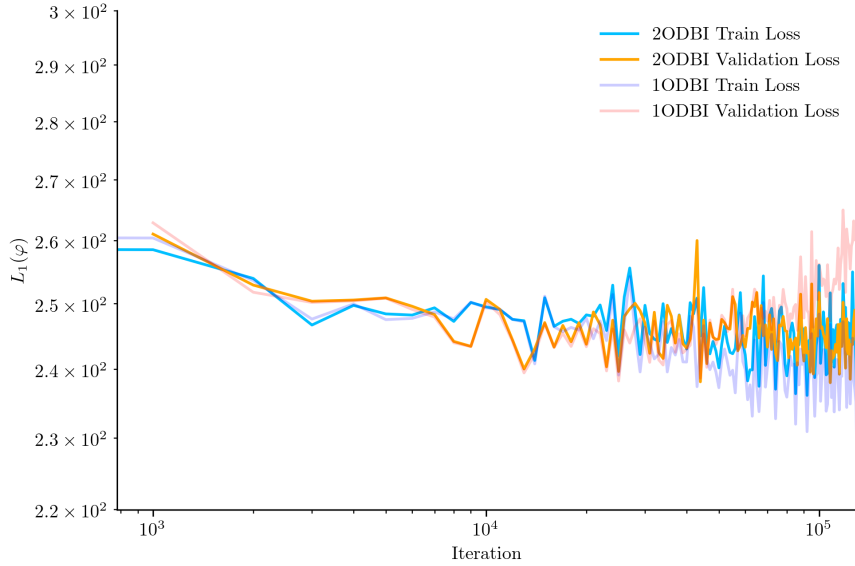


Figure 23: Diffusion Bayesian inference (Simformer) loss curve trained on the SLCP dataset, showing the original model (1ODBI) and the inclusion of 2nd order information in the loss function (2ODBI). Although trained using $L_2(\varphi)$, the loss shown for 2ODBI excludes the 2nd order term for parity with 1ODBI.

The 2nd order approximation in this instance was incorporated into the Simformer [42] benchmarking framework, rather than as a stand alone script. The training is therefore slightly different than from the example in the main script, most notably the presence of iterations rather than epochs. This model was trained to model both the posterior and likelihood through a fluctuating condition mask and trained on 10^4 generated samples of the SLCP dataset (Ref. [65]). For 2ODBI, $\gamma = 10^{-3}$.

C Parameter Quartile χ^2 Values

C.1 CNF

C.1.1 Natural Distribution

Table 12: CNF χ^2 values for \vec{r}_x across parameter quartile combinations.

Table 13: CNF χ^2 values for \vec{r}_y across parameter quartile combinations.

		P_c	w_c	δ_p	P_p	w_p	d_p	∇B								B_v																				
		Q1	Q2	Q3	Q4	Q1	Q2	Q3	Q4	Q1	Q2	Q3	Q4	Q1	Q2	Q3	Q4	Q1	Q2	Q3	Q4	Q1	Q2	Q3	Q4											
δ_c	Q1	0.80	1.23	0.86	0.64	1.17	0.92	1.37	1.04	1.15	1.24	0.60	0.78	0.81	0.97	1.09	1.20	1.34	1.28	1.38	0.81	1.66	1.73	1.02	0.79	0.87	1.03	1.12	0.92	0.58	0.98	0.97	0.94			
	Q2	0.80	0.64	0.72	0.71	1.04	1.14	1.22	0.83	0.70	0.48	0.87	0.80	0.95	0.65	0.71	1.17	0.72	0.79	0.57	0.66	0.71	0.70	0.48	1.23	1.36	0.61	0.86	0.72	1.02	1.15	1.02	1.08			
	Q3	0.81	0.49	0.86	0.65	1.00	0.63	1.05	0.84	1.24	1.00	0.72	0.79	1.05	0.80	1.07	0.97	1.26	1.04	0.73	0.79	0.69	0.94	0.79	0.63	0.84	1.11	1.01	1.33	1.49	0.63	0.57	0.94			
	Q4	0.83	0.72	0.76	0.47	0.95	0.82	1.03	0.90	0.89	1.18	1.16	1.43	1.14	0.82	0.67	0.98	1.03	0.96	0.84	1.11	1.22	1.14	1.17	1.73	0.66	0.90	0.99	0.92	1.35	0.74	0.90	0.88			
P_c	Q1	-	-	-	-	0.75	0.54	0.91	0.76	1.03	1.00	0.59	0.84	0.86	0.72	1.20	0.99	1.12	0.69	1.35	0.77	1.05	0.92	0.71	1.13	0.66	1.10	0.74	0.97	1.12	0.92	1.20	1.27			
	Q2	-	-	-	-	0.81	0.83	0.93	0.96	0.90	1.35	0.90	0.61	1.04	0.94	1.47	1.21	1.35	0.83	0.64	0.56	1.12	1.33	0.63	0.81	0.87	0.81	0.83	1.04	0.89	0.94	1.03	1.00			
	Q3	-	-	-	-	1.07	0.87	1.38	0.93	0.50	1.28	0.74	0.83	0.87	1.25	0.84	0.88	1.11	0.97	0.61	1.05	1.06	1.19	1.26	0.64	0.94	0.64	1.21	0.63	1.86	0.94	1.00				
	Q4	-	-	-	-	0.81	1.18	0.74	0.64	0.50	0.72	0.77	0.59	1.03	0.94	1.04	0.60	0.68	0.53	0.68	1.24	0.94	0.88	0.68	0.78	0.70	0.69	0.71	0.56	0.86	0.71	0.74				
w_c	Q1	-	-	-	-	-	-	-	-	0.81	0.83	1.32	1.27	0.55	0.61	0.85	1.10	0.60	1.12	0.89	0.81	0.92	0.74	0.91	1.05	1.50	1.70	0.71	1.02	0.94	0.83	0.86	0.78			
	Q2	-	-	-	-	-	-	-	-	1.28	1.09	0.58	0.97	0.61	1.06	0.72	0.93	0.56	0.85	0.56	0.89	1.12	0.74	0.76	1.19	1.45	0.96	1.32	1.00	0.70	1.18	0.77	0.86			
	Q3	-	-	-	-	-	-	-	-	0.88	0.94	0.98	0.67	1.61	0.91	1.09	0.98	0.84	1.07	0.81	0.74	0.55	0.96	1.05	1.11	0.84	0.79	0.98	1.17	0.96	0.95	1.02	1.35			
	Q4	-	-	-	-	-	-	-	-	1.83	1.46	0.79	0.93	1.55	1.12	0.81	0.70	0.86	0.78	1.04	0.49	1.25	1.73	0.96	0.81	1.17	0.88	0.80	0.67	0.76	0.71	1.48				
δ_p	Q1	-	-	-	-	-	-	-	-	-	-	-	-	0.83	0.94	1.03	0.63	0.97	1.29	0.80	0.80	0.78	0.57	1.36	1.38	0.94	0.91	1.63	0.96	0.86	0.72					
	Q2	-	-	-	-	-	-	-	-	-	-	-	-	0.93	0.71	1.01	0.90	1.41	1.17	1.03	0.41	0.76	0.93	0.94	1.03	1.52	0.58	0.96	1.10	0.99	0.81	0.89	0.93			
	Q3	-	-	-	-	-	-	-	-	-	-	-	-	0.91	0.92	1.05	1.28	0.69	0.79	0.70	0.57	1.07	1.33	0.90	0.62	1.29	0.86	1.28	1.41	0.71	0.94	0.47	1.77			
	Q4	-	-	-	-	-	-	-	-	-	-	-	-	1.64	0.68	1.08	0.85	0.87	1.05	0.86	0.87	1.04	0.82	1.34	1.36	1.30	0.59	0.77	0.73	1.24	0.78	1.44				
P_p	Q1	-	-	-	-	-	-	-	-	-	-	-	-	-	-	-	-	0.62	0.82	0.74	0.83	1.12	1.11	0.87	1.07	1.17	1.12	0.57	1.14	0.75	1.22	1.26	1.24			
	Q2	-	-	-	-	-	-	-	-	-	-	-	-	-	-	-	-	1.00	0.82	0.70	1.39	1.08	1.23	1.21	0.83	0.85	0.38	0.90	0.91	1.57	0.86	1.12	0.70			
	Q3	-	-	-	-	-	-	-	-	-	-	-	-	-	-	-	-	1.15	1.32	0.81	0.51	0.76	1.09	0.83	0.64	0.93	1.02	1.11	0.97	0.80	1.17	1.20	1.03			
	Q4	-	-	-	-	-	-	-	-	-	-	-	-	-	-	-	-	1.23	0.89	1.09	0.86	1.06	0.72	0.96	0.93	0.87	0.64	1.16	0.89	0.72	0.93	1.07	1.24			
w_p	Q1	-	-	-	-	-	-	-	-	-	-	-	-	-	-	-	-	-	-	-	-	0.71	1.06	1.25	0.91	1.56	1.05	1.38	0.79	0.89	1.46	1.38				
	Q2	-	-	-	-	-	-	-	-	-	-	-	-	-	-	-	-	-	-	-	-	0.83	1.31	1.09	0.73	0.79	0.70	0.56	0.80	1.13	1.18	0.55	0.90			
	Q3	-	-	-	-	-	-	-	-	-	-	-	-	-	-	-	-	-	0.61	1.56	0.73	0.92	0.86	0.99	1.04	0.84	0.77	1.04	0.91	0.70						
	Q4	-	-	-	-	-	-	-	-	-	-	-	-	-	-	-	-	-	0.78	0.94	0.80	0.61	0.90	0.68	1.01	0.93	0.53	0.63	1.02	0.97						
d_p	Q1	-	-	-	-	-	-	-	-	-	-	-	-	-	-	-	-	-	-	-	-	-	-	-	-	-	-	-	-	-	-	-	-	-	-	-
	Q2	-	-	-	-	-	-	-	-	-	-	-	-	-	-	-	-	-	-	-	-	-	-	-	-	-	-	-	-	-	-	-	-	-	-	-
	Q3	-	-	-	-	-	-	-	-	-	-	-	-	-	-	-	-	-	-	-	-	-	-	-	-	-	-	-	-	-	-	-	-	-	-	-
	Q4	-	-	-	-	-	-	-	-	-	-	-	-	-	-	-	-	-	-	-	-	-	-	-	-	-	-	-	-	-	-	-	-	-	-	-
∇B	Q1	-	-	-	-	-	-	-	-	-	-	-	-	-	-	-	-	-	-	-	-	-	-	-	-	-	-	-	-	-	-	-	-	-	-	-
	Q2	-	-	-	-	-	-	-	-	-	-	-	-	-	-	-	-	-	-	-	-	-	-	-	-	-	-	-	-	-	-	-	-	-	-	-
	Q3	-	-	-	-	-	-	-	-	-	-	-	-	-	-	-	-	-	-	-	-	-	-	-	-	-	-	-	-	-	-	-	-	-	-	-
	Q4	-	-	-	-	-	-	-	-	-	-	-	-	-	-	-	-	-	-	-	-	-	-	-	-	-	-	-	-	-	-	-	-	-	-	-

Table 14: CNF χ^2 values for v across parameter quartile combinations.

		P_c	w_c	δ_p	P_p	w_p	d_p	∇B								B_v																	
		Q1	Q2	Q3	Q4	Q1	Q2	Q3	Q4	Q1	Q2	Q3	Q4	Q1	Q2	Q3	Q4	Q1	Q2	Q3	Q4	Q1	Q2	Q3	Q4								
δ_c	Q1	2.30	0.96	1.49	1.51	1.00	0.92	1.47	1.73	2.29	0.88	1.00	1.53	1.23	1.03	0.97	1.16	1.86	1.10	1.43	1.73	0.97	0.74	0.91	0.61	1.29	1.65	0.90	1.49	1.44	1.33	1.60	
	Q2	1.14	1.10	1.59	1.39	2.36	1.17	1.34	0.99	1.88	1.99	1.43	0.97	1.63	1.14	1.60	1.17	1.70	1.80	1.50	1.19	0.88	1.05	1.41	1.39	1.54	2.02	1.32	1.40	1.84	1.30	1.28	
	Q3	2.54	2.71	1.29	1.04	1.32	2.28	1.44	2.02	1.16	2.37	1.57	2.02	1.78	2.53	1.50	1.49	2.23	1.86	1.78	2.09	1.91	1.24	1.51	1.78	2.22	1.90	1.07	1.22	2.16	2.41	1.58	1.84
	Q4	2.82	2.95	1.97	2.62	2.81	3.02	2.52	2.62	3.94	4.06	2.38	1.31	3.20	2.38	2.25	2.03	1.59	3.09	2.80	3.34	2.85	1.82	2.54	3.29	0.98	2.30	4.03	4.25	3.71	1.65	2.71	3.41
P_c	Q1	-	-	-	-	3.06	3.31	0.94	1.87	1.96	2.14	2.20	1.55	2.34	1.75	2.26	1.53	1.91	1.84	1.93	2.33	2.00	1.68	1.78	2.03	1.76	1.82	3.10	1.71	2.43	1.49	1.05</	

Table 16: CNF χ^2 values for θ across parameter quartile combinations.

C.1.2 Adaptive Sampling

Table 17: CNF χ^2 values for \vec{r}_x across parameter quartile combinations.

		P_c				w_c				δ_p				P_p				w_p				d_p				∇B				B_v			
		Q1	Q2	Q3	Q4	Q1	Q2	Q3	Q4	Q1	Q2	Q3	Q4	Q1	Q2	Q3	Q4	Q1	Q2	Q3	Q4	Q1	Q2	Q3	Q4	Q1	Q2	Q3	Q4	Q1	Q2	Q3	Q4
δ_c	Q1	1.07	1.18	1.39	1.39	0.96	0.94	1.69	1.75	1.34	1.00	1.71	1.26	0.90	0.70	0.74	2.24	0.89	1.24	1.32	0.91	0.60	1.00	1.15	1.67	0.87	1.95	1.13	1.19	0.63	1.02	0.77	2.06
	Q2	0.77	1.07	1.21	1.04	1.55	0.68	0.88	1.07	0.92	1.05	0.96	1.30	2.46	0.52	1.29	0.73	1.37	0.84	1.24	0.79	0.92	1.39	1.18	1.01	1.37	1.40	0.98	0.94	1.83	1.00	0.82	1.26
	Q3	1.01	1.50	0.88	0.28	0.86	0.98	1.07	1.60	0.86	0.75	1.10	1.17	0.83	1.06	0.93	1.00	1.29	1.21	1.34	1.50	1.01	1.09	1.44	1.81	1.34	1.55	0.70	0.90	0.86	0.83	1.09	0.90
	Q4	0.89	2.08	1.56	0.93	1.20	1.15	1.65	1.60	1.41	1.26	0.87	1.14	1.60	0.88	0.84	1.10	1.50	1.65	1.25	1.42	1.13	0.94	1.61	0.78	0.83	1.28	1.33	1.59	0.91	1.21	1.25	1.35
P_c	Q1	-	-	-	-	1.08	0.68	0.74	0.80	0.60	0.69	0.68	0.92	1.36	1.08	0.94	0.69	0.97	0.77	1.20	0.50	0.66	0.73	0.83	1.06	1.10	1.21	0.97	1.38	0.79	0.79	1.03	
	Q2	-	-	-	-	0.90	0.51	0.95	0.84	1.26	0.93	0.43	1.64	0.70	0.91	1.17	1.56	0.71	0.74	1.51	0.82	1.11	0.92	1.25	1.19	1.71	0.95	1.00	1.02	1.55	1.17	0.60	0.71
	Q3	-	-	-	-	1.45	0.92	1.02	1.40	0.88	1.41	1.10	0.69	1.34	1.18	1.33	1.57	1.57	0.82	0.88	1.22	0.88	0.83	1.39	1.59	1.02	0.78	1.31	1.18	0.88	1.15	1.32	1.22
	Q4	-	-	-	-	0.99	1.23	1.05	1.40	0.97	1.25	1.12	0.95	0.89	0.88	0.84	0.94	0.71	0.98	1.16	0.56	1.04	0.65	0.58	1.02	0.94	1.08	1.11	0.95	1.41	0.58	1.64	0.74
w_c	Q1	-	-	-	-	-	-	-	-	1.29	1.03	0.91	0.73	1.11	1.50	1.10	1.12	1.03	1.90	0.93	0.88	0.85	1.36	1.12	1.72	1.14	0.99	1.26	1.19	0.92	0.51	0.95	
	Q2	-	-	-	-	-	-	-	-	1.84	0.95	0.72	0.90	1.25	1.11	1.11	1.58	1.24	1.00	1.29	0.97	0.60	0.68	0.86	1.01	1.30	0.88	0.62	1.04	0.86	0.85	0.61	0.74
	Q3	-	-	-	-	-	-	-	-	0.98	1.08	0.86	0.87	0.60	1.12	1.44	0.47	1.10	0.64	1.10	1.16	0.97	0.86	1.09	0.91	1.64	0.65	0.58	1.02	0.94	1.08	1.11	0.95
	Q4	-	-	-	-	-	-	-	-	0.78	0.71	1.70	2.08	1.17	1.60	1.41	1.66	1.20	0.81	1.24	1.01	1.08	1.23	1.55	1.75	0.98	1.37	1.16	1.56	1.35	1.67	1.31	1.14
δ_p	Q1	-	-	-	-	-	-	-	-	-	-	-	-	0.97	0.99	0.80	0.62	0.83	0.90	0.90	0.96	1.06	1.00	0.80	0.59	1.13	0.85	0.69	1.20	0.88	1.10	0.43	0.82
	Q2	-	-	-	-	-	-	-	-	-	0.79	0.93	1.11	0.93	0.96	0.86	0.86	1.08	0.93	0.72	0.93	0.66	1.27	1.15	1.04	0.92	0.55	1.55	0.84	0.85			
	Q3	-	-	-	-	-	-	-	-	-	0.99	0.69	1.39	0.83	0.82	1.70	0.89	0.96	0.71	1.10	1.11	1.10	1.34	1.36	0.81	0.99	0.63	1.28	1.50	1.56			
	Q4	-	-	-	-	-	-	-	-	-	-	-	-	0.86	0.88	1.15	1.24	1.13	0.68	1.29	0.62	1.12	1.04	0.99	1.19	1.30	1.18	0.82	0.72	1.79	1.52	0.94	0.75
P_p	Q1	-	-	-	-	-	-	-	-	-	-	-	-	-	-	-	-	-	-	-	-	-	-	-	-	-	-	-	-	-	-	-	-
	Q2	-	-	-	-	-	-	-	-	-	-	-	-	-	-	-	-	-	-	-	-	-	-	-	-	-	-	-	-	-	-	-	-
	Q3	-	-	-	-	-	-	-	-	-	-	-	-	-	-	-	-	-	-	-	-	-	-	-	-	-	-	-	-	-	-	-	-
	Q4	-	-	-	-	-	-	-	-	-	-	-	-	-	-	-	-	-	-	-	-	-	-	-	-	-	-	-	-	-	-	-	-
w_p	Q1	-	-	-	-	-	-	-	-	-	-	-	-	-	-	-	-	-	-	-	-	-	-	-	-	-	-	-	-	-	-	-	-
	Q2	-	-	-	-	-	-	-	-	-	-	-	-	-	-	-	-	-	-	-	-	-	-	-	-	-	-	-	-	-	-	-	-
	Q3	-	-	-	-	-	-	-	-	-	-	-	-	-	-	-	-	-	-	-	-	-	-	-	-	-	-	-	-	-	-	-	-
	Q4	-	-	-	-	-	-	-	-	-	-	-	-	-	-	-	-	-	-	-	-	-	-	-	-	-	-	-	-	-	-	-	-
d_p	Q1	-	-	-	-	-	-	-	-	-	-	-	-	-	-	-	-	-	-	-	-	-	-	-	-	-	-	-	-	-	-	-	-
	Q2	-	-	-	-	-	-	-	-	-	-	-	-	-	-	-	-	-	-	-	-	-	-	-	-	-	-	-	-	-	-	-	-
	Q3	-	-	-	-	-	-	-	-	-	-	-	-	-	-	-	-	-	-	-	-	-	-	-	-	-	-	-	-	-	-	-	-
	Q4	-	-	-	-	-	-	-	-	-	-	-	-	-	-	-	-	-	-	-	-	-	-	-	-	-	-	-	-	-	-	-	-
∇B	Q1	-	-	-	-	-	-	-	-	-	-	-	-	-	-	-	-	-	-	-	-	-	-	-	-	-	-	-	-	-	-	-	-
	Q2	-	-	-	-	-	-	-	-	-	-	-	-	-	-	-	-	-	-	-	-	-	-	-	-	-	-	-	-	-	-	-	-
	Q3	-	-	-	-	-	-	-	-	-	-	-	-	-	-	-	-	-	-	-	-	-	-	-	-	-	-	-	-	-	-	-	-
	Q4	-	-	-	-	-	-	-	-	-	-	-	-	-	-	-	-	-	-	-	-	-	-	-	-	-	-	-	-	-	-	-	-

Table 18: CNF χ^2 values for \vec{r}_y across parameter quartile combinations.

		P_c				w_c				δ_p				P_p				w_p				d_p				∇B				B_v			
		Q1	Q2	Q3	Q4	Q1	Q2	Q3	Q4	Q1	Q2	Q3	Q4	Q1	Q2	Q3	Q4	Q1	Q2	Q3	Q4	Q1	Q2	Q3	Q4	Q1	Q2	Q3	Q4	Q1	Q2	Q3	Q4
δ_c	Q1	1.40	0.70	0.89	1.05	1.15	0.75	0.61	1.03	0.70	0.82	0.73	0.94	0.47	1.17	0.82	1.26	0.90	0.93	1.13	0.71	1.38	0.69	0.86	0.80	1.25	0.75	1.19	0.44	1.00	0.99	1.08	1.15
	Q2	1.52	0.92	0.68	1.11	1.12	1.06	0.86	1.04	0.74	0.59	0.94	0.82	1.27	0.95	1.03	1.14	1.00	0.75	0.51	1.07	0.53	0.89	0.93	1.14	0.89	1.28	0.42	0.53	0.66	1.23	0.88	1.03
	Q3	1.22	1.09	0.83	1.38	1.38	1.26	1.09	1.37	0.87	1.28	0.94	1.45	1.13	1.60	1.58	1.16	0.87	1.02	0.54	0.94	0.78	1.68	1.27	1.36	1.35	0.88	1.07	1.12	1.19	0.94	1.56	
	Q4	1.12	2.21	1.98	1.28	2.08	0.90	1.79	1.83	2.66	1.58	1.36	1.30	1.32	1.18	1.34	2.11	1.66	1.62	1.09	1.78	1.81	1.69	1.47	1.65	1.96	2.09	1.72	1.10	1.77	1.38	1.95	1.23
P_c	Q1	-	-	-	-	1.06	0.93	0.47	1.06	1.54	1.22	1.01	0.79	0.87	0.67	0.74	0.78	1.12	1.12	1.05	0.83	0.99	0.69	0.99	0.91								

		P_c				w_c				δ_p				P_p				w_p				d_p				∇B				B_v			
		Q1	Q2	Q3	Q4	Q1	Q2	Q3	Q4	Q1	Q2	Q3	Q4	Q1	Q2	Q3	Q4	Q1	Q2	Q3	Q4	Q1	Q2	Q3	Q4	Q1	Q2	Q3	Q4	Q1	Q2	Q3	Q4
δ_c	Q1	0.80	1.70	1.86	2.52	0.73	0.95	2.06	2.57	1.85	2.21	1.54	1.18	1.66	1.66	1.84	1.48	2.33	2.38	1.40	0.87	1.89	1.49	1.33	1.22	1.11	1.88	1.85	1.41	1.48	1.18	1.47	1.99
	Q2	1.01	0.82	1.01	1.02	1.45	1.20	1.18	1.71	0.55	1.33	1.26	1.08	0.84	0.51	1.19	2.32	0.92	1.06	0.95	1.25	0.91	0.89	1.05	0.76	1.03	0.76	1.36	1.11	1.05	0.80	1.56	1.04
	Q3	0.96	1.03	1.00	1.54	0.97	0.86	1.10	1.55	1.04	0.91	1.74	1.55	0.94	1.25	1.72	1.18	1.32	1.12	1.00	1.34	1.70	0.81	0.77	1.44	0.98	0.91	1.36	1.89	1.47	1.14	1.56	0.78
	Q4	1.94	2.71	1.49	2.11	1.71	2.96	2.35	2.17	3.67	2.00	1.82	1.78	2.51	2.03	2.50	2.13	2.58	2.01	1.91	2.22	2.06	1.72	1.76	2.89	2.08	1.99	3.12	4.33	2.59	2.06	1.77	2.34
P_c	Q1	-	-	-	-	1.30	0.64	1.12	1.04	1.34	1.13	1.07	1.03	0.78	0.63	1.78	1.10	1.47	1.09	1.19	0.84	1.39	1.01	0.85	0.62	1.22	1.05	1.25	1.55	1.04	1.21	1.02	1.26
	Q2	-	-	-	-	1.19	1.51	1.25	2.50	1.06	1.11	1.98	1.70	1.54	1.14	1.58	2.75	1.64	1.33	1.17	1.41	1.24	1.77	1.16	1.70	1.01	1.10	1.30	2.22	1.73	1.46	1.78	1.24
	Q3	-	-	-	-	0.80	1.00	1.65	2.04	1.30	1.03	1.19	1.33	0.77	1.80	0.98	1.36	1.32	1.07	1.28	1.63	1.10	1.13	1.23	1.51	0.57	1.44	1.68	1.65	0.94	1.06	1.90	0.73
	Q4	-	-	-	-	1.64	1.85	1.51	2.20	1.80	1.26	1.20	1.07	1.39	1.24	2.29	1.06	1.38	1.53	1.95	1.63	1.74	1.23	1.79	1.16	1.08	0.87	2.05	2.13	1.79	1.06	1.09	2.29
w_c	Q1	-	-	-	-	-	-	-	-	1.97	1.22	0.77	1.39	0.97	0.88	1.82	0.90	1.31	0.99	1.30	1.02	1.41	0.69	1.67	1.23	0.98	1.57	0.93	1.54	1.28	1.36	1.47	0.81
	Q2	-	-	-	-	-	-	-	-	1.02	1.97	1.22	1.50	0.76	0.98	2.12	1.52	1.20	1.26	1.15	1.33	1.39	1.06	1.62	1.43	1.08	1.58	1.33	1.53	1.42	1.85	0.56	1.21
	Q3	-	-	-	-	-	-	-	-	1.52	1.49	1.21	1.14	1.23	1.15	1.25	1.75	1.53	1.17	1.96	1.63	1.85	1.30	1.10	1.98	1.08	1.82	1.70	1.74	1.40	1.09	1.86	2.05
	Q4	-	-	-	-	-	-	-	-	2.14	2.88	2.16	1.69	1.20	1.42	1.93	2.61	1.81	2.40	1.73	3.29	1.02	1.71	2.19	2.51	2.01	2.74	2.02	1.40	1.28	3.03	2.08	
δ_p	Q1	-	-	-	-	-	-	-	-	-	-	-	-	-	-	-	-	-	-	-	-	-	-	-	-	-	-	-	-	-	-		
	Q2	-	-	-	-	-	-	-	-	-	-	-	-	-	-	-	-	-	-	-	-	-	-	-	-	-	-	-	-	-	-		
	Q3	-	-	-	-	-	-	-	-	-	-	-	-	-	-	-	-	-	-	-	-	-	-	-	-	-	-	-	-	-	-		
	Q4	-	-	-	-	-	-	-	-	-	-	-	-	-	-	-	-	-	-	-	-	-	-	-	-	-	-	-	-	-	-		
P_p	Q1	-	-	-	-	-	-	-	-	-	-	-	-	-	-	-	-	-	-	-	-	-	-	-	-	-	-	-	-	-	-		
	Q2	-	-	-	-	-	-	-	-	-	-	-	-	-	-	-	-	-	-	-	-	-	-	-	-	-	-	-	-	-	-		
	Q3	-	-	-	-	-	-	-	-	-	-	-	-	-	-	-	-	-	-	-	-	-	-	-	-	-	-	-	-	-	-		
	Q4	-	-	-	-	-	-	-	-	-	-	-	-	-	-	-	-	-	-	-	-	-	-	-	-	-	-	-	-	-	-		
w_p	Q1	-	-	-	-	-	-	-	-	-	-	-	-	-	-	-	-	-	-	-	-	-	-	-	-	-	-	-	-	-	-		
	Q2	-	-	-	-	-	-	-	-	-	-	-	-	-	-	-	-	-	-	-	-	-	-	-	-	-	-	-	-	-	-		
	Q3	-	-	-	-	-	-	-	-	-	-	-	-	-	-	-	-	-	-	-	-	-	-	-	-	-	-	-	-	-	-		
	Q4	-	-	-	-	-	-	-	-	-	-	-	-	-	-	-	-	-	-	-	-	-	-	-	-	-	-	-	-	-	-		
d_p	Q1	-	-	-	-	-	-	-	-	-	-	-	-	-	-	-	-	-	-	-	-	-	-	-	-	-	-	-	-	-	-		
	Q2	-	-	-	-	-	-	-	-	-	-	-	-	-	-	-	-	-	-	-	-	-	-	-	-	-	-	-	-	-	-		
	Q3	-	-	-	-	-	-	-	-	-	-	-	-	-	-	-	-	-	-	-	-	-	-	-	-	-	-	-	-	-	-		
	Q4	-	-	-	-	-	-	-	-	-	-	-	-	-	-	-	-	-	-	-	-	-	-	-	-	-	-	-	-	-	-		
∇B	Q1	-	-	-	-	-	-	-	-	-	-	-	-	-	-	-	-	-	-	-	-	-	-	-	-	-	-	-	-	-	-		
	Q2	-	-	-	-	-	-	-	-	-	-	-	-	-	-	-	-	-	-	-	-	-	-	-	-	-	-	-	-	-	-		
	Q3	-	-	-	-	-	-	-	-	-	-	-	-	-	-	-	-	-	-	-	-	-	-	-	-	-	-	-	-	-	-		
	Q4	-	-	-	-	-	-	-	-	-	-	-	-	-	-	-	-	-	-	-	-	-	-	-	-	-	-	-	-	-	-		

Table 20: CNF χ^2 values for ϕ across parameter quartile combinations.

		P_c				w_c				δ_p				P_p				w_p				d_p				∇B				B_v				
		Q1	Q2	Q3	Q4	Q1	Q2	Q3	Q4	Q1	Q2	Q3	Q4	Q1	Q2	Q3	Q4	Q1	Q2	Q3	Q4	Q1	Q2	Q3	Q4	Q1	Q2	Q3	Q4	Q1	Q2	Q3	Q4	
δ_c	Q1	0.89	0.98	0.76	1.15	0.78	1.03	1.17	0.76	0.82	0.80	0.82	0.94	0.88	0.58	1.19	0.92	0.97	1.06	1.01	0.85	0.95	0.64	0.76	0.64	1.49	1.45	0.96	0.90	1.12	1.40	0.86	1.12	
	Q2	0.91	1.01	0.93	1.33	1.52	0.97	0.95	0.64	0.79	0.96	1.01	0.94	0.79	0.78	1.22	0.80	0.94	0.81	0.73	1.14	1.02	0.54	0.90	0.80	1.22	0.65	1.03	0.71	1.09	0.72	1.74	1.14	1.14
	Q3	0.73	1.44	1.00	1.36	0.46	1.51	0.54	1.21	1.09	0.50	0.87	0.94	1.34	0.92	0.82	1.12	0.72	1.41	0.86	0.99	0.92	0.57	0.91	0.86	0.95	1.21	0.51	1.06	1.54	1.04	1.04		
	Q4	1.66	1.56	1.03	1.45	1.54	1.27	1.50	0.93	1.47	1.08	1.94	0.79	1.85	1.45	1.25	0.83	0.92	1.60	1.14	0.98	0.64	1.20	1.70	1.37	0.88	1.33	0.71	1.49	2.04	1.21	0.88	1.18	
P_c	Q1	-	-	-	-	1.22	1.02	1.17	1.03	1.37	0.94	0.89	1.24	0.63	1.30	0.99	1.12	0.63	1.12	1.20	1.26	0.99	0.76	0.74	2.18	0.96	1.24	1.21	0.46	1.02	0.53	0.68	1.51	
	Q2	-	-	-	-	0.62	1.14	1.22	0.72	1.05	0.87	0.98	0.78	1.42	1.17	0.78	0.90	0.93	1.04	1.20	1.22	1.00	0.80	0.88	1.02	1.69	0.86	0.61	1.13	1.03	1.06	0.97	1.10	
	Q3	-	-	-	-	0.86	0.86	0.68	0.74	0.66	1.22	0.77	0.70	0.81	1.45	0.95</td																		

C.2 CNF-PD

C.2.1 Natural Distribution

		P_c				w_c				δ_p				P_p				w_p				d_p				∇B				B_v						
		Q1	Q2	Q3	Q4	Q1	Q2	Q3	Q4	Q1	Q2	Q3	Q4	Q1	Q2	Q3	Q4	Q1	Q2	Q3	Q4	Q1	Q2	Q3	Q4	Q1	Q2	Q3	Q4	Q1	Q2	Q3	Q4			
δ_c	Q1	0.92	1.02	1.03	1.19	0.91	1.44	0.89	0.94	0.91	1.24	1.17	0.95	0.60	0.67	1.35	0.83	0.69	1.06	1.49	1.23	0.90	1.16	1.20	1.58	1.31	1.14	1.24	0.99	1.30						
	Q2	1.17	0.76	1.03	0.79	0.86	0.96	0.75	0.41	1.11	0.83	0.64	0.87	1.10	0.90	1.19	1.04	1.35	1.12	0.58	0.86	1.65	0.74	0.93	1.22	1.33	1.34	0.69	1.28	0.82	1.70	0.71	1.41			
	Q3	1.05	1.06	0.59	0.91	1.15	0.83	1.69	0.89	0.74	1.75	0.92	0.96	0.95	0.52	0.83	0.83	0.72	1.03	0.82	1.38	0.73	0.88	0.60	0.86	1.09	1.11	0.63	0.62	0.77	1.14	1.09	1.13			
	Q4	0.72	1.04	1.50	1.26	1.66	0.98	0.61	0.75	1.31	0.98	1.45	0.62	0.87	0.72	0.89	1.04	0.96	0.86	1.19	0.96	1.37	0.92	1.09	1.02	0.64	1.03	0.80	0.84	0.77	0.86	1.35	1.28			
P_c	Q1	-	-	-	-	0.81	0.91	0.87	1.61	0.77	0.64	1.27	1.16	0.51	0.81	1.38	0.70	1.03	0.69	1.27	1.15	1.13	0.53	1.33	1.09	1.17	0.89	0.61	0.68	1.11	1.03	1.49	0.90			
	Q2	-	-	-	-	1.28	1.01	1.27	0.77	1.08	0.90	0.88	0.74	0.91	0.98	0.76	0.75	1.04	0.75	0.87	1.13	0.91	1.00	0.67	0.94	0.97	0.87	0.58	0.68	0.90	1.06	0.68	1.04			
	Q3	-	-	-	-	1.53	0.63	0.67	0.57	1.10	1.00	0.64	1.11	0.68	0.65	0.86	1.32	0.89	1.06	0.58	1.35	0.75	0.83	0.78	1.03	0.68	1.11	1.11	1.47	0.86	0.97	0.69	0.62			
	Q4	-	-	-	-	1.42	0.73	1.15	0.97	0.99	0.69	1.01	1.29	1.06	1.28	1.17	1.04	1.18	0.67	1.42	0.68	0.64	0.90	1.03	1.32	1.10	1.46	0.94	1.24	0.99	1.02	0.95	1.25			
w_c	Q1	-	-	-	-	-	-	-	-	1.33	1.30	1.00	0.76	0.88	1.46	0.58	1.27	0.88	1.21	1.13	1.02	0.67	0.58	1.19	1.37	1.21	1.17	0.65	1.31	1.03	1.72	0.77	1.06			
	Q2	-	-	-	-	-	-	-	-	1.18	1.53	0.95	1.13	1.07	0.80	1.17	1.24	1.08	1.05	0.86	1.67	1.00	1.19	1.01	0.84	1.23	0.59	0.84	1.08	0.98	1.31	0.68	1.06			
	Q3	-	-	-	-	-	-	-	-	0.78	1.25	1.10	1.07	0.68	1.17	1.05	0.77	1.15	0.65	1.08	0.74	0.99	0.67	1.55	1.17	1.19	0.90	0.52	0.92	0.70	1.37	1.25	1.06			
	Q4	-	-	-	-	-	-	-	-	0.99	0.81	0.53	0.71	0.63	1.02	1.02	1.13	0.69	0.98	1.01	0.79	1.18	0.87	0.88	0.68	1.08	0.87	1.03	0.99	0.86	0.88	0.99				
δ_p	Q1	-	-	-	-	-	-	-	-	-	-	-	-	-	-	-	-	-	-	-	-	-	-	-	-	-	-	-	-	-	-	-	-	-	-	
	Q2	-	-	-	-	-	-	-	-	-	-	-	-	-	-	-	-	-	-	-	-	-	-	-	-	-	-	-	-	-	-	-	-	-	-	
	Q3	-	-	-	-	-	-	-	-	-	-	-	-	-	-	-	-	-	-	-	-	-	-	-	-	-	-	-	-	-	-	-	-	-	-	
	Q4	-	-	-	-	-	-	-	-	-	-	-	-	-	-	-	-	-	-	-	-	-	-	-	-	-	-	-	-	-	-	-	-	-	-	
P_p	Q1	-	-	-	-	-	-	-	-	-	-	-	-	-	-	-	-	-	-	-	-	-	-	-	-	-	-	-	-	-	-	-	-	-	-	-
	Q2	-	-	-	-	-	-	-	-	-	-	-	-	-	-	-	-	-	-	-	-	-	-	-	-	-	-	-	-	-	-	-	-	-	-	-
	Q3	-	-	-	-	-	-	-	-	-	-	-	-	-	-	-	-	-	-	-	-	-	-	-	-	-	-	-	-	-	-	-	-	-	-	-
	Q4	-	-	-	-	-	-	-	-	-	-	-	-	-	-	-	-	-	-	-	-	-	-	-	-	-	-	-	-	-	-	-	-	-	-	-
w_p	Q1	-	-	-	-	-	-	-	-	-	-	-	-	-	-	-	-	-	-	-	-	-	-	-	-	-	-	-	-	-	-	-	-	-	-	-
	Q2	-	-	-	-	-	-	-	-	-	-	-	-	-	-	-	-	-	-	-	-	-	-	-	-	-	-	-	-	-	-	-	-	-	-	-
	Q3	-	-	-	-	-	-	-	-	-	-	-	-	-	-	-	-	-	-	-	-	-	-	-	-	-	-	-	-	-	-	-	-	-	-	-
	Q4	-	-	-	-	-	-	-	-	-	-	-	-	-	-	-	-	-	-	-	-	-	-	-	-	-	-	-	-	-	-	-	-	-	-	-
d_p	Q1	-	-	-	-	-	-	-	-	-	-	-	-	-	-	-	-	-	-	-	-	-	-	-	-	-	-	-	-	-	-	-	-	-	-	-
	Q2	-	-	-	-	-	-	-	-	-	-	-	-	-	-	-	-	-	-	-	-	-	-	-	-	-	-	-	-	-	-	-	-	-	-	-
	Q3	-	-	-	-	-	-	-	-	-	-	-	-	-	-	-	-	-	-	-	-	-	-	-	-	-	-	-	-	-	-	-	-	-	-	-
	Q4	-	-	-	-	-	-	-	-	-	-	-	-	-	-	-	-	-	-	-	-	-	-	-	-	-	-	-	-	-	-	-	-	-	-	-
∇B	Q1	-	-	-	-	-	-	-	-	-	-	-	-	-	-	-	-	-	-	-	-	-	-	-	-	-	-	-	-	-	-	-	-	-	-	-
	Q2	-	-	-	-	-	-	-	-	-	-	-	-	-	-	-	-	-	-	-	-	-	-	-	-	-	-	-	-	-	-	-	-	-	-	-
	Q3	-	-	-	-	-	-	-	-	-	-	-	-	-	-	-	-	-	-	-	-	-	-	-	-	-	-	-	-	-	-	-	-	-	-	-
	Q4	-	-	-	-	-	-	-	-	-	-	-	-	-	-	-	-	-	-	-	-	-	-	-	-	-	-	-	-	-	-	-	-	-	-	-

Table 22: CNF-PD χ^2 values for \vec{r}_x across parameter quartile combinations.

		P_c				w_c				δ_p				P_p				w_p				d_p				∇B				B_v			
		Q1	Q2	Q3	Q4	Q1	Q2	Q3	Q4	Q1	Q2	Q3	Q4	Q1	Q2	Q3	Q4	Q1	Q2	Q3	Q4	Q1	Q2	Q3	Q4	Q1	Q2	Q3	Q4	Q1	Q2	Q3	Q4
δ_c	Q1	1.55	1.05	1.08	1.00	1.19	1.29	0.58	1.44	0.79	1.11	1.16	0.87	0.72	1.48	1.11	0.86	0.71	0.64	1.16	1.25	0.83	0.78	0.81	1.30	1.14	1.02	0.66	1.36	0.91	0.95	1.06	1.48
	Q2	0.81	1.43	1.41	0.96	1.52	0.96	1.10	1.16	1.04	1.36	0.83	1.11	1.34	0.74	1.25	1.53	0.77	1.49	0.78	0.99	1.20	1.00	1.03	1.43	0.96	1.44	1.05	1.32	1.87	0.90	0.85	1.01
	Q3	1.16	0.86	1.07	0.76	1.19	1.75	1.42	0.71	1.23	1.56	0.88	0.75	0.63	1.50	0.92	0.96	1.07	1.49	1.37	0.94	1.39	1.48	0.42	1.26	0.65	1.28	0.56	1.36	1.60	0.71	1.29	
	Q4	0.99	1.42	0.74	1.07	1.21	1.30	1.75	1.70	1.09	1.55	1.50	0.81	1.47	0.91	2.01	0.97	1.49	0.91	1.62	0.95	1.00	1.31	1.25	1.37	0.94	1.32	0.71	1.07	0.83	1.72	0.72	1.06
P_c	Q1	-	-	-	-	1.01	1.01	0.89	0.97	1.14	0.77	0.95	1.15	1.37	0.86	0.56	0.96	0.87	0.86	0.94	0.69												

		P_c	w_c	δ_p	P_p	w_p	d_p	∇B				B_v																					
		Q1	Q2	Q3	Q4	Q1	Q2	Q3	Q4	Q1	Q2	Q3	Q4	Q1	Q2	Q3	Q4	Q1	Q2	Q3	Q4	Q1	Q2	Q3	Q4								
δ_c	Q1	0.76	1.00	1.06	1.04	1.55	1.21	0.93	1.17	0.65	1.52	0.53	0.65	0.65	0.54	1.12	1.41	0.67	1.14	0.98	0.79	1.30	0.89	0.93	0.71	0.69	1.15	0.86	1.31	0.68	0.96	0.59	0.77
	Q2	0.91	0.72	1.13	1.14	1.03	0.99	2.08	1.22	0.70	0.92	1.96	1.41	0.81	0.90	0.84	1.63	1.49	1.29	0.95	0.83	1.89	0.94	0.79	0.91	1.48	1.00	0.86	0.37	1.05	0.92	1.24	1.11
	Q3	0.74	0.59	1.06	0.88	0.66	1.20	1.57	1.16	1.23	1.30	0.63	0.98	0.52	1.30	0.90	1.12	1.60	1.19	0.56	0.66	1.57	0.91	1.35	0.98	1.21	0.94	1.14	1.13	0.78	0.77	1.25	1.11
	Q4	1.66	0.84	0.93	0.44	0.79	1.19	1.09	1.05	0.72	1.17	1.20	1.17	0.93	1.12	1.12	0.86	1.03	0.84	0.73	0.87	1.30	1.22	0.93	1.25	0.81	1.07	0.86	1.00	1.22	1.09	1.15	0.73
P_c	Q1	-	-	-	-	0.96	1.07	1.34	0.94	1.03	0.79	1.34	0.67	0.62	0.89	1.02	0.90	0.96	1.16	0.98	0.73	1.08	1.27	0.64	0.97	1.03	0.43	1.08	1.21	0.36	1.23	1.22	1.70
	Q2	-	-	-	-	0.79	0.78	0.99	0.65	0.77	1.69	1.16	0.91	1.15	1.14	1.25	0.74	0.92	0.58	0.88	0.80	0.92	1.32	0.93	0.48	0.77	0.75	0.61	1.09	0.53	1.06	0.98	0.78
	Q3	-	-	-	-	1.14	0.95	1.25	0.61	1.20	1.08	0.95	0.86	1.21	0.91	0.78	1.33	1.41	0.83	0.50	1.03	1.12	1.10	0.57	0.63	0.65	1.02	1.08	0.46	0.99	0.91	0.71	
	Q4	-	-	-	-	1.45	0.84	1.37	1.08	0.86	0.71	1.13	1.18	0.48	0.61	1.29	0.88	0.72	1.14	0.83	0.63	0.72	1.89	0.73	0.78	1.32	1.00	1.09	1.02	0.61	1.09	0.81	0.58
w_c	Q1	-	-	-	-	-	-	-	-	0.89	0.91	0.98	1.26	0.69	0.85	0.94	0.81	1.76	0.74	0.66	0.72	1.30	0.82	0.87	0.73	0.91	0.85	1.30	1.21	1.33	1.09	0.93	0.91
	Q2	-	-	-	-	-	-	-	-	0.99	1.50	0.29	1.87	0.50	1.10	1.47	1.05	0.90	0.92	0.64	0.64	1.49	0.45	0.92	1.12	1.58	0.93	0.85	1.26	0.56	1.35	0.94	1.04
	Q3	-	-	-	-	-	-	-	-	1.01	1.72	0.96	0.99	1.99	1.28	1.16	0.74	1.84	1.01	0.83	0.73	1.98	1.02	1.19	1.76	1.24	1.16	1.13	1.34	1.73	0.93	0.90	
	Q4	-	-	-	-	-	-	-	-	0.76	0.95	0.92	1.17	0.80	1.13	0.79	1.02	0.68	1.21	1.06	0.42	0.98	1.35	0.81	0.84	1.15	1.21	0.54	0.88	0.77	0.61		
δ_p	Q1	-	-	-	-	-	-	-	-	-	-	-	0.85	1.17	0.61	0.59	0.71	1.02	0.94	0.54	0.67	1.34	1.08	0.72	1.43	0.97	0.77	0.60	1.17	0.78	0.45		
	Q2	-	-	-	-	-	-	-	-	-	-	-	0.92	0.99	1.34	1.41	1.25	0.99	0.67	0.55	0.87	0.83	1.21	1.10	1.55	0.83	1.03	0.93	0.64	0.83	1.17	1.59	
	Q3	-	-	-	-	-	-	-	-	-	-	-	0.93	0.48	0.56	0.95	0.47	0.84	0.74	0.35	1.05	0.95	0.77	0.58	0.83	1.01	0.83	1.10	0.27	0.99	0.86	1.39	
	Q4	-	-	-	-	-	-	-	-	-	-	-	-	0.71	0.77	0.74	1.00	0.94	1.11	0.55	1.28	0.90	1.09	1.04	1.00	1.12	1.04	1.42	0.94	1.35	0.41	0.99	
P_p	Q1	-	-	-	-	-	-	-	-	-	-	-	-	-	-	-	-	-	-	-	-	-	-	-	-	-	-	-	-	-	-	-	
	Q2	-	-	-	-	-	-	-	-	-	-	-	-	-	-	-	-	-	-	-	-	-	-	-	-	-	-	-	-	-	-	-	
	Q3	-	-	-	-	-	-	-	-	-	-	-	-	-	-	-	-	-	-	-	-	-	-	-	-	-	-	-	-	-	-	-	
	Q4	-	-	-	-	-	-	-	-	-	-	-	-	-	-	-	-	-	-	-	-	-	-	-	-	-	-	-	-	-	-	-	
w_p	Q1	-	-	-	-	-	-	-	-	-	-	-	-	-	-	-	-	-	-	-	-	-	-	-	-	-	-	-	-	-	-	-	
	Q2	-	-	-	-	-	-	-	-	-	-	-	-	-	-	-	-	-	-	-	-	-	-	-	-	-	-	-	-	-	-	-	
	Q3	-	-	-	-	-	-	-	-	-	-	-	-	-	-	-	-	-	-	-	-	-	-	-	-	-	-	-	-	-	-	-	
	Q4	-	-	-	-	-	-	-	-	-	-	-	-	-	-	-	-	-	-	-	-	-	-	-	-	-	-	-	-	-	-	-	
d_p	Q1	-	-	-	-	-	-	-	-	-	-	-	-	-	-	-	-	-	-	-	-	-	-	-	-	-	-	-	-	-	-	-	
	Q2	-	-	-	-	-	-	-	-	-	-	-	-	-	-	-	-	-	-	-	-	-	-	-	-	-	-	-	-	-	-	-	
	Q3	-	-	-	-	-	-	-	-	-	-	-	-	-	-	-	-	-	-	-	-	-	-	-	-	-	-	-	-	-	-	-	
	Q4	-	-	-	-	-	-	-	-	-	-	-	-	-	-	-	-	-	-	-	-	-	-	-	-	-	-	-	-	-	-	-	
∇B	Q1	-	-	-	-	-	-	-	-	-	-	-	-	-	-	-	-	-	-	-	-	-	-	-	-	-	-	-	-	-	-	-	
	Q2	-	-	-	-	-	-	-	-	-	-	-	-	-	-	-	-	-	-	-	-	-	-	-	-	-	-	-	-	-	-	-	
	Q3	-	-	-	-	-	-	-	-	-	-	-	-	-	-	-	-	-	-	-	-	-	-	-	-	-	-	-	-	-	-	-	
	Q4	-	-	-	-	-	-	-	-	-	-	-	-	-	-	-	-	-	-	-	-	-	-	-	-	-	-	-	-	-	-	-	

Table 24: CNF-PD χ^2 values for v across parameter quartile combinations.

		P_c	w_c	δ_p	P_p	w_p	d_p	∇B				B_v																					
		Q1	Q2	Q3	Q4	Q1	Q2	Q3	Q4	Q1	Q2	Q3	Q4	Q1	Q2	Q3	Q4	Q1	Q2	Q3	Q4	Q1	Q2	Q3	Q4								
δ_c	Q1	1.01	1.44	1.41	1.00	1.83	0.77	1.11	1.36	1.32	1.47	1.37	1.24	0.98	1.76	0.93	1.37	1.36	1.21	1.08	0.85	1.18	0.67	1.41	1.36	0.81	1.56	1.87	1.56	0.87	0.94	1.03	
	Q2	1.43	1.22	1.04	0.90	1.26	0.96	0.73	1.06	1.19	1.73	0.78	1.02	1.24	0.84	1.00	0.97	1.21	1.26	0.71	1.40	1.36	1.14	1.02	1.08	1.01	1.00	1.15	0.71	0.61	0.94	1.96	
	Q3	1.37	0.97	0.82	0.86	1.07	0.77	0.89	0.89	1.11	0.91	1.12	0.66	0.82	0.59	0.73	1.15	1.08	0.94	1.24	1.28	1.37	0.97	1.61	0.67	1.13	0.87	1.37	1.30	0.93	0.82	0.87	
	Q4	0.76	0.90	0.78	1.44	1.43	0.78	0.98	0.97	1.11	1.14	0.86	1.37	1.40	0.76	0.71	0.73	1.43	1.54	0.92	0.72	1.12	1.08	0.80	0.63	1.80	0.70	0.62	1.68	0.92			
P_c	Q1	-	-	-	-	1.28	0.91	1.01	1.12	1.02	1.02	1.00	0.80	0.58	0.97	1.04	1.13	1.17	0.64	0.56	1.12	1.00	0.87	1.57	0.63	1.54	1.41	1.29	1.37	0.45			
	Q2	-	-	-	-	1.29	0.80	0.79	0.86	1.55	1.25	1.24	1.03	1.00	1.61	0.71	0.90	1.07	1.18	0.91	1.31	1.50	1.34	0.85	1.69	1.01	0.92	1.57	1.18	0.86	1.20	1.18	0.81
	Q3	-	-	-	-	1.56	0.78	1.45	0.97	0.63	1.25	1.59	1.25	1.05	1.42	1.27	0.80	1.04	1.67	1.26	1.06	1.73	0.93	0.74	0.92	1.32	0.64	1.96	1.77	0.81			
	Q4	-	-	-	-	0.97	0.77	1.05	1.05	1.34	1.01	0.92	1.30	1.08	1.60	1.06	1.21	1.05	1.27	1.08	0.98	1.68	0.55	0.86	1.04	0.61	0.58	1.18	0.81	0.77	0.95	0.66	
w_c	Q1	-																															

		P_c				w_c				δ_p				P_p				w_p				d_p				∇B				B_v				
		Q1	Q2	Q3	Q4	Q1	Q2	Q3	Q4	Q1	Q2	Q3	Q4	Q1	Q2	Q3	Q4	Q1	Q2	Q3	Q4	Q1	Q2	Q3	Q4	Q1	Q2	Q3	Q4	Q1	Q2	Q3	Q4	
δ_c	Q1	0.93	1.49	1.37	1.09	1.03	1.36	1.17	0.79	1.30	1.69	0.87	1.58	1.00	0.91	1.30	1.02	1.45	1.27	1.23	1.26	1.19	0.98	1.54	0.42	1.10	0.66	0.59	1.26	1.06	1.51	0.78	0.85	
	Q2	0.63	0.89	1.24	1.22	0.83	0.94	1.17	1.43	0.61	1.07	0.71	1.12	0.67	0.97	0.90	1.29	0.86	1.26	1.22	1.09	0.93	1.37	0.94	0.90	1.34	1.04	0.68	1.18	0.82	0.89	0.82	1.32	
	Q3	1.24	0.64	0.82	1.25	0.65	1.72	0.99	0.85	0.91	1.01	0.94	0.97	0.79	0.82	0.91	1.31	0.63	0.98	1.09	1.63	1.14	1.67	0.99	0.77	0.97	0.89	0.85	1.14	1.57	1.79	0.77	1.29	
	Q4	0.52	0.56	0.98	1.44	0.80	0.66	1.12	1.39	0.98	1.07	1.04	1.04	0.78	0.89	0.99	0.95	0.97	0.97	0.71	0.96	1.36	0.82	0.85	0.88	0.71	1.27	0.89	1.60	0.79	0.84	1.15	0.74	0.97
P_c	Q1	-	-	-	-	1.15	0.89	1.33	0.84	0.62	1.24	0.50	1.21	1.09	1.20	0.91	1.10	1.18	0.77	0.47	0.76	0.99	1.02	1.02	0.56	1.23	0.87	1.34	0.88	0.71	1.07	0.92	0.87	
	Q2	-	-	-	-	1.27	0.67	0.59	1.14	0.92	1.15	0.57	0.81	0.97	1.06	0.72	0.31	1.27	1.00	0.49	0.87	0.75	0.75	1.03	1.02	1.39	0.59	0.97	0.76	1.70	1.14	1.16		
	Q3	-	-	-	-	1.07	1.30	0.83	1.00	0.98	1.04	1.00	0.78	0.68	1.26	1.04	1.37	1.12	1.01	0.99	0.98	0.92	0.69	0.92	1.21	1.20	0.90	0.84	1.34	1.47	0.70	0.90	1.62	
	Q4	-	-	-	-	0.95	1.02	1.12	1.23	0.95	1.21	1.30	0.89	0.90	1.18	0.88	1.45	1.08	0.94	1.27	1.04	0.92	1.22	1.59	1.25	0.73	1.41	0.93	0.97	0.77	1.05	1.05		
w_c	Q1	-	-	-	-	-	-	-	-	0.54	0.63	0.48	0.91	0.69	0.59	0.90	0.79	0.90	0.35	0.45	0.71	0.71	0.77	0.62	0.93	0.90	0.83	0.96	0.74	0.65	0.57	0.67	1.08	
	Q2	-	-	-	-	-	-	-	-	1.09	0.90	1.31	0.95	0.93	0.97	1.11	1.23	1.12	0.65	0.75	0.95	1.19	0.83	1.09	0.79	1.17	1.15	0.93	1.27	1.04	1.66	1.23	1.00	
	Q3	-	-	-	-	-	-	-	-	1.54	1.20	1.25	1.10	0.86	1.02	1.23	1.36	0.76	1.20	1.14	0.95	0.71	1.27	1.28	1.29	1.07	1.08	1.52	1.91	1.41	0.96	1.06	1.56	
	Q4	-	-	-	-	-	-	-	-	0.90	0.86	0.91	1.19	0.94	1.18	1.38	1.12	1.05	1.40	1.59	1.24	1.29	1.25	1.08	1.05	1.43	0.75	1.40	1.00	0.69	1.47	1.19	1.32	
δ_p	Q1	-	-	-	-	-	-	-	-	-	-	-	1.38	0.61	0.63	1.00	0.79	0.70	0.96	1.07	0.88	0.89	0.79	0.72	0.35	0.95	0.80	0.66	1.37	1.39	0.71	0.82		
	Q2	-	-	-	-	-	-	-	-	-	-	-	0.77	0.69	1.18	0.88	1.05	0.66	1.05	1.12	1.01	1.26	1.31	1.21	1.62	0.56	1.08	1.25	1.5	0.82	0.89	1.06		
	Q3	-	-	-	-	-	-	-	-	-	-	-	1.18	1.77	0.82	1.11	0.75	0.78	0.91	1.44	1.13	0.98	0.86	1.55	0.75	0.94	0.71	1.03	1.49	0.78	1.06	0.91		
	Q4	-	-	-	-	-	-	-	-	-	-	-	0.93	0.88	0.59	1.15	0.95	0.96	1.04	1.33	1.11	1.35	0.64	1.20	0.90	1.40	1.18	1.33	0.85	1.30	0.83	1.37		
P_p	Q1	-	-	-	-	-	-	-	-	-	-	-	-	-	-	-	-	-	0.85	1.21	0.96	1.39	-	1.05	0.93	0.65	1.29	0.52	1.08	1.11	1.25	1.84	0.92	0.91
	Q2	-	-	-	-	-	-	-	-	-	-	-	-	-	-	-	-	-	1.42	1.55	1.12	1.24	1.50	1.37	0.74	0.76	1.56	0.86	1.27	0.91	0.97	0.79	1.19	1.06
	Q3	-	-	-	-	-	-	-	-	-	-	-	-	-	-	-	-	-	1.43	0.86	1.33	0.78	0.70	1.08	1.11	0.55	0.80	0.76	0.85	1.44	1.03	1.28	1.46	1.16
	Q4	-	-	-	-	-	-	-	-	-	-	-	-	-	-	-	-	-	0.84	1.16	0.81	0.96	0.69	1.20	1.28	1.16	0.69	1.24	1.27	0.52				
w_p	Q1	-	-	-	-	-	-	-	-	-	-	-	-	-	-	-	-	-	-	-	-	-	-	-	-	-	-	-	-	-	-	-	-	
	Q2	-	-	-	-	-	-	-	-	-	-	-	-	-	-	-	-	-	-	-	-	-	-	-	-	-	-	-	-	-	-	-	-	
	Q3	-	-	-	-	-	-	-	-	-	-	-	-	-	-	-	-	-	-	-	-	-	-	-	-	-	-	-	-	-	-	-	-	
	Q4	-	-	-	-	-	-	-	-	-	-	-	-	-	-	-	-	-	-	-	-	-	-	-	-	-	-	-	-	-	-	-	-	
d_p	Q1	-	-	-	-	-	-	-	-	-	-	-	-	-	-	-	-	-	-	-	-	-	-	-	-	-	-	-	-	-	-	-	-	-
	Q2	-	-	-	-	-	-	-	-	-	-	-	-	-	-	-	-	-	-	-	-	-	-	-	-	-	-	-	-	-	-	-	-	-
	Q3	-	-	-	-	-	-	-	-	-	-	-	-	-	-	-	-	-	-	-	-	-	-	-	-	-	-	-	-	-	-	-	-	-
	Q4	-	-	-	-	-	-	-	-	-	-	-	-	-	-	-	-	-	-	-	-	-	-	-	-	-	-	-	-	-	-	-	-	-
∇B	Q1	-	-	-	-	-	-	-	-	-	-	-	-	-	-	-	-	-	-	-	-	-	-	-	-	-	-	-	-	-	-	-	-	-
	Q2	-	-	-	-	-	-	-	-	-	-	-	-	-	-	-	-	-	-	-	-	-	-	-	-	-	-	-	-	-	-	-	-	-
	Q3	-	-	-	-	-	-	-	-	-	-	-	-	-	-	-	-	-	-	-	-	-	-	-	-	-	-	-	-	-	-	-	-	-
	Q4	-	-	-	-	-	-	-	-	-	-	-	-	-	-	-	-	-	-	-	-	-	-	-	-	-	-	-	-	-	-	-	-	-

Table 26: CNF-PD χ^2 values for θ across parameter quartile combinations.

		P_c				w_c				δ_p				P_p				w_p				d_p				∇B				B_v			
		Q1	Q2	Q3	Q4	Q1	Q2	Q3	Q4	Q1	Q2	Q3	Q4	Q1	Q2	Q3	Q4	Q1	Q2	Q3	Q4	Q1	Q2	Q3	Q4	Q1	Q2	Q3	Q4	Q1	Q2	Q3	Q4
δ_c	Q1	1.36	1.05	1.12	0.59	1.72	0.59	0.89	1.08	0.92	0.74	1.41	1.36	1.00	1.14	0.95	1.24	1.09	0.89	1.02	1.60	1.18	0.72	0.93	1.12	0.57	1.13	0.93	1.20	1.06	0.93		
	Q2	0.65	0.80	0.90	1.39	1.02	0.95	0.90	1.20	1.30	1.06	1.14	0.77	0.68	1.05	0.87	1.10	0.74	0.82	0.83	1.44	0.88	0.68	1.15	0.59	1.18	1.22	0.49	0.49	0.72	0.72		
	Q3	0.64	0.80	0.82	0.80	1.17	1.07	0.88	1.16	0.42	1.67	0.85	0.72	1.12	0.73	0.70	1.04	0.74	0.75	0.86	0.88	0.77	1.14	0.95	1.47	0.69	0.65	0.97	0.61	1.17	0.99		
	Q4	0.93	0.85	0.72	1.07	0.51	0.75	1.08	0.82	0.86	0.56	0.70	0.66	1.01	0.60	0.62	0.70	0.67	0.74	0.78	0.80	0.81	0.70	0.90	0.84	0.77	0.81	1.00	1.70	1.20			

		P_c	w_c	δ_p	P_p	w_p	d_p	∇B				B_v																								
		Q1	Q2	Q3	Q4	Q1	Q2	Q3	Q4	Q1	Q2	Q3	Q4	Q1	Q2	Q3	Q4	Q1	Q2	Q3	Q4	Q1	Q2	Q3	Q4											
δ_c	Q1	1.33	1.13	1.31	1.33	0.64	1.57	0.63	0.93	1.17	1.03	1.42	1.90	1.36	1.11	1.64	0.78	1.04	1.54	1.02	1.26	1.25	0.87	1.03	1.20	1.01	1.20	1.10	0.90	0.89	0.86					
	Q2	1.31	2.35	0.94	0.98	1.67	1.02	1.03	1.22	1.24	1.49	2.19	0.80	1.77	0.85	1.36	1.03	1.75	0.86	1.44	1.05	0.91	1.56	2.04	1.41	1.17	1.54	1.26	1.17	1.46	1.36	0.87	1.49			
	Q3	1.01	1.14	1.10	1.22	0.76	0.82	0.72	0.68	0.69	1.36	0.85	1.01	0.67	1.21	0.85	1.20	0.89	0.95	1.03	1.36	1.15	0.55	1.09	1.56	1.23	1.60	1.27	0.83	1.33	1.35	1.23	0.93			
	Q4	0.77	1.17	1.17	1.99	0.76	1.02	1.14	1.20	1.01	1.35	0.54	0.79	1.02	1.56	1.01	0.61	1.06	1.20	0.99	0.61	0.74	0.79	1.24	1.13	1.42	1.18	0.94	0.96	0.91	1.23	0.85	0.63			
P_c	Q1	-	-	-	-	1.11	0.78	0.83	0.97	0.96	0.62	1.03	1.15	1.45	0.93	1.19	1.07	1.01	0.97	0.69	1.27	0.91	1.05	0.65	0.55	1.23	1.20	1.23	1.08	1.23	0.90	1.18	0.59			
	Q2	-	-	-	-	1.91	0.78	1.60	0.57	1.58	1.19	0.76	1.17	0.97	1.11	1.45	0.67	1.27	1.14	1.15	0.90	0.68	1.04	1.56	1.37	1.41	1.22	2.01	0.92	1.63	1.18	1.24	0.95			
	Q3	-	-	-	-	1.02	1.41	1.02	1.74	1.28	0.99	1.41	1.06	0.78	1.09	0.90	1.16	0.73	1.04	0.91	1.64	1.33	0.74	1.27	1.19	0.61	1.31	1.16	1.39	1.24	1.23	1.13	1.38			
	Q4	-	-	-	-	1.38	1.03	0.99	0.80	1.16	1.56	1.40	0.95	1.25	1.34	1.07	1.07	0.95	0.99	0.78	1.26	1.22	0.58	1.69	1.36	0.95	0.88	1.09	1.23	1.38	1.01	1.05	0.85			
w_c	Q1	-	-	-	-	-	-	-	-	-	1.40	0.79	1.61	0.78	0.78	0.86	0.85	1.07	1.35	0.71	0.94	1.07	0.85	0.51	1.04	1.28	1.51	1.11	0.87	0.95	1.02	0.85	0.80	1.07		
	Q2	-	-	-	-	-	-	-	-	-	1.05	0.68	1.08	1.19	0.86	0.74	1.94	0.62	0.68	0.77	0.67	1.25	1.38	0.85	1.06	1.22	1.38	1.12	0.88	0.66	1.03	1.02	0.95	0.79		
	Q3	-	-	-	-	-	-	-	-	-	1.13	1.16	1.10	1.29	0.77	1.27	1.44	0.80	1.54	0.83	1.16	0.49	0.85	0.87	1.40	0.72	1.08	1.40	0.68	1.22	1.01	0.68	1.30	0.63		
	Q4	-	-	-	-	-	-	-	-	-	0.48	1.12	1.10	0.97	0.55	0.77	1.05	1.08	1.78	1.00	0.85	0.63	0.94	0.94	1.15	0.48	0.60	0.83	0.74	0.70	0.64					
δ_p	Q1	-	-	-	-	-	-	-	-	-	-	-	-	-	-	-	0.77	1.74	1.30	1.24	0.95	1.23	1.16	1.04	1.31	1.11	0.87	1.22	1.27	0.90	1.36	0.94	0.93	1.64		
	Q2	-	-	-	-	-	-	-	-	-	-	-	-	-	-	-	0.51	0.77	1.80	1.13	1.02	0.75	1.84	1.56	1.11	0.68	1.37	1.54	1.48	0.88	0.98	1.47	1.28	0.63		
	Q3	-	-	-	-	-	-	-	-	-	-	-	-	-	-	-	2.03	0.97	0.83	1.10	0.96	1.49	1.48	1.40	1.04	1.23	1.51	1.32	2.00	0.86	1.42	0.83	1.07	1.09	1.69	1.48
	Q4	-	-	-	-	-	-	-	-	-	-	-	-	-	-	-	1.14	1.41	1.36	1.35	1.76	1.27	1.10	1.18	0.92	1.41	0.92	0.93	1.20	1.22	1.66	1.26	1.49	0.89	0.92	
P_p	Q1	-	-	-	-	-	-	-	-	-	-	-	-	-	-	-	-	-	-	-	-	-	-	-	-	-	-	-	-	-	-	-	-	-	-	
	Q2	-	-	-	-	-	-	-	-	-	-	-	-	-	-	-	-	-	-	-	-	-	-	-	-	-	-	-	-	-	-	-	-	-	-	
	Q3	-	-	-	-	-	-	-	-	-	-	-	-	-	-	-	-	-	-	-	-	-	-	-	-	-	-	-	-	-	-	-	-	-	-	
	Q4	-	-	-	-	-	-	-	-	-	-	-	-	-	-	-	-	-	-	-	-	-	-	-	-	-	-	-	-	-	-	-	-	-	-	
w_p	Q1	-	-	-	-	-	-	-	-	-	-	-	-	-	-	-	-	-	-	-	-	-	-	-	-	-	-	-	-	-	-	-	-	-	-	
	Q2	-	-	-	-	-	-	-	-	-	-	-	-	-	-	-	-	-	-	-	-	-	-	-	-	-	-	-	-	-	-	-	-	-	-	
	Q3	-	-	-	-	-	-	-	-	-	-	-	-	-	-	-	-	-	-	-	-	-	-	-	-	-	-	-	-	-	-	-	-	-	-	
	Q4	-	-	-	-	-	-	-	-	-	-	-	-	-	-	-	-	-	-	-	-	-	-	-	-	-	-	-	-	-	-	-	-	-	-	
d_p	Q1	-	-	-	-	-	-	-	-	-	-	-	-	-	-	-	-	-	-	-	-	-	-	-	-	-	-	-	-	-	-	-	-	-	-	
	Q2	-	-	-	-	-	-	-	-	-	-	-	-	-	-	-	-	-	-	-	-	-	-	-	-	-	-	-	-	-	-	-	-	-	-	
	Q3	-	-	-	-	-	-	-	-	-	-	-	-	-	-	-	-	-	-	-	-	-	-	-	-	-	-	-	-	-	-	-	-	-	-	
	Q4	-	-	-	-	-	-	-	-	-	-	-	-	-	-	-	-	-	-	-	-	-	-	-	-	-	-	-	-	-	-	-	-	-	-	
∇B	Q1	-	-	-	-	-	-	-	-	-	-	-	-	-	-	-	-	-	-	-	-	-	-	-	-	-	-	-	-	-	-	-	-	-	-	
	Q2	-	-	-	-	-	-	-	-	-	-	-	-	-	-	-	-	-	-	-	-	-	-	-	-	-	-	-	-	-	-	-	-	-	-	
	Q3	-	-	-	-	-	-	-	-	-	-	-	-	-	-	-	-	-	-	-	-	-	-	-	-	-	-	-	-	-	-	-	-	-	-	
	Q4	-	-	-	-	-	-	-	-	-	-	-	-	-	-	-	-	-	-	-	-	-	-	-	-	-	-	-	-	-	-	-	-	-	-	

Table 28: CNF-PD χ^2 values for \vec{r}_y across parameter quartile combinations.

		P_c	w_c	δ_p	P_p	w_p	d_p	∇B				B_v																					
		Q1	Q2	Q3	Q4	Q1	Q2	Q3	Q4	Q1	Q2	Q3	Q4	Q1	Q2	Q3	Q4	Q1	Q2	Q3	Q4	Q1	Q2	Q3	Q4								
δ_c	Q1	0.80	0.52	1.18	1.27	0.79	1.11	0.87	0.62	0.71	0.79	1.08	1.21	0.79	1.09	1.08	0.80	1.65	1.38	0.98	0.84	1.10	1.24	1.15	0.66	0.92	1.02	1.13	1.10	1.35			
	Q2	0.40	1.18	1.10	1.35	0.88	0.85	1.03	1.28	0.87	0.68	1.21	0.98	1.15	0.52	1.78	1.00	0.70	0.86	0.64	0.84	0.84	1.02	0.96	1.70	1.04	0.96	0.58	0.89	0.63	0.89	0.72	
	Q3	1.27	0.71	0.91	1.09	1.46	0.40	0.87	0.94	1.38	1.20	0.59	0.85	1.03	1.50	0.59	1.30	0.96	0.46	0.79	0.55	1.32	1.29	0.99	1.48	1.24	1.49	1.00	0.93	0.67	1.12		
	Q4	0.70	1.31	0.66	1.04	1.17	1.63	0.65	0.46	1.01	0.53	0.77	0.82	0.99	0.87	0.67	1.03	0.79	0.75	0.99	0.97	0.64	0.64	1.20	0.58	0.56	1.17	1.06	0.47	0.97	1.36	1.46	
P_c	Q1	-	-	-	-	0.97	0.78	0.55	0.90	0.81	1.09	1.18	0.74	0.94	0.79	1.27	1.29	0.96	0.95	0.94	0.76	1.39	1.30	0.97	0.81	1.34	0.71	1.12	0.88	0.87	1.15	1.23	
	Q2	-	-	-	-	0.94	0.92	0.84	1.01	1.02	0.99	0.83	0.66	1.03	0.80	1.05	0.84	0.99	0.96	0.67	1.46	1.04	0.93	0.63	1.21	0.90	0.87	1.07	1.25	0.62	0.98	0.86	1.31
	Q3	-	-	-	-	0.84	0.99	0.78	0.88	1.25	0.61	1.09	0.85	0.97	0.72	1.20	0.90	1.32	1.55	0.66	0.84	1.18	1.01	1.23	0.63	1.28	1.16	0.85	0.70	1.04			

		P_c				w_c				δ_p				P_p				w_p				d_p				∇B				B_v						
		Q1	Q2	Q3	Q4	Q1	Q2	Q3	Q4	Q1	Q2	Q3	Q4	Q1	Q2	Q3	Q4	Q1	Q2	Q3	Q4	Q1	Q2	Q3	Q4	Q1	Q2	Q3	Q4	Q1	Q2	Q3	Q4			
δ_c	Q1	2.51	1.05	1.11	0.88	0.95	1.46	0.83	0.61	1.59	1.66	1.09	1.35	1.18	1.10	0.73	1.67	0.92	0.75	1.33	0.69	1.25	0.78	0.91	1.17	1.46	1.20	1.19	0.99	0.89	1.47	1.11	1.12			
	Q2	1.06	0.89	1.50	0.81	1.29	1.20	1.82	0.90	1.00	1.20	1.58	0.96	1.10	0.91	1.15	1.56	0.94	0.72	1.42	0.91	0.43	1.18	1.19	1.28	0.77	1.11	0.99	1.45	1.07	1.41	1.27	1.35			
	Q3	1.86	0.89	1.22	1.05	1.21	0.53	0.66	1.02	1.51	0.91	0.63	0.87	1.30	0.83	1.36	0.95	1.54	1.03	0.82	0.96	0.93	0.99	0.92	1.44	2.09	1.07	1.12	0.76	1.51	1.51	1.27	0.58			
	Q4	1.83	1.67	1.16	1.31	1.84	1.78	1.10	1.46	2.83	1.28	1.07	1.00	2.62	1.32	1.37	1.91	1.42	1.49	1.31	2.12	1.15	1.32	1.75	3.07	2.06	0.87	2.02	1.81	1.29	1.65	2.18	1.68			
P_c	Q1	-	-	-	-	1.19	0.67	1.23	1.07	1.08	1.26	1.33	1.09	0.70	1.21	1.11	1.26	0.78	1.18	1.34	1.10	1.04	0.86	1.07	1.19	1.75	1.27	1.39	1.31	1.14	0.95	1.21	0.95			
	Q2	-	-	-	-	0.94	0.94	0.85	1.11	1.51	1.08	0.90	1.13	1.14	1.31	0.88	1.43	1.75	0.54	0.75	0.91	0.60	1.38	1.13	1.66	1.33	1.28	0.93	0.87	0.87	1.23	1.80	1.39			
	Q3	-	-	-	-	1.24	0.91	1.38	1.07	1.41	1.77	1.21	0.77	1.14	1.51	1.18	1.05	1.07	0.83	1.65	1.19	1.71	1.16	1.01	2.07	1.23	0.85	1.22	0.92	1.16	1.23					
	Q4	-	-	-	-	1.25	1.35	1.06	0.43	1.87	1.70	0.61	0.45	1.54	0.96	0.84	0.79	1.09	1.05	1.00	1.04	0.88	0.73	1.13	1.30	0.71	0.90	1.06	1.02	1.26	0.71	1.53				
w_c	Q1	-	-	-	-	-	-	-	-	1.41	1.19	0.74	0.93	0.73	0.91	0.92	1.67	1.09	1.11	1.10	0.69	1.12	1.04	1.10	1.59	0.90	1.23	0.63	1.13	1.52	1.15	1.43	1.30			
	Q2	-	-	-	-	-	-	-	-	1.11	1.12	0.76	1.03	1.06	1.14	0.97	0.99	1.01	0.74	1.06	1.08	1.01	0.79	0.90	1.10	0.88	0.75	1.17	0.92	1.11	1.70	1.19	0.75			
	Q3	-	-	-	-	-	-	-	-	1.03	1.20	1.12	0.70	0.86	0.86	1.06	1.38	0.58	1.60	0.83	1.59	1.11	0.91	1.21	1.44	0.70	0.60	1.24	2.00	1.53	1.00	0.63	0.79	1.22	0.90	1.14
	Q4	-	-	-	-	-	-	-	-	1.87	0.93	1.00	0.95	0.95	0.43	1.25	0.82	0.73	0.79	0.88	1.32	0.60	0.70	1.19	0.70	1.24	2.00	1.53	1.00	0.63	0.79	1.22	0.90	1.14		
δ_p	Q1	-	-	-	-	-	-	-	-	-	-	-	-	0.97	1.26	1.13	1.03	0.91	1.53	1.21	1.11	0.77	1.29	1.35	1.93	2.22	1.13	1.55	0.64	1.38	1.55	1.55	2.40			
	Q2	-	-	-	-	-	-	-	-	-	-	-	-	1.21	1.70	1.48	1.41	0.78	0.92	1.15	1.22	2.10	0.88	1.01	1.68	1.30	0.83	1.01	1.56	1.08	1.11	1.00	0.91			
	Q3	-	-	-	-	-	-	-	-	-	-	-	-	0.99	1.09	1.50	1.11	0.99	0.91	0.81	1.30	1.02	1.01	1.30	0.92	0.92	1.05	1.27	0.85	0.91	1.99	1.13				
	Q4	-	-	-	-	-	-	-	-	-	-	-	-	0.64	0.75	1.17	1.09	1.10	0.80	0.58	0.65	1.26	1.19	0.57	1.58	1.00	0.86	0.94	1.23	1.04	1.39	0.44				
P_p	Q1	-	-	-	-	-	-	-	-	-	-	-	-	-	-	-	-	-	-	-	-	-	-	-	-	-	-	-	-	-	-	-	-			
	Q2	-	-	-	-	-	-	-	-	-	-	-	-	-	-	-	-	-	-	-	-	-	-	-	-	-	-	-	-	-	-	-	-			
	Q3	-	-	-	-	-	-	-	-	-	-	-	-	-	-	-	-	-	-	-	-	-	-	-	-	-	-	-	-	-	-	-	-			
	Q4	-	-	-	-	-	-	-	-	-	-	-	-	-	-	-	-	-	-	-	-	-	-	-	-	-	-	-	-	-	-	-	-			
w_p	Q1	-	-	-	-	-	-	-	-	-	-	-	-	-	-	-	-	-	-	-	-	-	-	-	-	-	-	-	-	-	-	-	-			
	Q2	-	-	-	-	-	-	-	-	-	-	-	-	-	-	-	-	-	-	-	-	-	-	-	-	-	-	-	-	-	-	-	-			
	Q3	-	-	-	-	-	-	-	-	-	-	-	-	-	-	-	-	-	-	-	-	-	-	-	-	-	-	-	-	-	-	-	-			
	Q4	-	-	-	-	-	-	-	-	-	-	-	-	-	-	-	-	-	-	-	-	-	-	-	-	-	-	-	-	-	-	-	-			
d_p	Q1	-	-	-	-	-	-	-	-	-	-	-	-	-	-	-	-	-	-	-	-	-	-	-	-	-	-	-	-	-	-	-	-			
	Q2	-	-	-	-	-	-	-	-	-	-	-	-	-	-	-	-	-	-	-	-	-	-	-	-	-	-	-	-	-	-	-	-			
	Q3	-	-	-	-	-	-	-	-	-	-	-	-	-	-	-	-	-	-	-	-	-	-	-	-	-	-	-	-	-	-	-	-			
	Q4	-	-	-	-	-	-	-	-	-	-	-	-	-	-	-	-	-	-	-	-	-	-	-	-	-	-	-	-	-	-	-	-			
∇B	Q1	-	-	-	-	-	-	-	-	-	-	-	-	-	-	-	-	-	-	-	-	-	-	-	-	-	-	-	-	-	-	-	-			
	Q2	-	-	-	-	-	-	-	-	-	-	-	-	-	-	-	-	-	-	-	-	-	-	-	-	-	-	-	-	-	-	-	-			
	Q3	-	-	-	-	-	-	-	-	-	-	-	-	-	-	-	-	-	-	-	-	-	-	-	-	-	-	-	-	-	-	-	-			
	Q4	-	-	-	-	-	-	-	-	-	-	-	-	-	-	-	-	-	-	-	-	-	-	-	-	-	-	-	-	-	-	-	-			

Table 30: CNF-PD χ^2 values for ϕ across parameter quartile combinations.

		P_c				w_c				δ_p				P_p				w_p				d_p				∇B				B_v			
		Q1	Q2	Q3	Q4	Q1	Q2	Q3	Q4	Q1	Q2	Q3	Q4	Q1	Q2	Q3	Q4	Q1	Q2	Q3	Q4	Q1	Q2	Q3	Q4	Q1	Q2	Q3	Q4	Q1	Q2	Q3	Q4
δ_c	Q1	0.71	0.58	1.11	0.77	0.79	1.81	1.19	1.36	1.04	0.87	0.49	0.98	1.49	0.52	0.97	0.77	0.92	0.99	1.02	1.04	0.92	0.60	0.76	1.41	1.38	0.98	0.76	1.01	1.24	1.25	0.92	1.22
	Q2	1.14	1.22	0.90	0.60	0.88	1.26	1.54	0.94	1.28	0.69	0.77	0.75	0.94	0.58	0.94	0.90	0.78	0.96	0.92	0.56	0.76	1.06	1.45	0.82	1.29	0.86	1.02	0.88	0.30	1.28	0.76	1.12
	Q3	1.15	0.99	1.29	1.22	0.75	1.09	1.03	0.87	0.89	1.13	0.40	0.94	1.35	0.79	0.86	0.97	0.72	1.57	1.59	1.10	1.18	0.84	1.04	1.08	1.49	0.78	1.44	0.99	1.22	1.31	0.98	
	Q4	1.14	0.72	0.70	1.23	1.21	1.21	0.92	0.42	1.18	0.66	1.13	0.96	1.07	1.08	1.37	0.85	0.78	0.89	0.93	0.95	0.65	1.03	0.55	0.75	1.03	0.65	0.73	1.05	0.88	0.76	1.22	0.88
P_c	Q1	-	-	-	-	1.00	1.23	1.59	1.18	1.32	1.06	0.90	0.73	0.89	1.13	0.61	1.18	0.83	0.78	1.18	1.03	0.76	0.95	1.0									

C.3 1ODBI

C.3.1 Natural Distribution

		P_c				w_c				δ_p				P_p				w_p				d_p				∇B				B_v							
		Q1	Q2	Q3	Q4	Q1	Q2	Q3	Q4	Q1	Q2	Q3	Q4	Q1	Q2	Q3	Q4	Q1	Q2	Q3	Q4	Q1	Q2	Q3	Q4	Q1	Q2	Q3	Q4	Q1	Q2	Q3	Q4				
δ_c	Q1	0.90	0.95	0.89	0.96	1.22	1.92	1.04	1.44	0.63	0.69	1.47	0.75	1.16	1.01	1.06	0.90	1.42	0.68	1.42	1.39	1.04	1.24	1.11	1.44	1.37	0.96	1.70	1.75	1.40	1.31	0.74	0.88				
	Q2	1.14	1.11	0.78	0.97	0.81	0.66	0.91	0.95	1.06	0.69	1.07	0.91	0.61	0.68	1.04	0.83	0.87	0.81	0.57	1.27	0.95	1.36	0.90	0.93	1.11	0.98	0.77	1.50	0.69	1.05	0.73	0.97				
	Q3	0.85	1.04	0.85	1.23	1.08	1.72	0.86	0.77	0.85	1.62	0.92	1.16	0.44	0.69	0.97	0.94	0.91	0.73	1.14	0.90	1.37	1.22	0.60	0.96	0.88	0.95	0.69	0.76	0.90	0.77	0.90	0.89				
	Q4	1.20	1.13	1.12	1.29	0.85	1.20	1.27	0.96	1.09	0.54	1.14	0.74	1.23	0.78	1.49	1.07	1.07	0.84	1.27	0.86	0.84	1.07	1.28	1.31	0.90	1.21	0.85	1.01	1.17	0.90	1.50	1.05				
P_c	Q1	-	-	-	-	0.75	0.72	1.55	1.50	1.20	0.82	1.23	1.36	0.71	0.95	0.99	1.05	0.81	0.97	0.88	1.40	0.88	1.10	1.05	1.56	1.40	0.67	0.70	0.50	0.90	1.48	0.46	0.55				
	Q2	-	-	-	-	0.88	0.81	1.27	0.72	0.92	0.96	0.99	0.64	0.61	0.76	0.70	0.84	0.74	0.82	1.17	0.76	0.91	0.90	1.16	0.73	0.57	1.31	0.68	0.89	0.87	1.07	0.77	1.03				
	Q3	-	-	-	-	0.83	0.92	0.96	0.51	1.10	0.72	0.67	0.60	0.71	0.79	0.85	1.02	0.83	1.39	0.89	0.74	1.64	0.69	0.63	0.99	1.07	0.91	0.76	1.07	0.64	0.76	0.89	0.96				
	Q4	-	-	-	-	0.78	0.74	1.24	1.14	0.38	1.05	0.96	1.12	0.59	0.60	1.03	0.63	1.48	0.83	0.84	0.71	0.79	0.64	1.40	0.75	0.93	1.23	1.29	1.22	0.70	0.85	0.49	0.71				
w_c	Q1	-	-	-	-	-	-	-	-	-	-	1.12	0.93	1.47	0.79	0.68	1.40	0.99	0.72	0.71	1.00	1.15	1.19	0.72	0.88	1.45	1.29	0.70	0.73	0.52	1.20	0.72	0.74	0.68	0.82		
	Q2	-	-	-	-	-	-	-	-	-	-	0.98	1.70	1.00	0.84	0.80	0.80	1.31	1.47	1.04	1.14	1.26	1.05	0.96	1.05	0.76	1.16	1.30	1.02	1.06	1.16	0.67	0.97	0.97	0.77		
	Q3	-	-	-	-	-	-	-	-	-	-	0.51	0.89	0.83	0.77	0.82	0.90	0.88	0.76	0.86	0.87	1.30	0.84	0.72	1.11	0.83	1.35	0.70	1.22	0.86	0.93	1.11	0.71	0.95	0.86		
	Q4	-	-	-	-	-	-	-	-	-	-	0.78	0.76	0.91	0.48	0.80	1.02	1.22	0.55	1.22	0.77	0.80	1.05	1.15	1.27	0.83	0.72	0.88	1.07	1.12	0.62	0.64	1.15	0.78			
δ_p	Q1	-	-	-	-	-	-	-	-	-	-	-	-	-	-	-	-	0.65	0.97	1.06	0.99	0.72	1.35	0.97	1.04	0.68	0.91	2.28	1.73	0.76	0.96	1.23	1.02	1.68	0.84	1.00	0.89
	Q2	-	-	-	-	-	-	-	-	-	-	-	-	-	-	-	-	0.58	0.89	0.97	0.62	1.22	0.82	1.04	1.09	0.59	1.21	1.02	0.71	1.29	0.72	0.93	0.94	0.74	1.49	1.13	0.64
	Q3	-	-	-	-	-	-	-	-	-	-	-	-	-	-	-	-	0.54	1.70	1.09	0.82	0.37	1.07	0.95	0.88	0.51	0.93	0.79	0.65	1.02	0.46	0.61	0.91	0.65			
	Q4	-	-	-	-	-	-	-	-	-	-	-	-	-	-	-	-	0.70	0.72	1.06	0.96	0.75	0.79	0.78	1.61	1.54	0.82	1.18	1.02	1.40	0.76	0.62	0.96	0.82	0.74	1.04	
P_p	Q1	-	-	-	-	-	-	-	-	-	-	-	-	-	-	-	-	-	-	-	-	-	-	-	-	-	-	-	-	-	-	-	-	-	-		
	Q2	-	-	-	-	-	-	-	-	-	-	-	-	-	-	-	-	-	-	-	-	-	-	-	-	-	-	-	-	-	-	-	-	-	-		
	Q3	-	-	-	-	-	-	-	-	-	-	-	-	-	-	-	-	-	-	-	-	-	-	-	-	-	-	-	-	-	-	-	-	-	-		
	Q4	-	-	-	-	-	-	-	-	-	-	-	-	-	-	-	-	-	-	-	-	-	-	-	-	-	-	-	-	-	-	-	-	-	-		
w_p	Q1	-	-	-	-	-	-	-	-	-	-	-	-	-	-	-	-	-	-	-	-	-	-	-	-	-	-	-	-	-	-	-	-	-	-		
	Q2	-	-	-	-	-	-	-	-	-	-	-	-	-	-	-	-	-	-	-	-	-	-	-	-	-	-	-	-	-	-	-	-	-	-		
	Q3	-	-	-	-	-	-	-	-	-	-	-	-	-	-	-	-	-	-	-	-	-	-	-	-	-	-	-	-	-	-	-	-	-	-		
	Q4	-	-	-	-	-	-	-	-	-	-	-	-	-	-	-	-	-	-	-	-	-	-	-	-	-	-	-	-	-	-	-	-	-	-		
d_p	Q1	-	-	-	-	-	-	-	-	-	-	-	-	-	-	-	-	-	-	-	-	-	-	-	-	-	-	-	-	-	-	-	-	-	-		
	Q2	-	-	-	-	-	-	-	-	-	-	-	-	-	-	-	-	-	-	-	-	-	-	-	-	-	-	-	-	-	-	-	-	-	-		
	Q3	-	-	-	-	-	-	-	-	-	-	-	-	-	-	-	-	-	-	-	-	-	-	-	-	-	-	-	-	-	-	-	-	-	-		
	Q4	-	-	-	-	-	-	-	-	-	-	-	-	-	-	-	-	-	-	-	-	-	-	-	-	-	-	-	-	-	-	-	-	-	-		
∇B	Q1	-	-	-	-	-	-	-	-	-	-	-	-	-	-	-	-	-	-	-	-	-	-	-	-	-	-	-	-	-	-	-	-	-	-		
	Q2	-	-	-	-	-	-	-	-	-	-	-	-	-	-	-	-	-	-	-	-	-	-	-	-	-	-	-	-	-	-	-	-	-	-		
	Q3	-	-	-	-	-	-	-	-	-	-	-	-	-	-	-	-	-	-	-	-	-	-	-	-	-	-	-	-	-	-	-	-	-	-		
	Q4	-	-	-	-	-	-	-	-	-	-	-	-	-	-	-	-	-	-	-	-	-	-	-	-	-	-	-	-	-	-	-	-	-	-		

Table 32: 1ODBI χ^2 values for \vec{r}_x across parameter quartile combinations.

		P_c				w_c				δ_p				P_p				w_p				d_p				∇B				B_v			
		Q1	Q2	Q3	Q4	Q1	Q2	Q3	Q4	Q1	Q2	Q3	Q4	Q1	Q2	Q3	Q4	Q1	Q2	Q3	Q4	Q1	Q2	Q3	Q4	Q1	Q2	Q3	Q4	Q1	Q2	Q3	Q4
δ_c	Q1	0.84	0.58	0.75	1.02	0.77	0.91	0.58	0.95	1.16	0.86	1.37	0.96	0.99	1.33	1.18	0.35	0.77	0.56	1.01	1.04	1.31	1.51	0.69	1.28	1.05	1.09	0.79	1.26	0.68	1.23	1.38	0.84
	Q2	1.04	1.50	1.14	0.77	1.21	0.50	0.92	0.95	1.04	1.00	0.53	1.45	0.89	1.14	0.96	0.87	1.09	1.27	0.96	0.86	1.21	0.66	0.73	0.48	1.21	0.93	0.95	0.80	1.13	0.71	1.17	0.89
	Q3	0.73	1.02	0.94	0.81	0.97	1.21	0.89	0.66	0.83	0.79	0.85	1.13	0.87	1.07	0.64	1.15	1.06	1.06	0.80	0.65	0.52	0.92	1.10	0.98	0.65	0.81	1.15	0.56	0.69	0.47	1.31	
	Q4	0.60	0.99	0.84	1.49	0.74	1.50	1.14	0.94	1.01	0.81	0.74	1.17	0.87	1.17	0.75	1.14	0.92	0.74	1.11													

		P_c				w_c				δ_p				P_p				w_p				d_p				∇B				B_v						
		Q1	Q2	Q3	Q4	Q1	Q2	Q3	Q4	Q1	Q2	Q3	Q4	Q1	Q2	Q3	Q4	Q1	Q2	Q3	Q4	Q1	Q2	Q3	Q4	Q1	Q2	Q3	Q4	Q1	Q2	Q3	Q4			
δ_c	Q1	0.88	1.14	0.88	0.95	1.07	0.59	1.58	0.64	0.59	1.35	1.03	0.57	0.43	0.80	1.01	0.72	1.52	0.93	0.80	0.54	1.05	1.73	0.89	1.17	0.79	1.25	0.66	0.86	0.67	1.16	0.96	0.58			
	Q2	0.98	0.48	1.23	1.03	0.55	1.25	0.88	0.81	0.72	0.98	1.13	1.05	0.83	0.81	0.48	1.51	0.94	0.62	0.92	1.34	1.03	1.26	1.24	0.53	1.11	0.51	0.72	0.99	0.72	0.87	1.04	1.38			
	Q3	0.89	0.66	0.39	0.71	0.75	0.99	0.97	1.20	1.28	1.13	0.66	0.94	0.73	0.85	0.80	0.65	0.92	0.91	0.94	0.43	1.03	1.11	0.55	0.66	0.68	1.34	0.70	1.06	0.53	1.03	0.75	0.69			
	Q4	1.19	0.71	0.61	1.16	0.88	1.20	0.75	0.87	0.87	0.80	0.78	1.04	1.23	0.73	0.62	0.78	0.87	0.85	0.70	0.58	1.20	1.07	1.07	1.44	0.55	1.08	0.96	0.97	1.14	1.03	0.51	0.63			
P_c	Q1	-	-	-	-	0.79	0.87	0.67	1.07	0.97	0.80	0.61	0.46	0.72	0.89	0.72	0.62	0.89	0.96	0.67	0.66	0.99	1.93	0.67	0.90	0.78	0.81	0.67	0.81	1.07	1.12	1.25	1.16			
	Q2	-	-	-	-	1.04	1.19	0.46	0.98	0.92	1.17	0.84	0.63	1.24	0.82	0.69	0.70	1.15	1.17	0.80	0.79	0.80	0.77	1.02	0.64	0.95	0.82	0.71	1.13	0.55	0.64	1.02	0.91			
	Q3	-	-	-	-	0.81	0.93	0.66	0.62	0.81	1.09	0.69	0.85	1.09	0.94	0.68	0.54	1.46	0.80	1.17	0.34	1.37	1.18	0.69	0.66	0.53	0.44	0.91	0.68	0.57	1.29	0.77	1.00			
	Q4	-	-	-	-	1.30	1.04	1.25	1.04	0.62	0.52	1.04	1.25	1.11	0.79	1.06	1.08	0.95	0.79	0.86	1.10	0.77	2.04	0.82	1.26	0.65	1.18	0.93	0.65	0.94	0.89	0.88				
w_c	Q1	-	-	-	-	-	-	-	-	0.62	0.96	0.63	0.83	0.54	0.68	0.77	0.94	0.69	0.93	1.16	0.43	0.80	0.67	0.90	0.95	1.00	0.67	0.68	0.74	0.94	0.82	0.46	0.99			
	Q2	-	-	-	-	-	-	-	-	0.88	1.08	0.71	0.93	1.27	0.87	0.97	1.11	1.05	0.68	0.81	0.58	1.07	0.76	0.62	1.45	1.40	1.42	0.83	0.74	0.71	1.49	0.74	0.49			
	Q3	-	-	-	-	-	-	-	-	0.76	1.35	0.78	0.46	1.31	0.95	1.02	0.70	1.65	0.71	0.52	0.56	0.73	0.94	1.26	0.55	0.72	0.70	0.91	1.16	0.78	1.01	0.52	0.98			
	Q4	-	-	-	-	-	-	-	-	1.04	0.96	0.59	1.10	0.52	0.51	1.17	0.69	0.95	0.50	0.61	0.44	1.04	1.51	0.42	1.34	0.92	0.77	0.63	0.67	1.13	0.64	1.08	1.12			
δ_p	Q1	-	-	-	-	-	-	-	-	-	-	-	-	-	-	-	-	-	-	-	-	-	-	-	-	-	-	-	-	-	-	-	-	-	-	-
	Q2	-	-	-	-	-	-	-	-	-	-	-	-	-	-	-	-	-	-	-	-	-	-	-	-	-	-	-	-	-	-	-	-	-	-	-
	Q3	-	-	-	-	-	-	-	-	-	-	-	-	-	-	-	-	-	-	-	-	-	-	-	-	-	-	-	-	-	-	-	-	-	-	-
	Q4	-	-	-	-	-	-	-	-	-	-	-	-	-	-	-	-	-	-	-	-	-	-	-	-	-	-	-	-	-	-	-	-	-	-	-
P_p	Q1	-	-	-	-	-	-	-	-	-	-	-	-	-	-	-	-	-	-	-	-	-	-	-	-	-	-	-	-	-	-	-	-	-	-	-
	Q2	-	-	-	-	-	-	-	-	-	-	-	-	-	-	-	-	-	-	-	-	-	-	-	-	-	-	-	-	-	-	-	-	-	-	-
	Q3	-	-	-	-	-	-	-	-	-	-	-	-	-	-	-	-	-	-	-	-	-	-	-	-	-	-	-	-	-	-	-	-	-	-	-
	Q4	-	-	-	-	-	-	-	-	-	-	-	-	-	-	-	-	-	-	-	-	-	-	-	-	-	-	-	-	-	-	-	-	-	-	-
w_p	Q1	-	-	-	-	-	-	-	-	-	-	-	-	-	-	-	-	-	-	-	-	-	-	-	-	-	-	-	-	-	-	-	-	-	-	-
	Q2	-	-	-	-	-	-	-	-	-	-	-	-	-	-	-	-	-	-	-	-	-	-	-	-	-	-	-	-	-	-	-	-	-	-	-
	Q3	-	-	-	-	-	-	-	-	-	-	-	-	-	-	-	-	-	-	-	-	-	-	-	-	-	-	-	-	-	-	-	-	-	-	-
	Q4	-	-	-	-	-	-	-	-	-	-	-	-	-	-	-	-	-	-	-	-	-	-	-	-	-	-	-	-	-	-	-	-	-	-	-
d_p	Q1	-	-	-	-	-	-	-	-	-	-	-	-	-	-	-	-	-	-	-	-	-	-	-	-	-	-	-	-	-	-	-	-	-	-	-
	Q2	-	-	-	-	-	-	-	-	-	-	-	-	-	-	-	-	-	-	-	-	-	-	-	-	-	-	-	-	-	-	-	-	-	-	-
	Q3	-	-	-	-	-	-	-	-	-	-	-	-	-	-	-	-	-	-	-	-	-	-	-	-	-	-	-	-	-	-	-	-	-	-	-
	Q4	-	-	-	-	-	-	-	-	-	-	-	-	-	-	-	-	-	-	-	-	-	-	-	-	-	-	-	-	-	-	-	-	-	-	-
∇B	Q1	-	-	-	-	-	-	-	-	-	-	-	-	-	-	-	-	-	-	-	-	-	-	-	-	-	-	-	-	-	-	-	-	-	-	-
	Q2	-	-	-	-	-	-	-	-	-	-	-	-	-	-	-	-	-	-	-	-	-	-	-	-	-	-	-	-	-	-	-	-	-	-	-
	Q3	-	-	-	-	-	-	-	-	-	-	-	-	-	-	-	-	-	-	-	-	-	-	-	-	-	-	-	-	-	-	-	-	-	-	-
	Q4	-	-	-	-	-	-	-	-	-	-	-	-	-	-	-	-	-	-	-	-	-	-	-	-	-	-	-	-	-	-	-	-	-	-	-

Table 34: $1ODBI \chi^2$ values for v across parameter quartile combinations.

		P_c				w_c				δ_p				P_p				w_p				d_p				∇B				B_v			
		Q1	Q2	Q3	Q4	Q1	Q2	Q3	Q4	Q1	Q2	Q3	Q4	Q1	Q2	Q3	Q4	Q1	Q2	Q3	Q4	Q1	Q2	Q3	Q4	Q1	Q2	Q3	Q4	Q1	Q2	Q3	Q4
δ_c	Q1	1.20	0.80	1.02	0.63	0.99	0.53	0.67	0.94	1.56	0.95	0.72	0.86	0.83	1.19	1.09	0.97	1.04	0.84	0.87	0.82	0.83	0.81	0.68	1.08	0.97	0.56	1.01	0.87	0.80	0.65	0.87	0.55
	Q2	0.71	0.53	0.87	1.08	0.78	0.84	1.16	1.01	1.35	0.84	1.01	0.62	1.08	0.66	0.79	0.84	0.65	1.31	0.79	1.09	0.71	0.72	0.68	0.80	0.88	1.03	0.76	0.92	1.00	1.10	0.59	0.79
	Q3	0.90	1.08	0.70	1.02	1.10	0.84	1.12	1.30	1.56	0.59	1.11	0.98	0.87	0.72	1.03	0.78	1.03	0.80	1.24	1.21	1.09	0.96	0.98	0.87	1.30	0.70	0.68	1.59	1.12	0.52	0.52	
	Q4	1.11	0.72	0.94	0.97	1.25	1.30	0.98	0.70	1.18	1.74	0.89	0.83	0.76	1.11	0.60	1.15	1.02	0.98	1.06	0.81	0.61	1.15	0.81	0.75	0.88	1.07	0.82	0.86	0.50	1.24	1.26	
P_c	Q1	-	-	-	-	1.28	0.82	1.11	1.20	0.82	0.98	0.96	0.98	1.12	0.82	0.76	0.76	0.82	0.94	0.91	0.89	0.67	1.46	0.84	1.15	1.30	0.47</td						

		P_c				w_c				δ_p				P_p				w_p				d_p				∇B				B_v					
		Q1	Q2	Q3	Q4	Q1	Q2	Q3	Q4	Q1	Q2	Q3	Q4	Q1	Q2	Q3	Q4	Q1	Q2	Q3	Q4	Q1	Q2	Q3	Q4	Q1	Q2	Q3	Q4	Q1	Q2	Q3	Q4		
δ_c	Q1	0.87	1.04	0.88	1.14	0.71	0.82	1.30	0.83	0.87	0.89	0.73	0.88	1.78	0.96	0.60	0.69	1.20	1.04	1.14	0.74	1.40	1.20	1.15	0.91	0.92	0.64	0.85	1.23	1.11	0.77	0.74	0.70		
	Q2	0.63	1.16	0.87	1.28	0.70	0.77	1.10	1.24	0.60	0.70	0.63	0.93	0.35	0.55	1.32	1.08	0.65	0.98	1.54	0.90	0.79	0.75	0.91	1.13	0.72	0.73	1.02	1.19	0.74	0.79	1.04	1.08		
	Q3	1.19	0.67	0.81	1.25	1.08	1.84	0.98	0.83	1.19	0.92	1.17	0.91	1.25	1.38	1.12	1.24	1.08	0.87	1.46	0.63	1.23	1.41	0.62	1.15	1.23	0.58	1.19	0.73	1.39	1.24	1.24	1.02		
	Q4	0.77	0.43	0.98	0.78	0.93	0.78	0.83	0.60	0.79	0.74	1.34	1.15	0.88	1.55	0.79	1.01	0.79	0.83	1.60	0.64	1.02	1.18	0.95	0.89	0.87	0.92	1.28	0.99	1.22	0.70	0.88	0.87		
P_c	Q1	-	-	-	-	0.57	0.43	0.79	1.08	1.06	0.68	0.59	0.77	0.99	0.77	0.69	1.36	0.90	1.14	0.66	0.31	1.77	0.91	0.79	0.97	1.19	1.07	0.67	0.96	0.86	1.05	1.08	0.86	1.05	
	Q2	-	-	-	-	0.79	1.31	0.67	0.69	1.05	1.32	1.06	0.69	1.22	1.19	0.75	0.42	0.75	0.85	0.85	0.39	0.65	0.64	0.48	1.01	0.70	0.73	0.95	1.54	0.88	0.55	-	-		
	Q3	-	-	-	-	0.93	0.67	0.57	1.52	0.96	0.70	0.69	0.82	1.27	1.89	1.45	0.88	1.68	0.61	0.98	0.92	1.20	0.99	1.02	1.15	0.98	0.90	1.03	1.32	1.99	1.20	1.09	0.74	-	
	Q4	-	-	-	-	1.10	1.25	1.38	1.01	0.97	0.74	1.45	1.22	0.86	0.56	0.80	1.20	0.75	0.88	1.00	1.11	0.76	1.18	1.13	0.80	0.59	0.96	0.88	1.87	1.13	0.53	1.14	0.82	-	
w_c	Q1	-	-	-	-	-	-	-	-	0.78	1.17	0.90	1.09	1.18	0.76	1.41	0.68	0.58	0.78	1.08	1.02	1.01	0.64	0.66	1.43	0.98	0.37	0.78	0.83	1.56	1.12	0.83	1.33	-	
	Q2	-	-	-	-	-	-	-	-	0.70	0.54	0.91	0.77	0.94	1.28	0.60	0.67	1.05	0.91	1.42	0.53	1.28	0.67	0.92	0.69	0.85	1.15	1.01	0.94	0.74	0.52	0.69	0.51	-	-
	Q3	-	-	-	-	-	-	-	-	0.79	0.75	1.08	1.24	0.77	1.09	0.83	1.05	1.05	0.63	1.09	0.81	1.46	0.90	0.98	0.61	0.69	0.61	1.73	1.22	0.74	0.91	1.42	-		
	Q4	-	-	-	-	-	-	-	-	0.93	1.02	0.83	1.13	1.17	1.18	0.78	0.94	1.36	0.65	1.48	0.45	1.17	1.01	0.99	1.04	0.85	1.01	1.20	0.86	1.29	1.79	0.65	1.07	-	
δ_p	Q1	-	-	-	-	-	-	-	-	-	-	-	-	0.97	1.16	0.72	0.82	1.00	0.99	0.73	1.17	0.64	1.06	0.85	0.55	0.79	1.23	0.95	0.84	1.17	0.91	1.01	0.65	-	
	Q2	-	-	-	-	-	-	-	-	-	-	-	-	0.63	1.06	1.12	0.74	0.74	0.72	0.68	0.71	1.30	1.71	1.57	1.13	0.97	0.63	0.78	0.99	1.02	0.55	1.36	0.94	-	
	Q3	-	-	-	-	-	-	-	-	-	-	-	-	0.95	0.91	0.56	1.09	0.80	0.66	0.84	1.10	1.46	0.70	0.60	1.48	0.77	0.74	1.05	1.29	1.49	1.01	0.61	0.74	-	
	Q4	-	-	-	-	-	-	-	-	-	-	-	-	1.13	1.27	0.56	0.83	1.12	1.22	1.33	0.75	0.67	1.17	1.35	0.99	0.63	1.38	0.82	1.20	0.95	1.13	1.01	1.12	-	
P_p	Q1	-	-	-	-	-	-	-	-	-	-	-	-	-	-	-	-	-	-	-	-	-	-	-	-	-	-	-	-	-	-	-	-	-	
	Q2	-	-	-	-	-	-	-	-	-	-	-	-	-	-	-	-	-	-	-	-	-	-	-	-	-	-	-	-	-	-	-	-	-	
	Q3	-	-	-	-	-	-	-	-	-	-	-	-	-	-	-	-	-	-	-	-	-	-	-	-	-	-	-	-	-	-	-	-	-	
	Q4	-	-	-	-	-	-	-	-	-	-	-	-	-	-	-	-	-	-	-	-	-	-	-	-	-	-	-	-	-	-	-	-	-	
w_p	Q1	-	-	-	-	-	-	-	-	-	-	-	-	-	-	-	-	-	-	-	-	-	-	-	-	-	-	-	-	-	-	-	-	-	
	Q2	-	-	-	-	-	-	-	-	-	-	-	-	-	-	-	-	-	-	-	-	-	-	-	-	-	-	-	-	-	-	-	-	-	
	Q3	-	-	-	-	-	-	-	-	-	-	-	-	-	-	-	-	-	-	-	-	-	-	-	-	-	-	-	-	-	-	-	-	-	
	Q4	-	-	-	-	-	-	-	-	-	-	-	-	-	-	-	-	-	-	-	-	-	-	-	-	-	-	-	-	-	-	-	-	-	
d_p	Q1	-	-	-	-	-	-	-	-	-	-	-	-	-	-	-	-	-	-	-	-	-	-	-	-	-	-	-	-	-	-	-	-	-	
	Q2	-	-	-	-	-	-	-	-	-	-	-	-	-	-	-	-	-	-	-	-	-	-	-	-	-	-	-	-	-	-	-	-	-	
	Q3	-	-	-	-	-	-	-	-	-	-	-	-	-	-	-	-	-	-	-	-	-	-	-	-	-	-	-	-	-	-	-	-	-	
	Q4	-	-	-	-	-	-	-	-	-	-	-	-	-	-	-	-	-	-	-	-	-	-	-	-	-	-	-	-	-	-	-	-	-	
∇B	Q1	-	-	-	-	-	-	-	-	-	-	-	-	-	-	-	-	-	-	-	-	-	-	-	-	-	-	-	-	-	-	-	-	-	
	Q2	-	-	-	-	-	-	-	-	-	-	-	-	-	-	-	-	-	-	-	-	-	-	-	-	-	-	-	-	-	-	-	-	-	
	Q3	-	-	-	-	-	-	-	-	-	-	-	-	-	-	-	-	-	-	-	-	-	-	-	-	-	-	-	-	-	-	-	-	-	
	Q4	-	-	-	-	-	-	-	-	-	-	-	-	-	-	-	-	-	-	-	-	-	-	-	-	-	-	-	-	-	-	-	-	-	

Table 36: $10DBI \chi^2$ values for θ across parameter quartile combinations.

C.3.2 Adaptive Sampling

		P_c				w_c				δ_p				P_p				w_p				d_p				∇B				B_v			
		Q1	Q2	Q3	Q4	Q1	Q2	Q3	Q4	Q1	Q2	Q3	Q4	Q1	Q2	Q3	Q4	Q1	Q2	Q3	Q4	Q1	Q2	Q3	Q4	Q1	Q2	Q3	Q4	Q1	Q2	Q3	Q4
δ_c	Q1	1.16	0.95	0.75	0.73	0.89	0.72	0.69	1.05	1.28	0.85	0.97	1.25	0.98	1.09	1.18	1.08	1.28	0.81	1.11	1.25	1.04	0.74	0.59	1.11	1.17	0.99	1.05	1.01	0.91	0.99	0.72	
	Q2	1.27	1.07	0.54	0.68	0.87	1.12	0.79	1.10	1.34	0.81	0.78	0.76	1.39	0.87	1.11	1.63	0.74	0.90	0.76	0.79	1.33	0.63	0.91	0.95	1.16	0.62	0.89	1.09	1.08	1.10	0.62	
	Q3	1.08	1.30	0.64	0.85	1.24	0.81	0.46	0.84	0.90	0.99	0.59	1.10	0.78	1.11	0.86	1.11	1.34	0.80	0.94	0.90	0.64	0.57	0.85	0.94	0.85	0.73	0.67	0.45	0.55	1.07	0.45	
	Q4	0.97	1.01	1.02	0.47	0.90	1.61	0.96	0.83	1.11	0.71	0.61	1.23	0.84	0.52	1.07	1.45	1.35	1.04	1.34	0.84	1.51	0.61	1.48	0.90	0.84	1.15	1.73	0.76	1.20	0.78	1.62	1.23
P_c	Q1	-	-	-																													

Table 38: $10DBI \chi^2$ values for \vec{r}_y across parameter quartile combinations.

Table 39: $10DBI$ χ^2 values for v across parameter quartile combinations.

		P_c				w_c				δ_p				P_p				w_p				d_p				∇B				B_v					
		Q1	Q2	Q3	Q4	Q1	Q2	Q3	Q4	Q1	Q2	Q3	Q4	Q1	Q2	Q3	Q4	Q1	Q2	Q3	Q4	Q1	Q2	Q3	Q4	Q1	Q2	Q3	Q4	Q1	Q2	Q3	Q4		
δ_c	Q1	0.82	0.78	1.07	1.12	1.31	0.77	1.18	0.94	1.23	1.26	0.72	0.75	0.63	0.64	0.76	0.70	0.85	1.01	1.27	0.82	0.97	0.65	0.80	0.88	0.84	1.72	0.38	0.77	0.93	1.11	0.76	0.70		
	Q2	1.23	1.22	0.97	0.81	1.16	0.83	1.35	0.94	0.82	0.98	1.78	1.22	1.58	1.01	0.97	1.00	1.09	0.95	1.43	0.68	0.90	0.90	1.16	0.85	1.04	0.55	1.24	1.03	0.80	1.02	1.25	0.81		
	Q3	0.87	1.22	1.00	1.36	0.89	0.98	0.85	0.92	1.66	0.32	1.00	1.00	0.67	0.84	1.64	1.38	0.75	1.07	0.96	0.85	1.17	0.76	0.82	1.07	0.79	0.69	1.26	0.60	0.75	1.30	1.37	0.32		
	Q4	0.88	1.04	0.87	1.05	1.01	1.15	0.87	0.60	1.55	1.56	0.71	1.13	1.12	1.53	1.57	0.76	0.98	0.93	0.76	1.19	0.94	0.50	1.28	1.32	1.77	1.46	1.35	1.02	1.48	1.56	0.72	1.03		
P_c	Q1	-	-	-	-	0.87	0.97	0.93	1.04	0.80	1.12	1.04	1.40	1.05	0.72	1.42	1.04	0.75	1.25	1.11	0.67	1.42	0.67	1.15	0.88	0.92	0.52	1.20	1.12	0.80	1.77	0.77	0.80		
	Q2	-	-	-	-	1.11	1.29	0.73	0.47	0.88	0.81	0.81	0.87	0.79	1.33	1.16	1.37	0.88	0.92	0.90	1.03	0.94	0.61	1.10	0.88	0.90	0.80	0.54	1.03	0.99	0.74	0.83	0.83		
	Q3	-	-	-	-	1.24	0.83	0.96	0.89	1.68	1.45	0.86	1.22	1.56	1.29	0.89	0.75	0.62	0.89	1.16	0.80	0.97	0.95	1.63	1.17	0.81	1.11	1.18	0.82	1.28	0.66	0.83			
	Q4	-	-	-	-	1.31	1.03	0.99	0.85	1.49	1.41	0.48	1.52	1.16	0.99	1.48	0.69	0.78	0.86	1.26	1.10	0.76	1.30	1.07	1.05	1.21	1.32	1.10	0.84	0.37	1.07	0.91	1.56		
w_c	Q1	-	-	-	-	-	-	-	-	1.32	1.26	0.96	1.18	0.80	1.75	1.38	0.34	0.96	0.85	1.20	0.83	0.83	0.77	1.58	1.12	0.90	1.16	1.22	1.30	1.30	1.28	0.87	0.91		
	Q2	-	-	-	-	-	-	-	-	0.53	0.79	1.09	1.14	1.24	0.92	0.99	1.01	0.69	1.04	0.95	0.49	0.80	0.64	0.50	1.71	0.88	0.96	0.77	0.92	1.18	1.01	0.92	1.02		
	Q3	-	-	-	-	-	-	-	-	1.50	1.03	0.61	0.85	0.73	1.40	0.84	0.98	1.23	1.34	0.83	0.90	0.99	1.03	0.90	1.44	1.19	1.31	0.85	0.96	0.75	1.21	1.14	0.94		
	Q4	-	-	-	-	-	-	-	-	1.46	0.62	1.48	0.62	0.70	1.02	1.09	1.35	0.47	0.74	0.92	1.07	0.74	0.66	0.87	1.11	0.63	1.40	0.90	1.25						
δ_p	Q1	-	-	-	-	-	-	-	-	-	-	-	-	-	0.71	1.59	1.17	1.12	0.76	1.00	1.34	1.23	0.66	1.16	1.36	0.84	1.16	0.97	1.50	0.89	1.43	1.52	1.16	0.84	1.11
	Q2	-	-	-	-	-	-	-	-	-	-	-	-	-	1.66	0.84	0.57	0.91	0.86	0.93	1.10	1.33	1.57	0.86	1.40	0.69	0.85	0.69	1.18	1.79	0.73	0.79	0.66	0.68	
	Q3	-	-	-	-	-	-	-	-	-	-	-	-	-	0.88	0.94	1.26	0.94	0.75	0.81	0.95	0.79	1.10	0.48	0.89	0.93	0.72	0.88	1.11	0.94	0.93	0.82	1.27	1.04	
	Q4	-	-	-	-	-	-	-	-	-	-	-	-	-	0.59	1.14	1.55	0.95	0.93	0.82	1.21	1.72	1.07	0.61	1.06	1.10	1.29	0.74	0.63	0.74	0.83	1.34	0.74		
P_p	Q1	-	-	-	-	-	-	-	-	-	-	-	-	-	-	-	-	-	-	-	-	-	-	-	-	-	-	-	-	-	-	-	-		
	Q2	-	-	-	-	-	-	-	-	-	-	-	-	-	-	-	-	-	-	-	-	-	-	-	-	-	-	-	-	-	-	-	-		
	Q3	-	-	-	-	-	-	-	-	-	-	-	-	-	-	-	-	-	-	-	-	-	-	-	-	-	-	-	-	-	-	-	-		
	Q4	-	-	-	-	-	-	-	-	-	-	-	-	-	-	-	-	-	-	-	-	-	-	-	-	-	-	-	-	-	-	-	-		
w_p	Q1	-	-	-	-	-	-	-	-	-	-	-	-	-	-	-	-	-	-	-	-	-	-	-	-	-	-	-	-	-	-	-	-		
	Q2	-	-	-	-	-	-	-	-	-	-	-	-	-	-	-	-	-	-	-	-	-	-	-	-	-	-	-	-	-	-	-	-		
	Q3	-	-	-	-	-	-	-	-	-	-	-	-	-	-	-	-	-	-	-	-	-	-	-	-	-	-	-	-	-	-	-	-		
	Q4	-	-	-	-	-	-	-	-	-	-	-	-	-	-	-	-	-	-	-	-	-	-	-	-	-	-	-	-	-	-	-	-		
d_p	Q1	-	-	-	-	-	-	-	-	-	-	-	-	-	-	-	-	-	-	-	-	-	-	-	-	-	-	-	-	-	-	-	-		
	Q2	-	-	-	-	-	-	-	-	-	-	-	-	-	-	-	-	-	-	-	-	-	-	-	-	-	-	-	-	-	-	-	-		
	Q3	-	-	-	-	-	-	-	-	-	-	-	-	-	-	-	-	-	-	-	-	-	-	-	-	-	-	-	-	-	-	-	-		
	Q4	-	-	-	-	-	-	-	-	-	-	-	-	-	-	-	-	-	-	-	-	-	-	-	-	-	-	-	-	-	-	-	-		
∇B	Q1	-	-	-	-	-	-	-	-	-	-	-	-	-	-	-	-	-	-	-	-	-	-	-	-	-	-	-	-	-	-	-	-		
	Q2	-	-	-	-	-	-	-	-	-	-	-	-	-	-	-	-	-	-	-	-	-	-	-	-	-	-	-	-	-	-	-	-		
	Q3	-	-	-	-	-	-	-	-	-	-	-	-	-	-	-	-	-	-	-	-	-	-	-	-	-	-	-	-	-	-	-	-		
	Q4	-	-	-	-	-	-	-	-	-	-	-	-	-	-	-	-	-	-	-	-	-	-	-	-	-	-	-	-	-	-	-	-		

Table 40: 1ODBI χ^2 values for ϕ across parameter quartile combinations.

		P_c				w_c				δ_p				P_p				w_p				d_p				∇B				B_v			
		Q1	Q2	Q3	Q4	Q1	Q2	Q3	Q4	Q1	Q2	Q3	Q4	Q1	Q2	Q3	Q4	Q1	Q2	Q3	Q4	Q1	Q2	Q3	Q4	Q1	Q2	Q3	Q4	Q1	Q2	Q3	Q4
δ_c	Q1	0.66	0.78	0.98	0.69	1.34	1.42	1.29	0.83	1.03	0.70	1.00	0.53	1.26	1.25	1.32	0.90	0.87	1.22	1.02	0.97	1.33	0.88	0.77	0.85	1.04	1.29	0.89	0.74	0.63	1.07	0.40	0.96
	Q2	0.68	0.80	0.87	0.91	0.73	1.09	1.34	0.87	0.90	0.89	1.22	0.83	0.91	0.64	1.53	0.60	0.52	1.09	0.67	0.93	0.42	1.00	1.29	0.79	0.80	0.64	0.91	0.83	1.08	0.71	0.73	1.22
	Q3	0.60	1.34	1.35	1.12	0.66	0.97	0.79	0.71	0.95	0.84	0.88	0.81	1.35	1.77	1.05	1.00	1.42	1.28	1.32	1.15	1.17	0.99	0.95	1.34	1.30	1.75	0.75	0.95	0.87	1.15	0.9	0.66
	Q4	1.38	0.83	0.88	1.17	1.10	0.61	0.83	0.80	0.62	1.76	0.91	0.97	1.36	1.24	0.86	0.80	1.32	1.48	1.22	1.23	1.14	1.10	0.91	0.81	1.43	1.11	0.40	1.76	1.90	0.90		
P_c	Q1	-	-	-	-	0.59	0.71	0.79	1.00	1.30	0.82	0.97	0.70	0.62	0.95	1.00	1.20	0.45	1.24	1.41	1.29	1.10	0.62	0.63	1.85	0.81	1.						

C.4 2ODBI

C.4.1 Natural Distribution

		P_c				w_c				δ_p				P_p				w_p				d_p				∇B				B_v			
		Q1	Q2	Q3	Q4	Q1	Q2	Q3	Q4	Q1	Q2	Q3	Q4	Q1	Q2	Q3	Q4	Q1	Q2	Q3	Q4	Q1	Q2	Q3	Q4	Q1	Q2	Q3	Q4	Q1	Q2	Q3	Q4
δ_c	Q1	0.69	0.73	1.51	0.78	1.07	1.52	0.84	0.94	0.84	0.80	1.77	1.27	0.88	0.99	0.49	0.70	0.87	0.82	1.50	0.95	1.25	0.84	0.72	1.44	0.65	0.79	0.91	1.74	1.07	0.92	0.92	0.76
	Q2	0.61	1.09	0.73	0.68	0.75	1.03	0.57	0.74	1.07	0.91	1.24	0.83	0.50	0.85	1.24	0.71	1.14	0.76	0.50	0.82	0.66	1.12	0.63	1.47	1.13	0.90	0.67	1.21	0.77	1.32	0.76	0.74
	Q3	0.80	0.83	1.03	1.28	0.68	1.44	0.81	0.88	0.86	1.45	1.24	1.13	0.64	0.82	0.93	1.17	0.75	0.73	1.25	1.04	1.17	1.29	0.65	0.88	1.02	0.93	0.88	0.65	0.86	0.70	0.71	0.85
	Q4	1.32	0.87	0.88	0.80	1.05	1.20	0.66	0.73	0.92	0.68	0.75	0.89	0.59	0.73	0.95	1.39	1.12	0.53	0.78	0.67	0.73	0.73	1.33	1.34	0.49	1.51	0.75	0.60	1.07	0.66	0.84	1.01
P_c	Q1	-	-	-	-	0.92	1.11	0.93	1.08	1.40	0.81	1.11	1.47	0.81	0.68	1.43	0.95	1.00	1.00	1.01	1.51	0.96	1.28	1.01	1.39	1.34	0.99	0.56	0.93	1.16	1.45	0.81	1.01
	Q2	-	-	-	-	0.86	0.55	1.38	0.51	0.94	1.16	0.69	0.81	0.50	0.84	0.99	0.96	1.04	0.87	0.78	0.70	0.88	0.84	0.73	0.58	0.76	0.95	0.97	0.87	0.66	0.68	0.73	0.88
	Q3	-	-	-	-	0.78	1.14	1.00	0.75	0.85	0.92	0.87	0.95	0.56	0.84	0.78	1.19	0.69	1.11	1.05	0.76	1.59	0.97	0.79	1.14	1.04	0.96	0.87	1.20	1.17	0.90	0.94	0.82
	Q4	-	-	-	-	0.87	0.75	0.80	0.72	0.69	1.46	1.03	0.77	0.44	0.68	0.72	0.98	0.83	0.70	0.77	0.63	0.80	0.51	1.10	0.59	1.07	1.12	0.95	1.11	0.83	0.84	0.58	0.56
w_c	Q1	-	-	-	-	-	-	-	-	1.00	0.62	1.38	1.00	0.66	1.58	0.56	0.78	0.61	0.74	1.18	1.29	1.26	1.01	1.35	0.75	0.94	1.04	0.64	1.42	0.51	0.75	0.53	0.50
	Q2	-	-	-	-	-	-	-	-	1.10	1.14	1.34	0.54	0.78	1.24	0.91	0.97	1.32	1.24	0.89	0.92	1.34	0.88	0.68	0.91	0.95	1.12	1.02	0.99	0.47	0.98	0.62	1.03
	Q3	-	-	-	-	-	-	-	-	0.46	1.25	0.69	0.73	0.77	0.95	0.47	0.94	0.99	0.61	1.06	0.86	0.75	0.94	0.84	1.25	0.85	1.02	0.83	0.65	0.73	0.82	1.12	0.60
	Q4	-	-	-	-	-	-	-	-	1.22	0.53	0.66	0.79	0.71	0.70	1.06	0.92	0.95	0.74	0.72	0.55	1.03	0.91	0.86	1.02	0.71	0.90	1.03	0.88	0.85	0.87	0.73	1.49
δ_p	Q1	-	-	-	-	-	-	-	-	-	-	-	-	-	-	-	-	-	-	-	-	-	-	-	-	-	-	-	-	-	-	-	
	Q2	-	-	-	-	-	-	-	-	-	-	-	-	-	-	-	-	-	-	-	-	-	-	-	-	-	-	-	-	-	-	-	
	Q3	-	-	-	-	-	-	-	-	-	-	-	-	-	-	-	-	-	-	-	-	-	-	-	-	-	-	-	-	-	-	-	
	Q4	-	-	-	-	-	-	-	-	-	-	-	-	-	-	-	-	-	-	-	-	-	-	-	-	-	-	-	-	-	-	-	
P_p	Q1	-	-	-	-	-	-	-	-	-	-	-	-	-	-	-	-	-	-	-	-	-	-	-	-	-	-	-	-	-	-	-	
	Q2	-	-	-	-	-	-	-	-	-	-	-	-	-	-	-	-	-	-	-	-	-	-	-	-	-	-	-	-	-	-	-	
	Q3	-	-	-	-	-	-	-	-	-	-	-	-	-	-	-	-	-	-	-	-	-	-	-	-	-	-	-	-	-	-	-	
	Q4	-	-	-	-	-	-	-	-	-	-	-	-	-	-	-	-	-	-	-	-	-	-	-	-	-	-	-	-	-	-	-	
w_p	Q1	-	-	-	-	-	-	-	-	-	-	-	-	-	-	-	-	-	-	-	-	-	-	-	-	-	-	-	-	-	-	-	
	Q2	-	-	-	-	-	-	-	-	-	-	-	-	-	-	-	-	-	-	-	-	-	-	-	-	-	-	-	-	-	-	-	
	Q3	-	-	-	-	-	-	-	-	-	-	-	-	-	-	-	-	-	-	-	-	-	-	-	-	-	-	-	-	-	-	-	
	Q4	-	-	-	-	-	-	-	-	-	-	-	-	-	-	-	-	-	-	-	-	-	-	-	-	-	-	-	-	-	-	-	
d_p	Q1	-	-	-	-	-	-	-	-	-	-	-	-	-	-	-	-	-	-	-	-	-	-	-	-	-	-	-	-	-	-	-	
	Q2	-	-	-	-	-	-	-	-	-	-	-	-	-	-	-	-	-	-	-	-	-	-	-	-	-	-	-	-	-	-	-	
	Q3	-	-	-	-	-	-	-	-	-	-	-	-	-	-	-	-	-	-	-	-	-	-	-	-	-	-	-	-	-	-	-	
	Q4	-	-	-	-	-	-	-	-	-	-	-	-	-	-	-	-	-	-	-	-	-	-	-	-	-	-	-	-	-	-	-	
∇B	Q1	-	-	-	-	-	-	-	-	-	-	-	-	-	-	-	-	-	-	-	-	-	-	-	-	-	-	-	-	-	-	-	
	Q2	-	-	-	-	-	-	-	-	-	-	-	-	-	-	-	-	-	-	-	-	-	-	-	-	-	-	-	-	-	-	-	
	Q3	-	-	-	-	-	-	-	-	-	-	-	-	-	-	-	-	-	-	-	-	-	-	-	-	-	-	-	-	-	-	-	
	Q4	-	-	-	-	-	-	-	-	-	-	-	-	-	-	-	-	-	-	-	-	-	-	-	-	-	-	-	-	-	-	-	

Table 42: 2ODBI χ^2 values for \vec{r}_x across parameter quartile combinations.

		P_c				w_c				δ_p				P_p				w_p				d_p				∇B				B_v			
		Q1	Q2	Q3	Q4	Q1	Q2	Q3	Q4	Q1	Q2	Q3	Q4	Q1	Q2	Q3	Q4	Q1	Q2	Q3	Q4	Q1	Q2	Q3	Q4	Q1	Q2	Q3	Q4	Q1	Q2	Q3	Q4
δ_c	Q1	0.75	0.68	0.81	0.50	0.62	0.78	0.69	0.95	0.72	1.44	0.75	1.01	1.48	0.97	0.47	0.78	1.04	0.92	0.64	1.33	1.03	0.79	1.01	1.17	0.85	1.08	0.92	1.31	1.10	0.99	0.99	
	Q2	0.91	1.01	1.37	1.07	1.19	0.42	1.10	1.33	1.07	1.08	0.61	1.02	1.12	0.67	1.12	1.15	1.32	0.87	0.79	1.13	0.61	0.43	0.86	1.47	0.99	0.80	0.66	1.26	0.53	1.47	1.25	
	Q3	0.75	0.93	0.88	0.68	0.79	1.33	1.10	0.97	0.65	0.69	0.68	1.24	0.63	1.26	0.84	0.67	0.87	0.73	0.70	0.62	1.13	1.07	0.89	1.05	0.74	1.33	1.16	0.71	0.77	0.93	0.81	
	Q4	0.85	1.20	0.83	0.63	1.03	0.73	1.52	0.91	0.67	0.87	0.92	0.98	0.94	1.05	1.04	1.18	0.60	0.68	0.69	0.58	0.93	0.65	1.05	0.98	1.15	1.19	0.83	0.98	0.99	0.99		
P_c	Q1	-	-	-	-	0.69	0.92	0.53	0.70	0.92	0.71	0.57	1.00	0.61	0.86	0.88	1.09	0.99	0.77	0.82	0.74	0.43	1.20	0.64	1.05	0.91	0.94	0.63	0.73	0.40	0.89	0.92	1.11
	Q2	-	-	-	-	0.85	1.39	1.40	1.50	1.17	0.88	0.83	0.70	1.01	1.39	0.87	1.05	0.77	1.44	0.85	0.59	0.74	0.80	1.37	1.46	0.76	0.99	0.91	1.14	1.06	1.25	0.	

		P_c				w_c				δ_p				P_p				w_p				d_p				∇B				B_v			
		Q1	Q2	Q3	Q4	Q1	Q2	Q3	Q4	Q1	Q2	Q3	Q4	Q1	Q2	Q3	Q4	Q1	Q2	Q3	Q4	Q1	Q2	Q3	Q4	Q1	Q2	Q3	Q4	Q1	Q2	Q3	Q4
δ_c	Q1	1.12	0.79	0.91	0.91	1.08	0.65	1.25	1.05	0.90	1.07	1.14	0.50	0.40	0.78	1.13	0.60	1.38	0.63	0.98	0.53	1.32	1.47	0.99	0.80	0.90	0.70	0.78	0.63	1.04	1.11	0.65	0.50
	Q2	0.73	0.47	0.93	1.05	0.68	0.92	0.94	1.05	0.65	0.80	0.83	1.05	0.98	0.75	0.63	0.87	0.65	0.60	0.66	0.91	0.80	1.18	0.78	0.81	1.37	0.61	0.51	0.82	0.58	0.64	0.67	1.68
	Q3	0.86	0.65	0.52	0.53	1.00	0.75	0.84	1.21	1.36	1.11	0.68	0.80	1.20	0.89	0.77	0.99	1.00	0.41	0.72	0.49	1.03	0.80	0.61	0.75	0.68	1.15	0.75	0.96	0.93	0.90	0.51	1.03
	Q4	1.24	0.50	0.62	0.85	0.86	1.32	0.93	1.03	0.86	0.76	0.73	1.42	1.29	1.28	0.46	0.90	0.85	0.75	0.73	0.48	1.18	0.88	0.75	1.20	0.62	0.63	0.50	0.89	1.29	1.10	0.83	0.62
P_c	Q1	-	-	-	-	0.92	0.51	0.92	1.22	0.85	0.65	0.34	0.76	0.87	1.01	1.06	0.83	0.82	0.90	0.48	0.80	0.50	1.55	0.58	1.41	0.80	1.10	1.00	0.84	1.33	0.84	1.46	1.16
	Q2	-	-	-	-	0.97	0.85	0.55	0.96	0.97	0.97	0.78	0.71	1.24	0.85	0.54	0.67	0.83	0.95	0.84	0.80	0.94	0.77	0.90	0.63	1.37	0.70	0.67	0.75	0.61	0.76	0.70	0.73
	Q3	-	-	-	-	0.60	0.97	0.84	0.78	1.13	1.06	0.81	0.80	0.99	1.15	0.80	0.55	1.40	0.96	0.73	0.55	1.58	1.05	0.89	0.63	0.75	0.74	0.91	0.58	1.15	1.07	0.57	0.96
	Q4	-	-	-	-	1.16	1.15	1.32	1.24	0.55	0.60	0.92	1.07	0.64	0.88	0.59	0.92	0.91	0.59	1.30	0.68	1.44	1.47	0.76	1.01	0.97	1.04	0.74	0.97	0.87	0.68		
w_c	Q1	-	-	-	-	-	-	-	-	0.72	0.65	0.79	1.29	0.60	0.73	0.86	0.81	0.77	1.16	1.00	0.45	0.76	0.65	0.99	1.06	1.17	0.70	0.96	0.77	0.78	0.67	0.74	0.80
	Q2	-	-	-	-	-	-	-	-	0.88	0.99	0.54	0.70	0.86	0.69	0.73	0.84	0.88	0.71	0.70	0.46	1.15	0.92	0.43	0.97	1.65	1.00	1.06	0.76	0.61	1.42	0.77	0.49
	Q3	-	-	-	-	-	-	-	-	1.27	1.47	0.58	0.79	1.57	0.92	0.83	0.80	1.40	0.79	0.61	0.70	0.96	1.14	0.94	0.51	1.08	0.57	1.32	0.72	0.85	1.21	0.73	0.77
	Q4	-	-	-	-	-	-	-	-	1.55	0.78	0.77	1.14	0.66	0.74	0.98	1.10	0.74	0.74	0.61	0.62	1.15	0.99	0.79	0.77	0.94	0.74	0.89	1.39				
δ_p	Q1	-	-	-	-	-	-	-	-	-	-	-	-	0.91	0.95	0.77	0.36	0.79	0.96	0.90	0.55	0.61	0.70	1.08	0.96	1.44	0.93	0.69	0.59	0.74	1.00	0.67	0.60
	Q2	-	-	-	-	-	-	-	-	-	-	-	-	1.17	1.80	1.00	0.57	1.33	0.96	0.50	0.18	1.03	1.11	0.83	1.11	1.32	0.54	0.61	0.98	0.75	0.91	0.69	1.31
	Q3	-	-	-	-	-	-	-	-	-	-	-	-	0.88	1.23	0.31	1.16	0.72	0.81	0.63	0.60	0.82	1.09	0.96	0.85	1.18	0.64	1.17	0.90	0.94	0.63	0.55	1.20
	Q4	-	-	-	-	-	-	-	-	-	-	-	-	1.12	0.55	0.57	0.90	1.05	0.72	0.81	0.62	1.38	0.64	0.86	1.30	1.18	1.09	0.58	0.63	0.70	1.19	0.95	1.10
P_p	Q1	-	-	-	-	-	-	-	-	-	-	-	-	-	-	-	-	-	-	-	-	-	-	-	-	-	-	-	-	-	-	-	
	Q2	-	-	-	-	-	-	-	-	-	-	-	-	-	-	-	-	-	-	-	-	-	-	-	-	-	-	-	-	-	-	-	
	Q3	-	-	-	-	-	-	-	-	-	-	-	-	-	-	-	-	-	-	-	-	-	-	-	-	-	-	-	-	-	-	-	
	Q4	-	-	-	-	-	-	-	-	-	-	-	-	-	-	-	-	-	-	-	-	-	-	-	-	-	-	-	-	-	-	-	
w_p	Q1	-	-	-	-	-	-	-	-	-	-	-	-	-	-	-	-	-	-	-	-	-	-	-	-	-	-	-	-	-	-	-	
	Q2	-	-	-	-	-	-	-	-	-	-	-	-	-	-	-	-	-	-	-	-	-	-	-	-	-	-	-	-	-	-	-	
	Q3	-	-	-	-	-	-	-	-	-	-	-	-	-	-	-	-	-	-	-	-	-	-	-	-	-	-	-	-	-	-	-	
	Q4	-	-	-	-	-	-	-	-	-	-	-	-	-	-	-	-	-	-	-	-	-	-	-	-	-	-	-	-	-	-	-	
d_p	Q1	-	-	-	-	-	-	-	-	-	-	-	-	-	-	-	-	-	-	-	-	-	-	-	-	-	-	-	-	-	-	-	
	Q2	-	-	-	-	-	-	-	-	-	-	-	-	-	-	-	-	-	-	-	-	-	-	-	-	-	-	-	-	-	-	-	
	Q3	-	-	-	-	-	-	-	-	-	-	-	-	-	-	-	-	-	-	-	-	-	-	-	-	-	-	-	-	-	-	-	
	Q4	-	-	-	-	-	-	-	-	-	-	-	-	-	-	-	-	-	-	-	-	-	-	-	-	-	-	-	-	-	-	-	
∇B	Q1	-	-	-	-	-	-	-	-	-	-	-	-	-	-	-	-	-	-	-	-	-	-	-	-	-	-	-	-	-	-	-	
	Q2	-	-	-	-	-	-	-	-	-	-	-	-	-	-	-	-	-	-	-	-	-	-	-	-	-	-	-	-	-	-	-	
	Q3	-	-	-	-	-	-	-	-	-	-	-	-	-	-	-	-	-	-	-	-	-	-	-	-	-	-	-	-	-	-	-	
	Q4	-	-	-	-	-	-	-	-	-	-	-	-	-	-	-	-	-	-	-	-	-	-	-	-	-	-	-	-	-	-	-	

Table 44: 2ODBI χ^2 values for v across parameter quartile combinations.

		P_c				w_c				δ_p				P_p				w_p				d_p				∇B				B_v			
		Q1	Q2	Q3	Q4	Q1	Q2	Q3	Q4	Q1	Q2	Q3	Q4	Q1	Q2	Q3	Q4	Q1	Q2	Q3	Q4	Q1	Q2	Q3	Q4	Q1	Q2	Q3	Q4	Q1	Q2	Q3	Q4
δ_c	Q1	0.90	0.97	0.79	0.73	0.96	0.52	0.61	1.04	0.84	1.21	0.50	0.82	0.71	0.93	1.49	0.87	0.74	0.72	0.79	0.85	0.70	0.61	0.62	1.18	0.97	0.75	0.76	0.91	0.74	0.77	0.80	0.75
	Q2	0.94	0.81	1.14	1.22	0.82	0.98	1.23	0.92	1.38	0.88	1.55	0.65	1.06	0.82	1.35	1.36	0.53	1.35	0.77	1.07	0.96	0.84	0.95	1.03	1.42	1.11	0.52	1.23	1.09	1.17	1.27	
	Q3	1.07	0.79	0.76	1.09	0.97	0.85	0.96	1.06	1.38	0.74	0.84	0.98	1.04	1.02	0.78	1.10	1.00	0.68	0.81	1.45	1.18	0.69	0.55	1.21	1.21	0.61	1.34	0.87	1.26	0.78	0.78	
	Q4	0.98	0.95	1.03	0.86	1.50	1.10	1.30	0.93	0.98	1.01	0.92	0.53	0.99	0.70	0.57	0.64	1.25	1.15	0.76	1.07	0.84	1.50	1.07	0.65	0.88	1.08	0.55	0.60	0.37	1.03	1.42	
P_c	Q1	-	-	-	-	1.40	1.17	1.40	1.52	0.89	0.94	1.04	1.00	1.25	1.10	0.93	0.97	1.11	0.80	1.14	0.94	1.30	0.91	0.94	1.28	0.65	1.39	1.17	1.00	0.99	0.71	0.91	1.04
	Q2	-	-	-	-	0.84	0.71																										

		P_c				w_c				δ_p				P_p				w_p				d_p				∇B				B_v			
		Q1	Q2	Q3	Q4	Q1	Q2	Q3	Q4	Q1	Q2	Q3	Q4	Q1	Q2	Q3	Q4	Q1	Q2	Q3	Q4	Q1	Q2	Q3	Q4	Q1	Q2	Q3	Q4	Q1	Q2	Q3	Q4
δ_c	Q1	1.19	0.83	0.88	1.47	0.50	1.08	1.42	1.30	0.95	0.64	0.86	0.90	0.91	1.05	0.67	0.54	1.08	0.75	1.57	0.86	1.69	0.93	0.75	0.78	0.86	0.69	0.68	0.99	1.12	0.82	0.55	0.82
	Q2	0.64	1.51	1.23	1.31	0.94	1.00	0.99	0.96	0.54	0.52	0.40	0.81	0.59	0.80	0.64	0.82	0.92	0.81	0.82	0.98	0.90	0.78	1.11	0.78	0.63	0.99	0.52	1.06	1.01	0.90	1.25	1.13
	Q3	1.04	0.82	0.97	0.93	0.67	1.46	0.81	0.83	0.85	0.66	1.43	1.00	1.13	0.92	1.25	1.00	0.82	1.06	1.28	0.92	1.15	1.36	1.03	1.34	0.82	0.63	1.17	0.96	1.29	1.01	1.14	
	Q4	0.84	0.80	0.69	0.83	0.88	0.71	0.79	0.80	0.64	0.82	0.95	0.74	0.83	1.36	0.95	1.62	1.17	0.78	1.67	0.64	1.22	0.75	1.01	0.75	0.55	0.76	1.79	0.96	0.81	0.60	0.85	0.76
P_c	Q1	-	-	-	-	0.78	0.51	0.78	1.48	0.96	0.70	1.08	0.83	1.18	0.60	1.00	0.82	1.05	1.28	0.91	0.46	1.47	0.81	1.13	1.00	1.08	1.10	1.10	1.02	1.00	1.32	0.59	0.84
	Q2	-	-	-	-	1.01	1.28	1.12	1.29	0.93	1.08	0.78	1.05	1.17	0.97	0.54	0.65	0.71	1.17	0.98	0.81	1.20	0.61	0.59	0.60	1.04	1.10	0.73	0.73	0.87	1.78	0.97	0.96
	Q3	-	-	-	-	0.62	0.80	0.57	1.16	0.80	0.71	0.95	0.91	0.98	1.41	0.95	1.30	1.17	0.62	1.13	1.09	1.25	1.02	0.60	0.99	0.41	1.14	0.84	1.49	1.41	1.53	1.10	0.77
	Q4	-	-	-	-	1.06	1.10	1.25	1.26	1.33	0.63	1.27	0.90	0.65	0.51	0.82	1.51	0.61	0.86	0.81	0.69	0.81	1.20	0.81	1.11	0.93	0.88	0.96	1.52	1.24	1.21	0.86	1.22
w_c	Q1	-	-	-	-	-	-	-	-	0.86	0.48	0.43	1.22	0.85	0.58	1.24	0.50	0.52	0.96	0.73	1.07	0.84	0.53	0.95	1.38	0.89	0.82	0.69	0.66	0.99	0.59	0.88	0.90
	Q2	-	-	-	-	-	-	-	-	0.70	0.72	0.64	0.93	1.34	0.88	0.89	0.80	0.95	0.81	1.41	0.62	1.19	1.12	0.74	0.73	0.57	1.16	1.19	0.83	0.89	1.01	1.26	0.83
	Q3	-	-	-	-	-	-	-	-	0.56	0.45	1.36	1.02	0.86	1.08	1.56	1.22	0.70	0.77	1.09	1.08	0.81	1.20	0.81	1.11	0.93	0.88	0.96	1.20	0.85	0.86	1.13	1.27
	Q4	-	-	-	-	-	-	-	-	0.72	0.73	0.93	1.03	0.76	0.92	1.01	1.05	0.77	0.44	1.13	0.89	0.99	1.66	0.78	0.77	0.60	0.81	1.41	0.80	0.92	1.09	0.81	0.85
δ_p	Q1	-	-	-	-	-	-	-	-	-	0.66	0.49	0.90	0.42	0.49	0.61	0.95	0.54	0.63	0.53	0.52	0.38	0.58	0.82	0.79	0.92	1.39	0.70	0.44	0.67			
	Q2	-	-	-	-	-	-	-	-	-	0.58	0.93	0.46	0.64	0.67	0.78	0.74	0.52	1.29	1.11	1.51	0.62	0.82	0.54	0.71	0.91	0.68	0.55	1.20	0.92			
	Q3	-	-	-	-	-	-	-	-	-	-	1.11	1.13	0.77	0.87	1.03	0.70	1.15	0.99	1.33	0.61	0.50	1.47	1.20	0.90	1.27	0.79	1.37	1.00	0.63	0.99		
	Q4	-	-	-	-	-	-	-	-	-	-	1.44	0.92	0.39	1.28	1.13	0.99	1.24	0.92	0.82	1.22	0.96	1.55	0.83	0.73	0.77	0.76	0.56	0.88	0.99	1.23		
P_p	Q1	-	-	-	-	-	-	-	-	-	-	-	-	-	-	-	-	-	-	-	-	-	-	-	-	-	-	-	-	-	-	-	
	Q2	-	-	-	-	-	-	-	-	-	-	-	-	-	-	-	-	-	-	-	-	-	-	-	-	-	-	-	-	-	-	-	
	Q3	-	-	-	-	-	-	-	-	-	-	-	-	-	-	-	-	-	-	-	-	-	-	-	-	-	-	-	-	-	-	-	
	Q4	-	-	-	-	-	-	-	-	-	-	-	-	-	-	-	-	-	-	-	-	-	-	-	-	-	-	-	-	-	-	-	
w_p	Q1	-	-	-	-	-	-	-	-	-	-	-	-	-	-	-	-	-	-	-	-	-	-	-	-	-	-	-	-	-	-	-	
	Q2	-	-	-	-	-	-	-	-	-	-	-	-	-	-	-	-	-	-	-	-	-	-	-	-	-	-	-	-	-	-	-	
	Q3	-	-	-	-	-	-	-	-	-	-	-	-	-	-	-	-	-	-	-	-	-	-	-	-	-	-	-	-	-	-	-	
	Q4	-	-	-	-	-	-	-	-	-	-	-	-	-	-	-	-	-	-	-	-	-	-	-	-	-	-	-	-	-	-	-	
d_p	Q1	-	-	-	-	-	-	-	-	-	-	-	-	-	-	-	-	-	-	-	-	-	-	-	-	-	-	-	-	-	-	-	-
	Q2	-	-	-	-	-	-	-	-	-	-	-	-	-	-	-	-	-	-	-	-	-	-	-	-	-	-	-	-	-	-	-	
	Q3	-	-	-	-	-	-	-	-	-	-	-	-	-	-	-	-	-	-	-	-	-	-	-	-	-	-	-	-	-	-	-	
	Q4	-	-	-	-	-	-	-	-	-	-	-	-	-	-	-	-	-	-	-	-	-	-	-	-	-	-	-	-	-	-	-	
∇B	Q1	-	-	-	-	-	-	-	-	-	-	-	-	-	-	-	-	-	-	-	-	-	-	-	-	-	-	-	-	-	-	-	
	Q2	-	-	-	-	-	-	-	-	-	-	-	-	-	-	-	-	-	-	-	-	-	-	-	-	-	-	-	-	-	-	-	
	Q3	-	-	-	-	-	-	-	-	-	-	-	-	-	-	-	-	-	-	-	-	-	-	-	-	-	-	-	-	-	-	-	
	Q4	-	-	-	-	-	-	-	-	-	-	-	-	-	-	-	-	-	-	-	-	-	-	-	-	-	-	-	-	-	-	-	

Table 46: 2ODBI χ^2 values for θ across parameter quartile combinations.

		P_c				w_c				δ_p				P_p				w_p				d_p				∇B				B_v			
		Q1	Q2	Q3	Q4	Q1	Q2	Q3	Q4	Q1	Q2	Q3	Q4	Q1	Q2	Q3	Q4	Q1	Q2	Q3	Q4	Q1	Q2	Q3	Q4	Q1	Q2	Q3	Q4	Q1	Q2	Q3	Q4
δ_c	Q1	1.60	1.36	1.07	0.63	0.95	1.29	1.18	1.33	1.12	0.61	1.00	1.65	0.92	0.94	1.02	1.24	0.97	0.94	1.66	1.36	1.06	1.07	0.80	0.87	0.94	1.25	1.07	1.32	0.97	0.99	1.14	
	Q2	0.84	1.17	0.54	0.82	1.38	0.96	0.63	1.20	0.96	0.55	1.08	0.72	1.35	0.74	0.83	1.33	0.46	0.89	1.01	1.13	1.01	0.77	0.81	0.84	1.24	0.64	0.87	1.47	0.90	0.45	1.01	
	Q3	0.92	0.93	0.66	1.07	1.35	0.87	0.50	1.32	0.98	0.96	1.19	1.08	0.81	0.93	1.26	1.26	0.95	1.06	0.62	0.63	0.97	0.50	0.98	1.21	0.94	0.70	0.99	0.61	0.95	0.77	0.61	0.95
	Q4	0.78	0.87	1.14	0.66	0.75	1.40	0.98	1.05	1.02	0.84	0.59	1.28	0.78	0.76	0.95	1.05	0.91	0.89	1.47	0.92	1.41	0.61	0.94	1.12	0.95	1.01	1.63	0.73	1.07	0.66	0.60	1.39
P_c	Q1	-	-	-	-	1.51	0.88	0.91	1.22	0.81	1.16	0.92	0.73	0.89	0.98	1.57	1.19	1.13	1.44	0.51	1.28	0.20	0.65	1.55	1.20	1.56	1.50	1.00	0.83	1.03	0.90	0.62	1.08
	Q2	-	-	-	-	1.00																											

		P_e	w_c	δ_p	P_p	w_p	d_p	∇B	B_v																									
		Q1	Q2	Q3	Q4	Q1	Q2	Q3	Q4	Q1	Q2	Q3	Q4	Q1	Q2	Q3	Q4	Q1	Q2	Q3	Q4													
δ_c	Q1	1.27	0.72	1.09	1.77	0.72	1.11	1.21	1.35	1.25	0.68	1.08	1.46	1.29	1.16	0.75	1.02	0.78	1.22	0.99	0.52	0.78	1.09	1.06	1.23	1.19	1.24	1.10	0.47	0.92	0.83	1.05	0.99	
	Q2	0.66	1.39	0.72	0.92	1.35	0.75	0.83	0.88	1.34	0.67	0.81	0.76	1.85	0.92	0.59	1.08	1.12	0.75	1.09	0.82	0.65	1.20	0.80	0.73	0.96	1.20	0.83	1.56	1.82	0.79	0.86	1.05	
	Q3	0.93	0.82	0.67	0.95	0.65	0.72	0.52	1.05	0.90	0.72	1.12	0.88	0.58	0.98	0.92	0.58	1.20	0.52	1.34	1.06	0.93	0.85	0.78	1.85	1.40	0.78	0.97	0.94	0.82	0.96	0.84	0.53	
	Q4	0.95	1.08	0.87	1.49	0.80	0.79	1.17	1.28	0.57	0.74	0.91	0.80	1.22	0.79	1.07	0.74	0.87	0.94	1.15	0.92	1.75	0.85	0.82	0.78	0.78	0.93	0.92	1.50	0.81	1.03	0.66	0.75	
P_c	Q1	-	-	-	-	0.85	0.96	0.88	0.73	1.31	0.64	0.60	0.90	1.72	0.91	1.16	0.87	1.03	0.72	1.06	0.97	0.76	0.77	1.13	0.67	1.06	0.93	0.69	0.97	1.43	0.95	1.00		
	Q2	-	-	-	-	1.56	0.59	0.84	0.62	1.85	0.85	0.68	0.97	1.09	1.21	1.52	1.25	0.99	0.74	1.12	0.81	1.21	1.25	1.18	0.66	1.24	0.49	1.26	0.68	0.94	0.73	0.38	0.95	
	Q3	-	-	-	-	1.09	1.22	1.07	0.81	1.43	1.22	0.73	0.95	0.98	1.26	0.54	0.93	1.48	1.13	0.85	1.38	1.10	1.25	1.19	1.24	0.47	0.95	0.89	1.08	0.95	0.74	0.84	1.41	
	Q4	-	-	-	-	1.24	1.13	0.72	1.80	0.46	1.05	1.89	1.53	0.89	1.35	1.20	0.70	1.37	1.32	1.47	1.21	1.03	1.16	1.35	1.50	1.12	0.62	1.85	0.83	1.22	1.12	1.60		
w_c	Q1	-	-	-	-	-	-	-	-	1.40	1.12	1.18	0.46	0.78	0.50	1.11	0.75	1.28	0.94	1.66	1.08	0.94	1.63	0.43	1.34	1.42	0.97	0.98	1.07	1.16	0.69	0.58	0.98	
	Q2	-	-	-	-	-	-	-	-	1.15	0.76	0.35	1.00	1.07	0.93	1.31	0.72	1.34	0.83	1.31	1.04	1.04	0.55	0.93	0.80	0.84	0.59	0.76	0.87	1.21	0.56	1.08	1.12	
	Q3	-	-	-	-	-	-	-	-	1.02	0.86	0.68	0.63	0.84	1.03	0.70	0.77	0.84	0.95	0.84	0.78	0.70	0.90	1.01	1.27	0.61	0.89	0.99	0.83	0.70	0.72	1.21		
	Q4	-	-	-	-	-	-	-	-	0.96	0.65	0.81	0.80	1.30	1.17	0.65	1.06	1.30	0.76	0.94	0.71	0.85	0.71	0.76	0.90	1.20	1.21	1.20	1.09	0.58	0.84	1.26	0.94	0.70
δ_p	Q1	-	-	-	-	-	-	-	-	-	-	-	0.47	1.31	1.21	1.04	0.91	1.08	1.16	1.28	0.65	1.11	1.04	0.88	1.23	0.94	0.55	1.04	1.25	1.06	1.39	0.91		
	Q2	-	-	-	-	-	-	-	-	-	-	-	0.71	0.76	1.12	0.81	0.83	0.82	1.03	1.34	0.92	0.39	0.89	1.27	1.11	1.11	1.03	0.98	0.73	1.52	0.59	0.57		
	Q3	-	-	-	-	-	-	-	-	-	-	-	0.83	1.14	0.70	0.75	1.20	1.04	0.97	0.79	0.93	0.96	0.93	1.17	1.46	0.71	0.80	0.76	0.80	0.65	1.14	1.38		
	Q4	-	-	-	-	-	-	-	-	-	-	-	0.80	0.86	0.84	1.17	0.89	0.67	1.08	0.63	1.14	1.11	1.02	1.28	1.21	0.94	1.11	0.88	0.89	0.67	0.90	0.81		
P_p	Q1	-	-	-	-	-	-	-	-	-	-	-	-	-	-	-	-	-	-	-	-	-	-	-	-	-	-	-	-	-	-	-	-	-
	Q2	-	-	-	-	-	-	-	-	-	-	-	-	-	-	-	-	-	-	-	-	-	-	-	-	-	-	-	-	-	-	-	-	-
	Q3	-	-	-	-	-	-	-	-	-	-	-	-	-	-	-	-	-	-	-	-	-	-	-	-	-	-	-	-	-	-	-	-	-
	Q4	-	-	-	-	-	-	-	-	-	-	-	-	-	-	-	-	-	-	-	-	-	-	-	-	-	-	-	-	-	-	-	-	-
w_p	Q1	-	-	-	-	-	-	-	-	-	-	-	-	-	-	-	-	-	-	-	-	-	-	-	-	-	-	-	-	-	-	-	-	-
	Q2	-	-	-	-	-	-	-	-	-	-	-	-	-	-	-	-	-	-	-	-	-	-	-	-	-	-	-	-	-	-	-	-	-
	Q3	-	-	-	-	-	-	-	-	-	-	-	-	-	-	-	-	-	-	-	-	-	-	-	-	-	-	-	-	-	-	-	-	-
	Q4	-	-	-	-	-	-	-	-	-	-	-	-	-	-	-	-	-	-	-	-	-	-	-	-	-	-	-	-	-	-	-	-	-
d_p	Q1	-	-	-	-	-	-	-	-	-	-	-	-	-	-	-	-	-	-	-	-	-	-	-	-	-	-	-	-	-	-	-	-	-
	Q2	-	-	-	-	-	-	-	-	-	-	-	-	-	-	-	-	-	-	-	-	-	-	-	-	-	-	-	-	-	-	-	-	-
	Q3	-	-	-	-	-	-	-	-	-	-	-	-	-	-	-	-	-	-	-	-	-	-	-	-	-	-	-	-	-	-	-	-	-
	Q4	-	-	-	-	-	-	-	-	-	-	-	-	-	-	-	-	-	-	-	-	-	-	-	-	-	-	-	-	-	-	-	-	-
∇B	Q1	-	-	-	-	-	-	-	-	-	-	-	-	-	-	-	-	-	-	-	-	-	-	-	-	-	-	-	-	-	-	-	-	-
	Q2	-	-	-	-	-	-	-	-	-	-	-	-	-	-	-	-	-	-	-	-	-	-	-	-	-	-	-	-	-	-	-	-	-
	Q3	-	-	-	-	-	-	-	-	-	-	-	-	-	-	-	-	-	-	-	-	-	-	-	-	-	-	-	-	-	-	-	-	-
	Q4	-	-	-	-	-	-	-	-	-	-	-	-	-	-	-	-	-	-	-	-	-	-	-	-	-	-	-	-	-	-	-	-	-

Table 48: 2ODBI χ^2 values for \vec{r}_y across parameter quartile combinations.

		P_e	w_c	δ_p	P_p	w_p	d_p	∇B	B_v																								
		Q1	Q2	Q3	Q4	Q1	Q2	Q3	Q4	Q1	Q2	Q3	Q4	Q1	Q2	Q3	Q4	Q1	Q2	Q3	Q4												
δ_c	Q1	1.20	0.74	0.75	1.21	1.11	0.67	1.09	0.81	0.80	0.66	1.05	1.33	0.48	0.76	1.52	1.01	0.79	1.13	1.05	1.01	1.43	1.26	0.86	0.68	0.88	0.94	0.70	0.94	0.95	0.66	1.15	1.87
	Q2	0.62	1.06	0.68	1.04	1.15	1.01	0.94	0.97	0.66	0.96	0.99	1.20	1.01	1.05	0.63	0.92	0.77	1.25	0.41	0.91	0.53	0.71	0.97	0.69	0.73	0.85	0.80	1.16	1.75	0.48	0.72	0.97
	Q3	0.97	0.73	0.84	1.06	1.03	0.69	0.66	1.40	0.73	0.89	1.04	0.71	0.86	0.94	0.89	0.35	0.44	1.09	0.86	0.65	1.16	1.03	1.05	0.56	0.66	0.48	0.46	0.77	0.50			
	Q4	0.51	0.86	0.94	0.85	0.86	0.75	0.91	0.63	1.00	0.72	0.70	1.00	1.26	1.06	0.79	0.74	0.75	0.51	1.08	0.91	0.48	1.05	0.83	1.23	1.14	1.14	0.70	0.58	0.91	0.60	0.65	0.90
P_c	Q1	-	-	-	-	1.22	0.46	0.97	0.70	0.83	0.79	1.13	1.04	0.84	1.14	1.08	0.83	0.68	1.40	0.80	0.83	1.60	0.86	0.87	0.92	0.91	0.75	1.17	1.20	0.71	1.13	0.88	1.12
	Q2	-	-	-	-	1.14	0.79	0.68	1.50	0.70	0.72	0.45	1.38	0.72	1.70	0.83	0.65	0.77	0.63	0.75	0.70	1.03	0.55	0.72	1.49	1.08	0.70	1.11	0.94	0.76	1.16	1.38	0.07
	Q3	-	-	-	-	1.30	0.63	0.88	0.59	0.94	0.86	0.78	1.02	0.93	1.05	1.05	0.86	0.88	0.82	0.51	0.98	1.01	1.27	0.56	0.82	1.13	0.94	0.69	0.95	1.23	0.88	1.04	0.85
	Q4	-	-	-	-	1.36	0.91	0.99	0.77	0.62	1.32	0.82	0.80	1.09	1.05	0.78	1.03	0.80	0.72	0.77	0.72	0.60	0.55	0.7									

		P_c	w_c	δ_p	P_p	w_p	d_p	∇B				B_v																									
		Q1	Q2	Q3	Q4	Q1	Q2	Q3	Q4	Q1	Q2	Q3	Q4	Q1	Q2	Q3	Q4	Q1	Q2	Q3	Q4	Q1	Q2	Q3	Q4												
δ_c	Q1	1.02	1.01	0.99	1.00	1.28	0.98	1.20	0.84	1.09	1.20	1.04	1.00	0.81	0.89	1.00	0.89	0.72	1.16	1.07	0.66	0.97	0.60	0.93	0.60												
	Q2	1.17	0.79	0.94	0.77	1.34	0.82	1.04	1.07	0.57	0.64	1.35	0.81	1.59	0.79	0.81	1.35	1.05	0.73	1.24	0.81	0.65	0.53	1.02	0.67	0.80											
	Q3	1.08	0.83	1.26	1.52	1.23	0.95	1.04	0.78	2.04	0.44	1.14	0.65	0.83	0.77	1.62	0.98	1.17	0.91	0.76	0.79	1.02	0.97	0.95	0.85												
	Q4	0.87	0.77	0.72	0.95	0.94	1.55	1.07	0.57	1.32	1.39	0.78	1.57	1.05	1.34	1.30	0.71	0.80	0.90	1.06	1.10	1.00	0.68	0.87	1.01												
P_c	Q1	-	-	-	-	1.23	1.24	1.05	1.12	0.95	0.91	1.28	1.35	1.25	0.69	1.11	1.10	0.82	0.86	1.38	0.90	1.61	0.67	0.92	0.73	0.92	0.77										
	Q2	-	-	-	-	0.71	1.12	0.88	0.45	0.94	0.55	0.76	0.85	0.73	1.02	0.72	1.57	0.45	0.76	0.79	0.71	0.62	0.97	1.28	0.82	0.63	0.75										
	Q3	-	-	-	-	1.31	0.88	0.70	1.05	1.39	1.32	0.86	1.31	1.40	1.09	1.03	0.80	0.61	0.92	1.02	1.01	0.68	1.14	1.66	1.02	0.73	0.86										
	Q4	-	-	-	-	1.46	1.00	1.50	0.80	1.28	1.68	0.75	1.07	1.34	0.84	1.12	0.60	0.93	0.84	1.45	1.01	1.37	0.87	1.02	1.08	1.18	1.09										
w_c	Q1	-	-	-	-	-	-	-	-	1.44	0.85	1.18	1.18	0.85	1.53	1.84	0.67	1.11	0.84	1.43	0.69	0.71	0.85	1.47	1.12	1.07	1.29	1.47	1.36	1.48	1.81	0.84	1.21				
	Q2	-	-	-	-	-	-	-	-	0.94	0.96	1.10	1.01	1.13	0.82	0.88	1.03	1.05	0.84	1.08	1.06	0.80	0.82	0.71	1.49	0.83	0.99	1.22	0.73	1.44	0.86	1.22	0.71				
	Q3	-	-	-	-	-	-	-	-	1.74	0.80	0.89	1.30	0.64	1.22	1.10	0.51	0.71	0.89	1.18	1.09	1.04	1.00	1.06	1.36	0.81	0.79	1.00	1.14	1.22	1.43	1.07	0.97	0.57			
	Q4	-	-	-	-	-	-	-	-	0.80	1.10	0.91	0.88	1.00	0.42	0.96	1.28	0.74	0.53	0.92	1.38	0.87	0.62	1.00	0.48	1.00	0.93	0.94	1.16	0.76	1.41	0.77	1.21				
δ_p	Q1	-	-	-	-	-	-	-	-	-	-	-	-	-	-	-	-	0.76	1.30	1.01	0.99	0.90	1.02	1.40	1.24	0.61	0.97	1.02	1.09	1.16	1.09	0.94	1.46	1.35	1.02	1.14	1.20
	Q2	-	-	-	-	-	-	-	-	-	-	-	-	-	-	-	-	1.41	1.34	0.60	0.90	0.69	1.06	1.15	1.65	0.97	0.98	1.44	0.73	0.73	0.85	0.81	1.48	0.89	0.62	0.52	0.79
	Q3	-	-	-	-	-	-	-	-	-	-	-	-	-	-	-	-	1.27	0.77	1.17	0.82	0.64	0.79	1.21	0.94	1.22	0.75	1.12	0.86	0.71	1.02	0.92	0.81	1.00	0.93	1.66	1.12
	Q4	-	-	-	-	-	-	-	-	-	-	-	-	-	-	-	-	0.37	1.18	1.26	0.73	0.72	0.70	0.99	1.11	1.20	1.22	0.70	0.87	0.85	0.85	0.84	0.66	0.94	0.67	1.24	1.05
P_p	Q1	-	-	-	-	-	-	-	-	-	-	-	-	-	-	-	-	-	-	0.81	1.15	0.79	0.56	1.60	0.80	0.74	0.88	0.88	0.90	1.14	1.14	0.84	1.08	1.18	0.95		
	Q2	-	-	-	-	-	-	-	-	-	-	-	-	-	-	-	-	-	-	0.76	1.33	0.51	1.01	0.58	0.75	1.21	0.44	0.85	1.45	0.25	1.03	1.41	1.31	1.24	0.61		
	Q3	-	-	-	-	-	-	-	-	-	-	-	-	-	-	-	-	-	-	1.02	1.02	0.98	1.44	1.38	0.85	1.43	0.92	1.62	0.67	0.85	1.39	0.84	1.48	1.63	0.99		
	Q4	-	-	-	-	-	-	-	-	-	-	-	-	-	-	-	-	-	-	0.85	1.08	1.20	1.43	0.74	0.71	0.59	0.84	1.24	1.11	1.05	0.85	0.87	1.69	0.74	1.05		
w_p	Q1	-	-	-	-	-	-	-	-	-	-	-	-	-	-	-	-	-	-	-	-	-	-	-	-	-	-	-	-	-	-	-	-	-	-		
	Q2	-	-	-	-	-	-	-	-	-	-	-	-	-	-	-	-	-	-	-	-	-	-	-	-	-	-	-	-	-	-	-	-	-	-		
	Q3	-	-	-	-	-	-	-	-	-	-	-	-	-	-	-	-	-	-	-	-	-	-	-	-	-	-	-	-	-	-	-	-	-	-		
	Q4	-	-	-	-	-	-	-	-	-	-	-	-	-	-	-	-	-	-	-	-	-	-	-	-	-	-	-	-	-	-	-	-	-	-		
d_p	Q1	-	-	-	-	-	-	-	-	-	-	-	-	-	-	-	-	-	-	-	-	-	-	-	-	-	-	-	-	-	-	-	-	-	-		
	Q2	-	-	-	-	-	-	-	-	-	-	-	-	-	-	-	-	-	-	-	-	-	-	-	-	-	-	-	-	-	-	-	-	-	-		
	Q3	-	-	-	-	-	-	-	-	-	-	-	-	-	-	-	-	-	-	-	-	-	-	-	-	-	-	-	-	-	-	-	-	-	-		
	Q4	-	-	-	-	-	-	-	-	-	-	-	-	-	-	-	-	-	-	-	-	-	-	-	-	-	-	-	-	-	-	-	-	-	-		
∇B	Q1	-	-	-	-	-	-	-	-	-	-	-	-	-	-	-	-	-	-	-	-	-	-	-	-	-	-	-	-	-	-	-	-	-	-		
	Q2	-	-	-	-	-	-	-	-	-	-	-	-	-	-	-	-	-	-	-	-	-	-	-	-	-	-	-	-	-	-	-	-	-	-		
	Q3	-	-	-	-	-	-	-	-	-	-	-	-	-	-	-	-	-	-	-	-	-	-	-	-	-	-	-	-	-	-	-	-	-	-		
	Q4	-	-	-	-	-	-	-	-	-	-	-	-	-	-	-	-	-	-	-	-	-	-	-	-	-	-	-	-	-	-	-	-	-	-		

Table 50: 2ODBI χ^2 values for ϕ across parameter quartile combinations.

		P_c	w_c	δ_p	P_p	w_p	d_p	∇B				B_v																					
		Q1	Q2	Q3	Q4	Q1	Q2	Q3	Q4	Q1	Q2	Q3	Q4	Q1	Q2	Q3	Q4	Q1	Q2	Q3	Q4	Q1	Q2	Q3	Q4								
δ_c	Q1	0.80	0.59	0.86	0.84	0.93	0.98	0.88	0.90	1.16	0.73	0.55	0.87	1.22	1.10	0.90	1.01	0.76	1.03	0.78	1.25	0.80	0.73	1.42	1.28	0.84	0.78	1.35	1.14	1.34	0.87	0.80	
	Q2	0.77	1.05	1.33	0.94	1.00	0.79	1.40	0.74	1.13	1.03	1.10	1.17	0.94	1.12	1.19	0.60	0.74	1.70	1.11	1.04	0.96	0.93	0.95	0.88	1.36	1.05	1.01	0.89	0.99	1.00	1.56	
	Q3	0.79	1.41	1.47	0.89	0.85	0.84	0.60	1.00	0.92	0.61	0.76	1.72	1.34	0.70	0.44	1.09	0.97	1.41	0.73	0.92	0.51	1.25	1.23	1.23	1.27	1.27	1.27	1.27	1.27	1.27	1.27	1.27
	Q4	0.89	0.77	0.86	1.02	0.56	1.14	0.94	0.83	0.79	0.46	0.98	0.76	0.88	1.27	1.12	0.52	0.65	1.48	0.96	0.98	0.72	1.05	1.11	0.68	0.90	0.80	0.70	1.78	0.58	0.61	0.88	
P_c	Q1	-	-	-	-	0.63	0.84	0.68	0.94	1.11	0.77	1.06	0.80	0.89	0.98	1.41	1.01	0.77	0.88	1.06	0.57	0.74	0.83	0.93	1.91	0.85	1.18	0.89	0.71	0.95	0.83	0.35	1.11
	Q2	-	-	-	-	0.98	0.60	1.26	1.16	1.25	0.98	1.10	0.79	1.30	0.84	0.76	0.55	0.92	1.25	1.00	0.53	0.80	1.01	1.55	0.87	0.68	0.66	0.96	0.86	0.53	1.26	0.74	0.91
	Q3	-	-	-	-	0.41	0.83	0.88	1.55	1.23	0.98	1.29	0.86	0.97	1.22	1.18	0.80	0.83	0.91	0.96	1.20	1.08	0.95	1.10	1.21	0.68	0.92	0.48	1.23	1.45	1.23	1.02	
	Q4	-	-	-	-	1.00	0.69	1.14	0.62	0.76</td																							